AD_____

Award Number: W81XWH-13-1-0129

TITLE: “Maximizing PTH Anabolic Osteoporosis Therapy”

PRINCIPAL INVESTIGATOR: Joseph Bidwell

CONTRACTING ORGANIZATION: INDIANA UNIVERSITY
INDIANAPOLIS IN 46202-5130

REPORT DATE: September 2015

TYPE OF REPORT: Annual

PREPARED FOR: U.S. Army Medical Research and Materiel Command
Fort Detrick, Maryland 21702-5012

DISTRIBUTION STATEMENT: Approved for Public Release;
Distribution Unlimited

The views, opinions and/or findings contained in this report are those of the author(s) and should not be construed as an official Department of the Army position, policy or decision unless so designated by other documentation.

REPORT DOCUMENTATION PAGE

Form Approved
OMB No. 0704-0188

1. REPORT DATE	2. REPORT TYPE	3. DATES COVERED
September 2015	Annual	15 Aug 2014 - 14 Aug 2015

4. TITLE AND SUBTITLE

"Maximizing PTH Anabolic Osteoporosis Therapy"

5a. CONTRACT NUMBER
W81XWH-13-1-0129

5b. GRANT NUMBER

5c. PROGRAM ELEMENT NUMBER

6. AUTHOR(S)

Joseph Bidwell

email: jbidwell@iupui.edu

5d. PROJECT NUMBER

5e. TASK NUMBER

5f. WORK UNIT NUMBER

7. PERFORMING ORGANIZATION NAME(S) AND ADDRESS(ES)

INDIANA UNIVERSITY
980 INDIANA AVE RM 2232
INDIANAPOLIS IN 46202-5130

8. PERFORMING ORGANIZATION REPORT NUMBER

9. SPONSORING / MONITORING AGENCY NAME(S) AND ADDRESS(ES)
U.S. Army Medical Research and Materiel Command
Fort Detrick, Maryland 21702-5012

10. SPONSOR/MONITOR'S ACRONYM(S)

11. SPONSOR/MONITOR'S REPORT NUMBER(S)

12. DISTRIBUTION / AVAILABILITY STATEMENT
Approved for Public Release; Distribution Unlimited

13. SUPPLEMENTARY NOTES

14. ABSTRACT

The purpose of this study is to test the efficacy of parathyroid hormone (PTH) mono-therapy and PTH+ anti-catabolic combination therapies on *Nmp4*$^{-/-}$ and wild type (WT) mice. **The scope of** the research comprises the following specific aims: (i & ii) to determine the impact of Nmp4 on the efficacy of PTH mono- and combination therapies with various anti-catabolics in ovariectomized (ovx) mice; (iii) to determine the cell type-specific contributions to the enhanced response of the *Nmp4*$^{-/-}$ mouse to these osteoporosis therapies. In **YEAR 2** we completed experiments comparing the response of ovx WT and *Nmp4*$^{-/-}$ mice to PTH+anti-catabolic therapies. **The most significant findings during the YEAR 2 period include the following**:

- **KEY FINDING:** *Mice receiving PTH+RAL (raloxifene) and PTH+ZOL (zolendronate) showed the largest BMD (bone mineral density) increase.*
- **KEY FINDING:** *The PTH+RAL therapy was the only treatment to exhibit a synergistic effect on total WB (whole body) and spine BMD*
- **KEY FINDING:** *Disabling Nmp4 enhanced PTH+RAL-induced increases in femoral BV/TV and increased the synergistic action of PTH with RAL and ZOL in both the femur and spine.*
- **KEY FINDING**: *Disabling Nmp4 enhanced the distinction between the PTH+RAL-induced increase in cortical bone area and the other treatments*
- **KEY FINDING:** *Nmp4*$^{-/-}$ *mice under the PTH+RAL therapy harbored more bone marrow osteoprogenitors than mice under the other treatments*
- **KEY FINDING:** *Raloxifene enhanced WT mesenchymal stem/progenitor cell (MSPC) mineralization*

Our key discovery in YEAR 2 is that disabling Nmp4 in a pre-clinical osteoporosis model improves the bone-forming efficacy of PTH+RAL therapy.

15. SUBJECT TERMS
Nmp4-knockout (KO) mice, osteoporosis, ovariectomy, PTH combination therapies

16. SECURITY CLASSIFICATION OF:			17. LIMITATION OF ABSTRACT	18. NUMBER OF PAGES	19a. NAME OF RESPONSIBLE PERSON
a. REPORT	b. ABSTRACT	c. THIS PAGE			USAMRMC
U	U	U	UU	167	19b. TELEPHONE NUMBER *(include area code)*

Table of Contents

INTRODUCTION: The subject of this research is the need for improved osteoporosis therapies. The purpose of this study is to test the efficacy of parathyroid hormone (PTH) mono-therapy and PTH + anti-catabolic combination therapies on *Nmp4*$^{-/-}$ and wild type (WT) mice. We have previously determined that Nmp4 represses the response of bone to osteoanabolics[1-3]. The scope of this research comprises the following specific aims: (i & ii) to determine the impact of Nmp4 on the efficacy of PTH mono- and combination therapies with bisphosphonates and the selective estrogen receptor modulator (SERM) raloxifene in ovariectomized (ovx) mice; (iii) to determine the cell type-specific contributions to the enhanced response of the *Nmp4*$^{-/-}$ mouse to these osteoporosis therapies.

BODY:

During Year 2 we successfully accomplished a number of objectives in the following Tasks and Subtasks:

i. *Task 2: Conduct PTH mono-therapy and PTH combination therapies with bisphosphonates*: A *revised* manuscript describing the impact of Nmp4 on ovx-induced bone loss and the response of ovx mice to PTH mono-therapy is in review at Molecular Endocrinology (see Appendix Manuscript Number ME-14-1406R1). Note: this manuscript contains all details for the materials and methods used to generate the PTH+anti-catabolic data described below.

ii. *Task 3: Conduct PTH combination therapy with raloxifene*: The treatment of the WT and *Nmp4*$^{-/-}$ mice with the PTH + anti-catabolic therapies (raloxifene and bisphosphonates) is finished and the analyses underway. The PTH+raloxifene combination therapy has been identified as the optimum combination treatment to be used in Task 4 (see below for details of results and ongoing analyses).

iii. *Subtasks 4.2.a and 4.3.a: Breed 54 female Nmp4fl/fl3.6Col-Cre+ & 54 Nmp4fl/fl-Cre– mice*: We are backcrossing our Nmp4$^{flox/flox}$ mice onto a C57BL/6J for production of conditional knockout animals (see below for details).

iv. *Subtask 6.2: Culture, expand, and characterize the phenotype of both WT and Nmp4*$^{-/-}$ *mesenchymal stem/progenitor cells (MSPCs)*: These experiments are described in the revised manuscript ME-14-1406R1 (Appendix) and we have started experiments designed to characterize the impact of raloxifene on MSPCs (see below)

Overview of Objectives and Results During Year 2:

During Year 1 we determined that the exaggerated response to anabolic doses of PTH was preserved in ovx *Nmp4*$^{-/-}$ mice but that disabling this transcription factor did not protect them from ovx-induced bone loss without therapy. During Year 2 we addressed whether various PTH+anti-catabolic combination therapies are more efficacious in osteoporotic *Nmp4*$^{-/-}$ than wild type (WT) mice. Animals were ovx at 12wks. Therapies were initiated at 16wks of age including PTH only, alendronate (ALN) only, raloxifene (RAL) only, zolendronate (ZOL) only, and the combination treatments PTH+ALN, PTH+RAL, PTH+ZOL. The vehicle control (VEH) was comprised of all the carriers used in the study. At 24wks of age (8wks treatment) mice were euthanized for analysis.

Doses:

- PTH: 30µg/kg/d
- ALN: 1µg/kg/d
- ZOL: 80µg/kg 1x dose:
- RAL: 1mg/kg/d

Doses of anti-resorptive agents are based on human clinical doses.

The standard ALN dose for treatment of osteoporosis typically given as either a daily (10mg) or weekly (70mg) dose. Based on a 60kg individual this is roughly 1.17 mg/kg/week. The human dose is oral and has an estimated bioavailability of around 0.6%, meaning that the absorbed dose is roughly 0.007 mg/kg/week (or 7 µg/kg/week). We dosed via injection, assuming 100% absorption, thus we delivered ALN at 1µg/kg/day[4-6].

RAL is typically given as a 60 mg daily dose. Based on a 60 kg patient, the dose would be 1 mg/kg/day. The assumption is 100% absorption thus the full dose is used when injecting[5, 7].

ZOL is typically given yearly at a dose of 5 mg. Based on a 60 kg patient, the dose is 0.083 mg/kg. Our single dose of 80 µg/kg approximates this amount[8, 9].

SUMMARY OF KEY FINDINGS FOR YEAR 2:

We have generated an extensive data set from the combination experiments and although the analysis is not complete the preliminary statistical evaluation provides an exciting emerging picture, which is presented here. Note that Nmp4 targets cancellous bone thus we will specify what skeletal compartments comprise the endpoint under consideration.

- The PTH+RAL combination therapy typically added more bone to both WT and *Nmp4*$^{-/-}$ ovx skeletons than the other treatments (whole body [WB] and spine BMD and femoral and spine BV/TV)
- The PTH+RAL treatment was the most effective at out-performing the PTH mono-therapy in both genotypes (whole body [WB] and spine BMD and femoral and spine BV/TV)
- Disabling Nmp4 significantly improved the efficacy of the PTH+RAL therapy but typically had little to no effect on the PTH+bisphosphonate treatments (whole body [WB] and spine BMD and femoral and spine BV/TV)
- The anti-catabolic mono-therapies, as expected, added only a modest amount of bone to the ovx WT and *Nmp4*$^{-/-}$ skeletons, compared to PTH mono-therapy. Disabling Nmp4 did not enhance the response of the ovx skeleton to the anti-catabolic mono-therapies.
- The *Nmp4*$^{-/-}$ PTH+RAL treatment group exhibited the largest pool of bone marrow osteoprogenitors [identified by $CD45^{-}/CD105^{+}/Nestin^{+}/CD146^{+}$].
- Raloxifene enhanced the mineralization capacity of WT mesenchymal stem/progenitor cells (MSPCs) but did not further augment the precocious *Nmp4*$^{-/-}$ MSPC mineralization.

STATSTICAL TREATMENT:

We have tested 7 therapies and a vehicle control using two genotypes of mice yielding a total of 16 treatment groups. To date we have used the following statistical methods:

- Raw data:
  - **μ**CT trabecular data: Cancellous bone is the primary target of Nmp4. To determine if there was a genotype x treatment interaction for any of the combination treatments we performed a series of 2W ANOVAs using Genotype and Treatment (veh vs PTH+anti-catabolic; PTH vs PTH+anti-catabolic) as the independent variables and femoral BV/TV, femoral Tb N and Tb Th, or spine BV/TV as the dependent endpoints. We set $p<0.01$ to avoid Type I errors. Similarly, to determine if the combination treatments provided a synergistic effect over their respective mono-therapies we performed a series of 2W ANOVAs using PTH and the anti-catabolic treatments as the independent variables.
  - **μ**CT cortical data: There was no indication of a genotype x treatment interaction therefore the raw cortical data was treated with a 1W ANOVA followed by a Tukey-Kramer HSD post hoc test to compare means.
- % Change BMD data: For these data we used the Kruskal–Wallis 1W ANOVA by ranks for non-parametric data.
- FACS data: The raw FACS data is reported as % of total cells analyzed. We used the Kruskal–Wallis 1W ANOVA followed by nonparametric comparisons with control using the Dunn method for joint ranking.

KEY FINDING: *Mice receiving PTH+RAL and PTH+ZOL showed the largest BMD increase after ovx.*

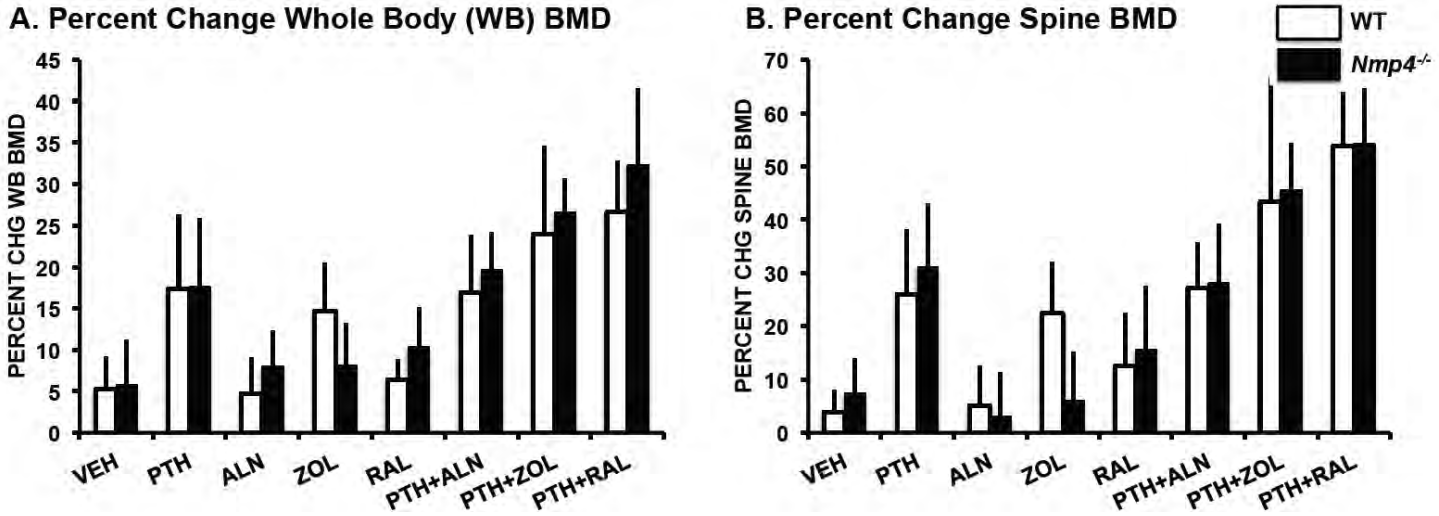

Figure 1: Percent change [A] whole body bone mineral density (WB BMD) (16wks to 24wks of age) and [B] spine BMD (L3-L5) for WT and *Nmp4*$^{-/-}$ [KO] mice under various treatment groups. The PTH+RAL and PTH+ZOL stimulated the largest changes in WB and spine BMD. The data were analyzed using the Kruskal-Wallis test for non-parametric statistics ($p < 0.0001$) followed by a comparison for all pairs using Dunn method for joint ranking post hoc test. The data represents average±SD, n=7-12 mice/group.

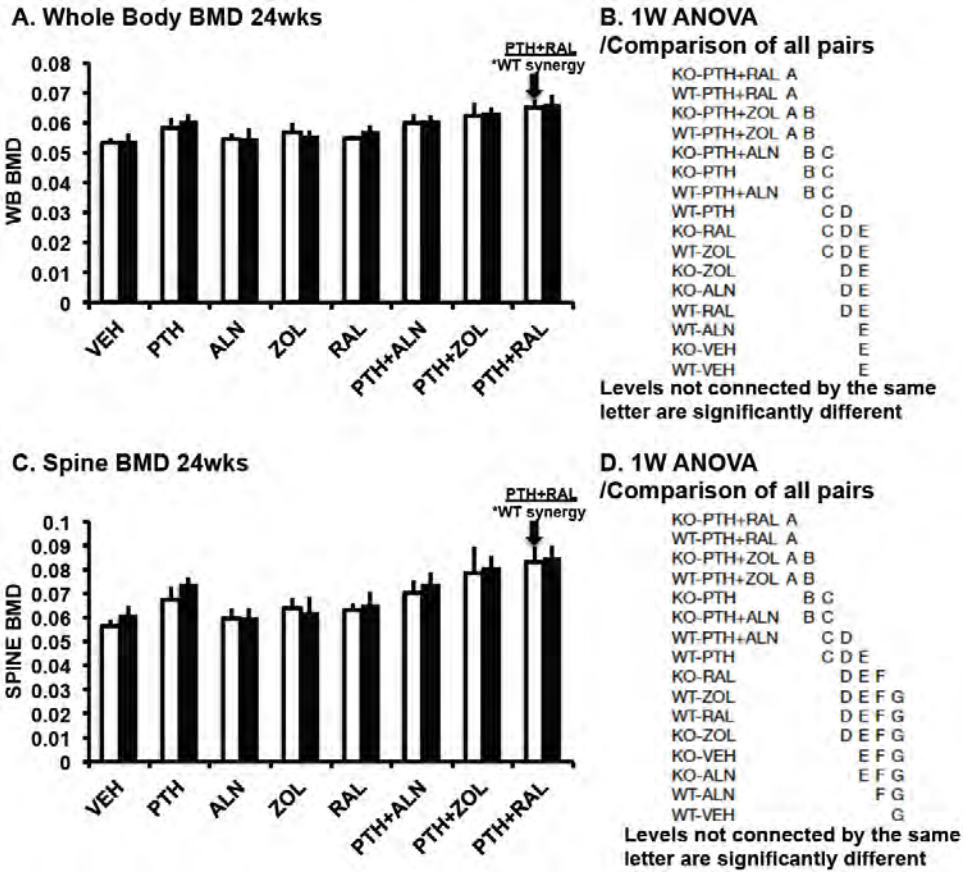

Figure 2: [A] WB BMD (24wks of age) and [B] spine BMD (L3-L5) for WT and *Nmp4*$^{-/-}$ [KO] mice under various treatment groups. [C], [D] The data were analyzed using a 1W ANOVA followed by a comparison for all pairs using a Tukey-Kramer ($p<0.05$). The mice from the PTH+RAL (and PTH+ZOL) exhibited the largest WB and spine BMDs. The WT mice exhibited a synergistic response to the PTH+RAL combination therapy (see Table 1, next page). The data represents average±SD, n=7-12 mice/group.

Figure 1 illustrates the percent change of WB and spine BMD of the WT and *Nmp4*$^{-/-}$ mice from the 16 different treatment groups. The use of the Kruskal-Wallis test for non-parametric statistics showed a significant difference between the groups ($p<0.0001$). The use of a Dunn's post-hoc test comparing all pair-wise comparisons indicated that the PTH+RAL and PTH+ZOL groups were distinct in that they were different from most of the other treatments (statistical output not shown in graphs for simplicity).

Figure 2 compares the raw WB and spine BMD of the different treatment groups at the end of the experiment (8wks of therapy, 24wks of age). The use of a 1W ANOVA followed by a Tukey-Kramer HSD shows that the PTH+RAL and the PTH+ZOL treatments were the most effective at adding bone after ovx.

These results raise the question as to whether any of the combination treatments show a synergistic response at the levels of WB and spine BMD.

KEY FINDING: *The PTH+RAL therapy was the only treatment to exhibit a synergistic effect on total WB and spine BMD*

TABLE 1

WHOLE BODY BMD			
THERAPY	p-value PTH Treatment	p-value Anti-catabolic Treatment	p-value PTH x Anti-catabolic interaction
PTH+ALN [WT mice]	<0.0001	0.04	0.65
PTH+ALN [*Nmp4*$^{-/-}$ mice]	<0.0001	0.50	0.64
PTH+RAL [WT mice]	<0.0001	<0.0001	**0.0007**
PTH+RAL [*Nmp4*$^{-/-}$ mice]	<0.0001	<0.0001	0.1025
PTH+ZOL [WT mice]	<0.0001	0.0003	0.8258
PTH+ZOL [*Nmp4*$^{-/-}$ mice]	<0.0001	0.0023	0.3662
SPINE BMD (L3-L5)			
THERAPY	p-value PTH Treatment	p-value Anti-catabolic Treatment	p-value PTH x Anti-catabolic interaction
PTH+ALN [WT mice]	<0.0001	0.02	0.94
PTH+ALN [*Nmp4*$^{-/-}$ mice]	<0.0001	0.69	0.79
PTH+RAL [WT mice]	<0.0001	<0.0001	**0.003**
PTH+RAL [*Nmp4*$^{-/-}$ mice]	<0.0001	<0.0001	0.0175
PTH+ZOL [WT mice]	<0.0001	<0.0001	0.3807
PTH+ZOL [*Nmp4*$^{-/-}$ mice]	<0.0001	0.0101	0.0561

To determine if the combination treatments provided a synergistic effect over their respective mono-therapies we performed a series of 2W ANOVAs using PTH and the anti-catabolic treatments as the independent variables and either WB BMD or spine BMD (at 8wks of therapy, 24wks of age) as the dependent endpoint (see Table 1). Note that these analyses used the actual BMD value and not the % change. We set $p<0.01$ to avoid Type I errors. Only the PTH+RAL combination therapy yielded a synergistic effect for the WT (WB BMD/spine BMD). The *Nmp4*$^{-/-}$ showed a nearly significant synergistic effect for spine BMD.

The PTH+ bisphosphonate therapies (ALN and ZOL) did not act synergistically on either the WT and *Nmp4*$^{-/-}$ mice. ALN induced the weakest response in both genotypes for these endpoints (% change BMD and BMD, Figures, 1, 2, and Table 1).

Potential interpretations of some of the data:

- WB BMD is primarily cortical bone (Nmp4 non-target) whereas the spine BMD (L3-L5) has a comparatively larger proportion of cancellous bone (Nmp4 target). This may explain the lack of a synergistic effect for the *Nmp4*$^{-/-}$ mice for the WB BMD parameter but near synergistic effect for spine BMD.
- The difference in the response to ALN mono-therapy between WT and *Nmp4*$^{-/-}$ mice is consistent with our previous observation that null osteoclasts are more active than WT cells[2]. These differences may be overwhelmed in the presence of the stronger bisphosphonate ZOL.

KEY FINDING: *Disabling Nmp4 enhanced PTH+RAL-induced increases in femoral BV/TV and increased the synergistic action of PTH with RAL and ZOL in both the femur and spine.*

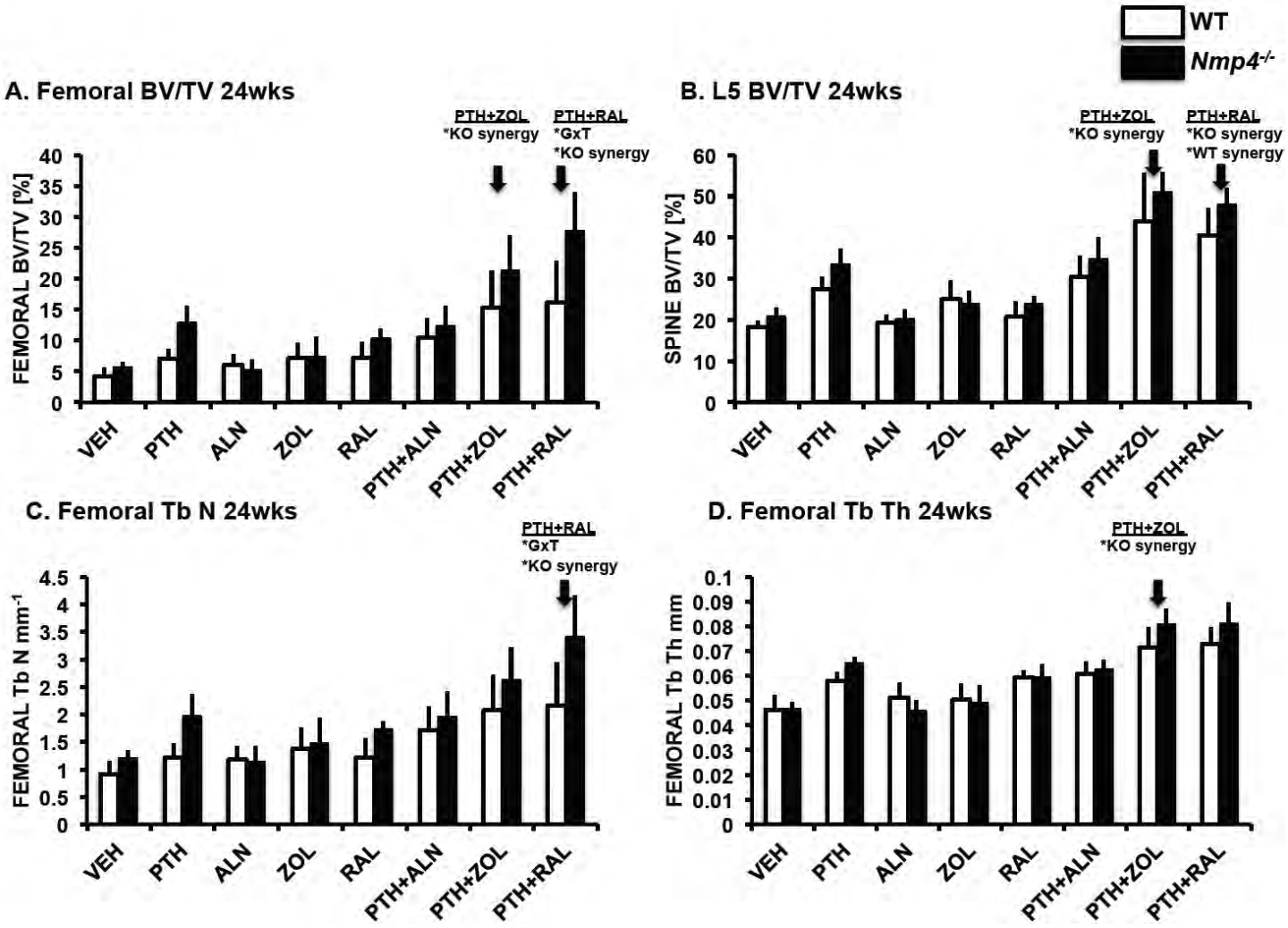

Figure 3: [A] Femoral BV/TV (24wks of age); [B] spine BV/TV (L5) [C] Femoral trabecular number (Tb N); and [D] Femoral trabecular thickness (Tb Th) for WT and *Nmp4*$^{-/-}$ mice under various treatment groups. The data were analyzed using a series of 2W ANOVAs. The PTH combination treatment groups were compared for genotype x treatment interactions (G x T). They were also compared for treatment synergy (PTH x anti-catabolic) for the WT and *Nmp4*$^{-/-}$ mice separately. The detailed results of the statistical analyses are shown in Tables 2-4. There was a G x T interaction in the PTH+RAL therapy (femoral BV/TV and Tb N, veh vs PTH+RAL). The *Nmp4*$^{-/-}$ mice exhibited a synergistic response to the PTH+RAL therapy (femoral BV/TV, femoral Tb N, L5 BV/TV) and to the PTH+ZOL therapy (femoral BV/TV, femoral Tb Th, spine BV/TV). The WT mice showed a synergistic response to PTH+RAL in the spine. The data represents average±SD, n=7-12 mice/group.

Table 2: FEMUR BV/TV

Therapy	*Independent variable #1*	*Independent variable #2*	*Interaction var#1 x var#2*
PTH+RAL: Gene x Treat[a]	Genotype: p<0.0001	Treatment: p<0.0001	G x T: p=0.0010
PTH+RAL: Gene x Treat[b]	Genotype: p<0.0001	Treatment: p<0.0001	G x T: p=0.0485
PTH+RAL: KO Synergy	PTH treatment: p<0.0001	RAL treatment: p<0.0001	PTH x RAL: p=0.0010
PTH+RAL: WT Synergy	PTH treatment: p<0.0001	RAL treatment: p<0.0001	PTH x RAL: p=0.0139
PTH+ZOL: Gene x Treat[a]	Genotype: p=0.0059	Treatment: p<0.0001	G x T: p=0.0760
PTH+ZOL: Gene x Treat[b]	Genotype: p=0.0059	Treatment: p<0.0001	G x T: p=0.9101
PTH+ZOL: KO Synergy	PTH treatment: p<0.0001	ZOL treatment: p<0.0001	PTH x ZOL: p=0.0067
PTH+ZOL: WT Synergy	PTH treatment: p<0.0001	ZOL treatment: p<0.0001	PTH x ZOL: p=0.0188
PTH+ALN: Gene x Treat[a]	Genotype: p=0.0295	Treatment: p<0.0001	G x T: p=0.7344
PTH+ALN: Gene x Treat[b]	Genotype: p<0.0001	Treatment: p=0.0779	G x T: p=0.0197
PTH+ALN: KO Synergy	PTH treatment: p<0.0001	ALN treatment: p=0.5540	PTH x ALN: p=0.9148
PTH+ALN: WT Synergy	PTH treatment: p<0.0001	ALN treatment: p=0.0001	PTH x ALN: p=0.1944

a: Genotype x treatment comparing vehicle-treated mice to PTH+ anti-catabolic therapy
b: Genotype x treatment comparing PTH-treated mice to PTH+ anti-catabolic therapy

Table 3: FEMUR Tb N and Tb Th

Therapy	*Independent variable #1*	*Independent variable #2*	*Interaction var#1 x var#2*
Femur Tb N			
PTH+RAL: Gene x Treat[a]	Genotype: p<0.0001	Treatment: p<0.0001	G x T: p=0.0090
PTH+RAL: Gene x Treat[b]	Genotype: p<0.0001	Treatment: p<0.0001	G x T: p=0.1641
PTH+RAL: KO Synergy	PTH treatment: p<0.0001	RAL treatment: p<0.0001	PTH x RAL: p<0.0001
PTH+RAL: WT Synergy	PTH treatment: p<0.0001	RAL treatment: p<0.0001	PTH x RAL: p=0.0313
PTH+ZOL: Gene x Treat[a]	Genotype: p=0.0046	Treatment: p<0.0001	G x T: p=0.4041
PTH+ZOL: Gene x Treat[b]	Genotype: p<0.0001	Treatment: p<0.0001	G x T: p=0.4838
PTH+ZOL: KO Synergy	PTH treatment: p<0.0001	ZOL treatment: p=0.0030	PTH x ZOL: p=0.1691
PTH+ZOL: WT Synergy	PTH treatment: p<0.0001	ZOL treatment: p=0.0004	PTH x ZOL: p=0.1415
Femur Tb Th			
PTH+RAL: Gene x Treat[a]	Genotype: p=0.0337	Treatment: p<0.0001	G x T: p=0.0422
PTH+RAL: Gene x Treat[b]	Genotype: p<0.0001	Treatment: p<0.0001	G x T: p=0.7730
PTH+RAL: KO Synergy	PTH treatment: p<0.0001	RAL treatment: p<0.0001	PTH x RAL: p=0.3820
PTH+RAL: WT Synergy	PTH treatment: p<0.0001	RAL treatment: p<0.0001	PTH x RAL: p=0.6140
PTH+ZOL: Gene x Treat[a]	Genotype: p=0.0127	Treatment: p<0.0001	G x T: p=0.0166
PTH+ZOL: Gene x Treat[b]	Genotype: p<0.0001	Treatment: p<0.0001	G x T: p=0.5458
PTH+ZOL: KO Synergy	PTH treatment: p<0.0001	ZOL treatment: p<0.0001	PTH x ZOL: p=0.00o2
PTH+ZOL: WT Synergy	PTH treatment: p<0.0001	ZOL treatment: p<0.0001	PTH x ZOL: p=0.0172

a: Genotype x treatment comparing vehicle-treated mice to PTH+ anti-catabolic therapy
b: Genotype x treatment comparing PTH-treated mice to PTH+ anti-catabolic therapy

Table 4: L5 BV/TV

Therapy	*Independent variable #1*	*Independent variable #2*	*Interaction var#1 x var#2*
PTH+RAL: Gene x Treat[a]	Genotype: p=0.0002	Treatment: p<0.0001	G x T: p=0.0.0417
PTH+RAL: Gene x Treat[b]	Genotype: p<0.0001	Treatment: p<0.0001	G x T: p=0.5999
PTH+RAL: KO Synergy	PTH treatment: p<0.0001	RAL treatment: p<0.0001	PTH x RAL: p<0.0001
PTH+RAL: WT Synergy	PTH treatment: p<0.0001	RAL treatment: p<0.0001	PTH x RAL: p=0.0002
PTH+ZOL: Gene x Treat[a]	Genotype: p=0.0205	Treatment: p<0.0001	G x T: p=0.2534
PTH+ZOL: Gene x Treat[b]	Genotype: p=0.0026	Treatment: p<0.0001	G x T: p=0.8175
PTH+ZOL: KO Synergy	PTH treatment: p<0.0001	ZOL treatment: p<0.0001	PTH x ZOL: p<0.0001
PTH+ZOL: WT Synergy	PTH treatment: p<0.0001	ZOL treatment: p<0.0001	PTH x ZOL: p=0.0235
PTH+ALN: Gene x Treat[a]	Genotype: p=0.0045	Treatment: p<0.0001	G x T: p=0.4050
PTH+ALN: Gene x Treat[b]	Genotype: p=0.0002	Treatment: p=0.1281	G x T: p=0.5125
PTH+ALN: KO Synergy	PTH treatment: p<0.0001	ALN treatment: p=0.8438	PTH x ALN: p=0.3830
PTH+ALN: WT Synergy	PTH treatment: p<0.0001	ALN treatment: p=0.0472	PTH x ALN: p=0.3131

a: Genotype x treatment comparing vehicle-treated mice to PTH+ anti-catabolic therapy
b: Genotype x treatment comparing PTH-treated mice to PTH+ anti-catabolic therapy

- To determine if the combination treatments provided a synergistic effect over their respective mono-therapies we performed a series of 2W ANOVAs using PTH and the anti-catabolic treatments as the independent variables and Femoral BV/TV (Table 2), Femoral Tb N and Tb Th (Table 3), or Spine BV/TV (Table 4) as the dependent endpoints (8wks of therapy, 24wks of age). We set p<0.01 to avoid Type I errors.
  - *Nmp4*$^{-/-}$ mice show a synergistic response to PTH+RAL (Femoral BV/TV, Femoral Tb N, and Spine BV/TV)
  - The WT mice show a synergistic response to PTH+RAL (Spine BV/TV)
  - *Nmp4*$^{-/-}$ mice show a synergistic response to PTH+ZOL (Femoral BV/TV, Femoral Tb Th, and Spine BV/TV)
- To determine if there was a genotype x treatment interaction for any of the combination treatments we performed a series of 2W ANOVAs using Genotype and Treatment (veh vs PTH+anti-catabolic; PTH vs PTH+anti-catabolic) as the independent variables and Femoral BV/TV (Table 2), Femoral Tb N and Tb Th (Table 3), or Spine BV/TV (Table 4) as the dependent endpoints. We set p<0.01 to avoid Type I errors.
  - Genotype x treatment interactions were observed for femoral BV/TV and femoral Tb N under the PTH+RAL therapy when compared to the vehicle-treated mice
  - No genotype x treatment interactions were obtained for the PTH+ZOL therapy

KEY FINDING: *Disabling Nmp4 enhanced the distinction between the PTH+RAL-induced increase in* cortical bone area *and the other combination treatments*

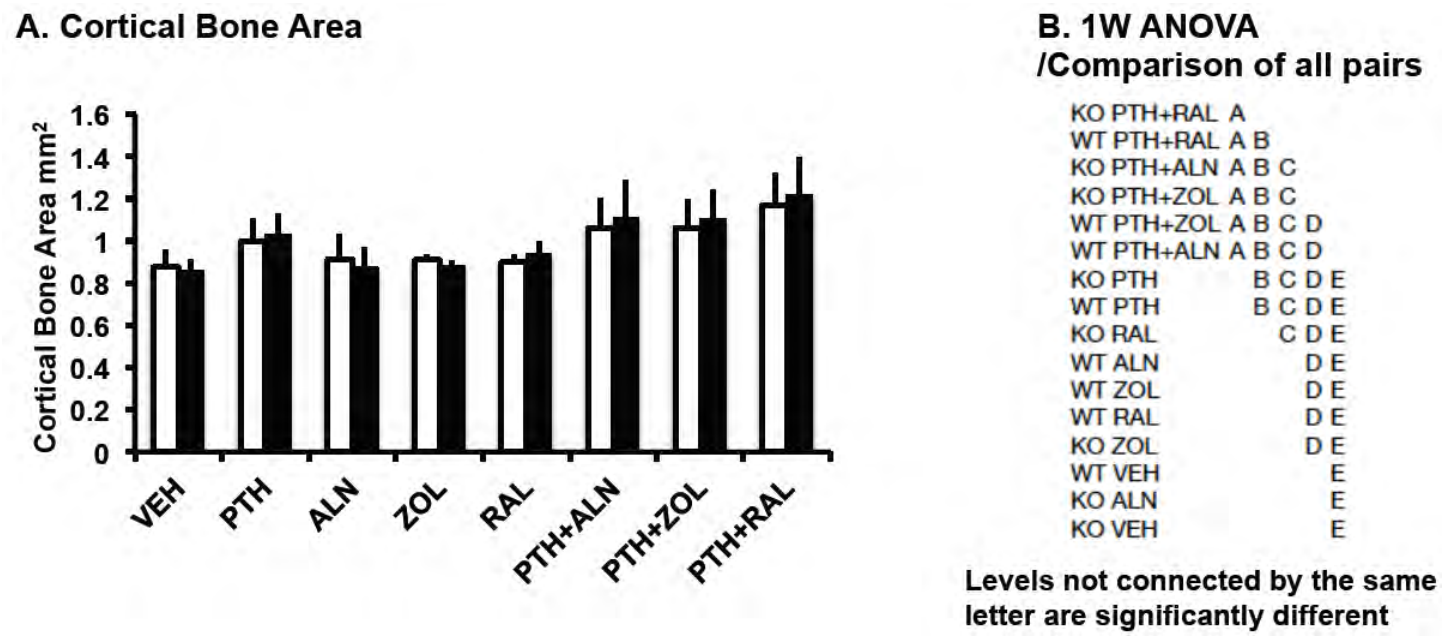

Figure 4: [A] Femoral cortical bone area of ovx WT and *Nmp4*$^{-/-}$ mice at 24wks of age, 8wks of treatment. Statistical analysis included a 1W ANOVA ($p < 0.0001$) followed by a Tukey-Kramer HSD post-hoc test. Data are average ± SD, number of mice/experimental group = 9-13.

We have previously shown that disabling Nmp4 enhances the response of trabecular bone to PTH without compromising the cortical compartment[3]. This is consistent with our observation that *Nmp4*$^{-/-}$ mice from the PTH+RAL therpay group had the largest cortical bone area (Figures 4A and 4B). However, there was no evidence of synergy in this or any of the combination treatments for this parameter nor was there a genotype x treatment effect.

KEY FINDING: *Nmp4*$^{-/-}$ *mice under the PTH+RAL combination therapy harbored more bone marrow osteoprogenitors than mice under the other treatments*

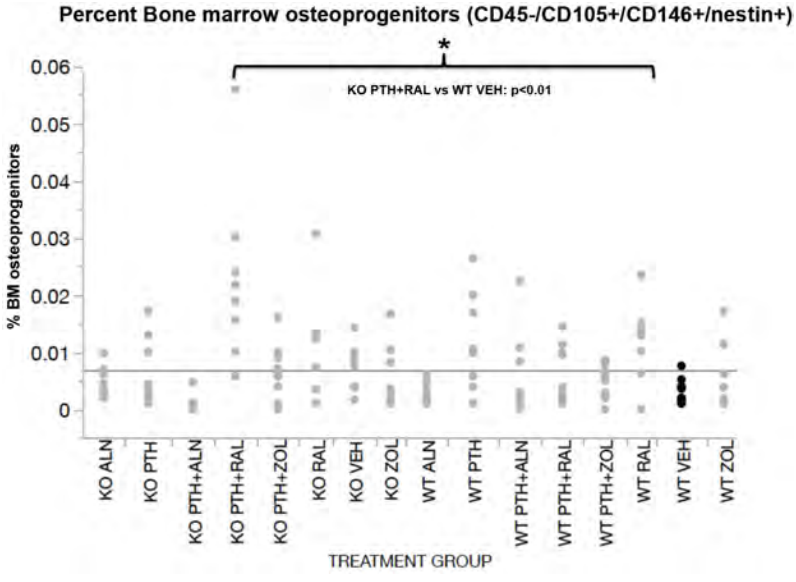

Figure 5: Percent bone marrow (BM) osteoprogenitors as evaluated by CD45^{-}/CD105^{+}/CD146^{+}/Nestin^{+} cells. Statistical analysis used a non-parametric Kruskal-Wallis test followed by a Dunn's post hoc. See text for details.

We have reported that healthy, non-ovariectomized *Nmp4*$^{-/-}$ mice exhibit an increased number of bone marrow (BM) osteoprogenitor cells irrespective of treatment[1]. We also demonstrated that the percentage of BM CD45^{-}/CD105^{+}/CD146^{+}/Nestin^{+} cells paralleled the number of CFU-F$^{alk\ phos+}$ cells in our mice[1]. During the first year of this DOD study we showed that this enhanced number of *Nmp4*$^{-/-}$ osteoprogenitors wanes 12wks post-ovariectomy. Here we report that this increased pool of osteoprogenitors is maintained 12wks post-op in *null* mice under the PTH+RAL therapy (see Figure 5). A Kruskal-Wallis analysis with Dunn's post hoc test comparing the % BM osteoprogenitors in the WT-VEH cohort with all the other groups show that the *Nmp4*$^{-/-}$ mice under the PTH+RAL therapy cohort are the only treatment group that exhibit a significant difference from the control.

KEY FINDING: *Raloxifene enhanced WT mesenchymal stem/progenitor cell (MSPC) mineralization*
We have shown that *Nmp4*$^{-/-}$ expanded MSPCs exhibit a precocious mineralization (see Appendix Manuscript Number ME-14-1406R1). The null cells begin to mineralize by Days 4-7 in culture whereas the WT cells have a very weak mineralization response. There are a number of studies showing that osteoprogenitors and osteoblasts respond directly to raloxifene[10-15]. It has also been demonstrated that raloxifene has a mineralization-promoting effect on female mesenchymal stem cells[13]. As part of Subtask 6.2: Phenotype analyses of WT and *Nmp4*$^{-/-}$ mesenchymal stem progenitor cells (MSPCs) we addressed whether raloxifene enhances the mineralization response to ex vivo cultures of expanded MSPCs. Figure 6 outlines the experimental protocol and results

These cells were derived from bone marrow mononuclear cells of male mice and expanded in MesenCult for 5 passages before use in osteogenic differentiation studies. Cells are used between passages 5 and 10[16].

- **Day 0: Seed 25K cells into each well in αMEM complete as shown in the Figure. [03/16/15]**
- **Day 2: Transfer cells to osteogenic medium [VEH3] or RAL+osteogenic medium.**
- **For RAL supplement, add 1.02µl of Raloxifene Secondary Stock to 1mls of complete medium. To VEH3 add 1.02µl RAL diluent/1ml of complete medium.**
- **Feed the cells every MWF.**
- **Day 5, Day 9, and Day 16, stain the cells with alizarin red.**

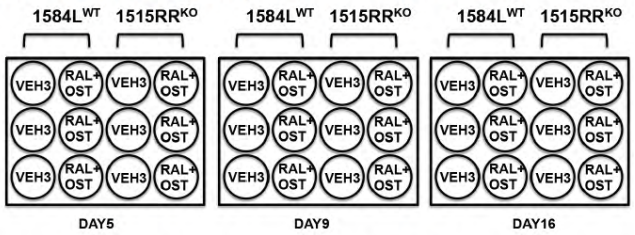

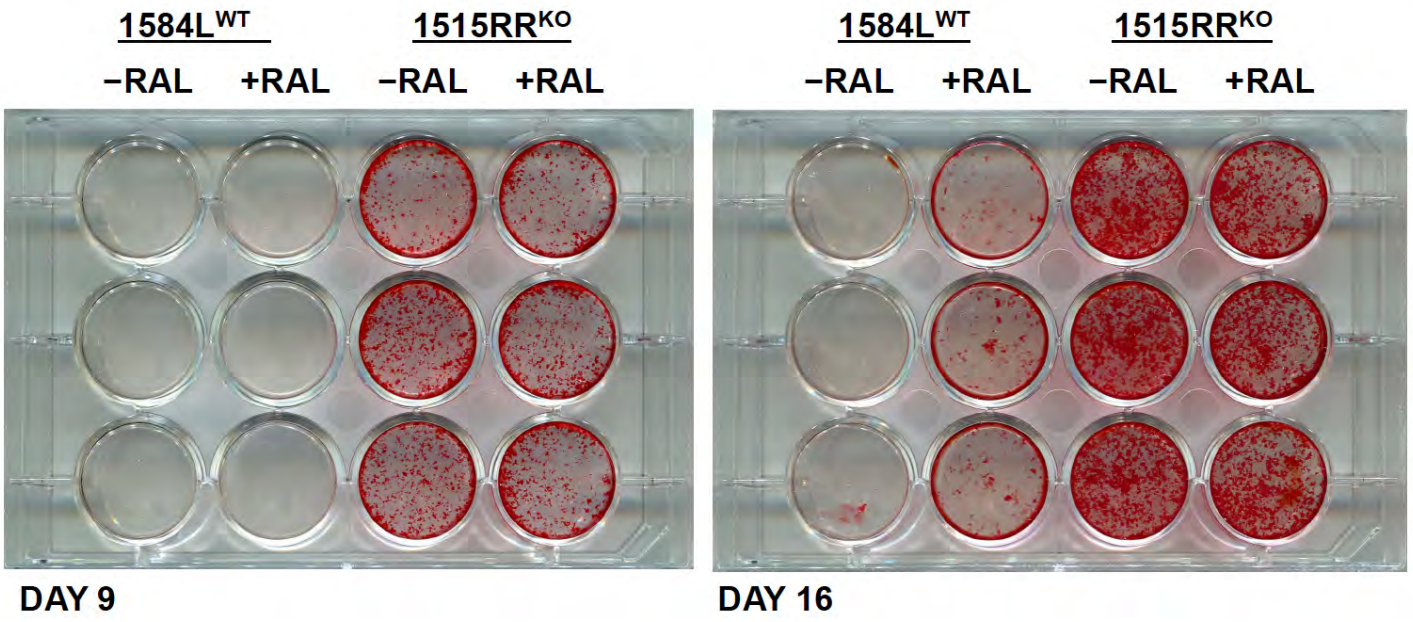

Figure 6: Raloxifene (100nM) clearly enhances WT MSPC mineralization. Whether it has an impact on the precocious mineralization of the *Nmp4*$^{-/-}$ (KO) remains to be determined. See text for details

We made the following observations from this single preliminary experiment:

- At Day 9, post-seeding the *Nmp4*$^{-/-}$ cells show a strong mineralization response in both the presence and absence of raloxifene (100nM), but the WT cells have little to no evidence of mineralization.
- At Day 16 the WT cells in raloxifene are showing a significant increase in mineralization compared to the cells in the absence of this drug
- The *Nmp4*$^{-/-}$ cells have mineralized to the point of obscuring any potential effect of the drug using this qualitative assay

ADDITIONAL RESEARCH ACTIVITIES:

Breeding of conditional knockout (KO) mice

The objectives for subtasks 4.2.a and 4.3.a are the breeding of *Nmp4$^{fl/fl}$ 3.6Col-Cre+*, *Nmp4$^{fl/fl}$ Cathepsin K-Cre+*, and *Nmp4$^{fl/fl}$-Cre–* mice. After breeding our germline transmission mice with the B6.129S4-Gt(ROSA)26Sortum2(FLP)Sor/J mice to remove the *Neo* gene we obtained evidence that the 5' floxed site was absent in the offspring. We are currently repeating these analyses and if necessary will devise a strategy for restoring this site.

KEY RESEARCH ACCOMPLISHMENTS FOR 2ND YEAR:

- KEY FINDING: *Mice receiving PTH+RAL and PTH+ZOL showed the largest BMD increase after ovx.*
- KEY FINDING: *The PTH+RAL therapy was the only treatment to exhibit a synergistic effect on total WB and spine BMD*
- KEY FINDING: *Disabling Nmp4 enhanced PTH+RAL-induced increases in femoral BV/TV and increased the synergistic action of PTH with RAL and ZOL in both the femur and spine.*
- KEY FINDING: *Disabling Nmp4 enhanced the distinction between the PTH+RAL-induced increase in cortical bone area and the other combination treatments*
- KEY FINDING: *Nmp4$^{-/-}$ mice under the PTH+RAL combination therapy harbored more bone marrow osteoprogenitors than mice under the other treatments*
- KEY FINDING: *Raloxifene enhanced WT mesenchymal stem/progenitor cell (MSPC) mineralization*

REPORTABLE OUTCOMES:

Abstract presentations in which the DOD support was acknowledged:

1. American Society for Bone & Mineral Research:
a. Date/location: October 9-12 2015, Seattle, WA
b. Title: Improving PTH/Raloxifene Combination Osteoporosis Therapy In a Preclinical Model
c. Authors: Yu Shao, Selene Hernandez-Buquer, Paul Childress, Dan Brown, Yongzheng He, Marta Alvarez, Feng-chun Yang, Stuart J Warden, Matthew R Allen, Joseph P Bidwell

Manuscripts submitted:

1. Molecular Endocrinology:
a. Date: July 8, 2015 [revised, see Appendix]
b. Title: Genome-wide mapping and interrogation of the Nmp4 anti-anabolic bone axis
c. Authors: Paul Childress, Keith Stayrook, Marta B Alvarez, Zhiping Wang, Yu Shao, Selene Hernandez-Buquer, Justin K Mack, Zachary R Grese, Yongzheng He, Daniel Horan, Fredrick M Pavalko, Stuart J Warden, Alexander G Robling, Feng-chun Yang, Matthew R Allen, Venkatesh Krishnan, Yunlong Liu, Joseph P Bidwell

Funding applied for based on work supported by this award:

Agency: NIH
Program: NIAMS
Title: Boosting Bone Anabolism and Bone Regeneration
Date submitted: 10/05/2014
Total costs & dates if funding awarded: $3,010,660 [03/01/2015-02/28/2020]

CONCLUSION: Key experimental discovery for 2nd year of DOD study

Our key discovery is that disabling Nmp4 significantly improves PTH+raloxifene combination therapy in an ovariectomized preclinical osteoporosis model but does not have a strong impact on PTH+bisphosphonate combination treatments

"So what?'

Women comprise the fastest growing group of the US veterans contributing to the looming osteoporosis epidemic within the veteran population. The Veterans Affairs (VA) health care system will be in high demand by female veterans of Operation Enduring Freedom and Operation Iraqi Freedom. PTH is the only FDA-approved anabolic osteoporosis therapy and adds significant amounts of bone to the osteoporotic skeleton. Therefore, this drug has the potential to restore the bone lost in a variety of VA clinical settings. However, a drawback to PTH use is that potency declines within 2 years and thus it is not suitable as a long-term therapy, which is problematic in treating a chronic degenerative disease. Clinicians have attempted to improve PTH therapy by adding an anti-catabolic (e.g. raloxifene or a bisphosphonate) to the treatment. This has not met with success. The present discovery supports our contention that disabling Nmp4 or some component of its pathway will unlock the block on PTH combination therapies and enhance/extend regeneration of osteoporotic bone in post-menopausal female veterans.

REFERENCES:

1. He Y, Childress P, Hood M Jr, Alvarez M, Kacena MA, Hanlon M, McKee B, Bidwell JP, Yang FC. 2013 Nmp4/CIZ suppresses the parathyroid hormone anabolic window by restricting mesenchymal stem cell and osteoprogenitor frequency. Stem Cells Dev. 22(3):492-500
2. Childress P, Philip BK, Robling AG, Bruzzaniti A, Kacena MA, Bivi N, Plotkin LI, Heller A, Bidwell JP. 2011 Nmp4/CIZ suppresses the response of bone to anabolic parathyroid hormone by regulating both osteoblasts and osteoclasts. Calcif Tissue Int. 89(1):74-89.
3. Robling AG, Childress P, Yu J, Cotte J, Heller A, Philip BK, Bidwell JP. 2009 Nmp4/CIZ suppresses parathyroid hormone-induced increases in trabecular bone. J Cell Physiol219(3):734-43.
4. Lui PP, Lee YW, Mok TY, Cheuk YC, Chan KM. 2013 Alendronate reduced peri-tunnel bone loss and enhanced tendon graft to bone tunnel healing in anterior cruciate ligament reconstruction. Eur Cell Mater. 25:78-96.
5. Ettinger B, San Martin J, Crans G, Pavo I. 2004 Differential effects of teriparatide on BMD after treatment with raloxifene or alendronate. J Bone Miner Res. 19(5):745-51.
6. Muschitz C, Kocijan R, Fahrleitner-Pammer A, Lung S, Resch H. 2013 Antiresorptives overlapping ongoing teriparatide treatment result in additional increases in bone mineral density. J Bone Miner Res. 28(1):196-205.
7. Cano A, Dapía S, Noguera I, Pineda B, Hermenegildo C, del Val R, Caeiro JR, García-Pérez MA. 2008 Comparative effects of 17beta-estradiol, raloxifene and genistein on bone 3D microarchitecture and volumetric bone mineral density in the ovariectomized mice. Osteoporos Int. 19(6):793-800.
8. Cosman F, Eriksen EF, Recknor C, Miller PD, Guañabens N, Kasperk C, Papanastasiou P, Readie A, Rao H, Gasser JA, Bucci-Rechtweg C, Boonen S. 2011 Effects of intravenous zoledronic acid plus subcutaneous teriparatide [rhPTH(1-34)] in postmenopausal osteoporosis. J Bone Miner Res. 26(3):503-11.
9. Sheng ZF1, Xu K, Ma YL, Liu JH, Dai RC, Zhang YH, Jiang YB, Liao EY. 2009 Zoledronate reverses mandibular bone loss in osteoprotegerin-deficient mice. Osteoporos Int. 20(1):151-9.
10. Viereck V, Gründker C, Blaschke S, Niederkleine B, Siggelkow H, Frosch KH, Raddatz D, Emons G, Hofbauer LC. 2003 Raloxifene concurrently stimulates osteoprotegerin and inhibits interleukin-6 production by human trabecular osteoblasts. J Clin Endocrinol Metab. 88(9):4206-13.
11. Taranta A, Brama M, Teti A, De luca V, Scandurra R, Spera G, Agnusdei D, Termine JD, Migliaccio S. 2002 The selective estrogen receptor modulator raloxifene regulates osteoclast and osteoblast activity in vitro. Bone. 30(2):368-76.
12. Lin Y, Liu LJ, Murray T, Sodek J, Rao L.J 2004 Effect of raloxifene and its interaction with human PTH on bone formation. Endocrinol Invest. 27(5):416-23.
13. Matsumori H, Hattori K, Ohgushi H, Dohi Y, Ueda Y, Shigematsu H, Satoh N, Yajima H, Takakura Y. 2009 Raloxifene: its ossification-promoting effect on female mesenchymal stem cells. J Orthop Sci. 14(5):640-5.
14. Giner M, Rios MJ, Montoya MJ, Vázquez MA, Miranda C, Pérez-Cano R. 2011 Alendronate and raloxifene affect the osteoprotegerin/RANKL system in human osteoblast primary cultures from patients with osteoporosis and osteoarthritis. Eur J Pharmacol. 15;650(2-3):682-7.

15. Somjen D, Katzburg S, Sharon O, Knoll E, Hendel D, Stern N. 2011 Sex specific response of cultured human bone cells to ERα and ERβ specific agonists by modulation of cell proliferation and creatine kinase specific activity. J Steroid Biochem Mol Biol. 125(3-5):226-30.
16. Wu X, Estwick SA, Chen S, Yu M, Ming W, Nebesio TD, Li Y, Yuan J, Kapur R, Ingram D, Yoder MC, Yang FC. 2006 Neurofibromin plays a critical role in modulating osteoblast differentiation of mesenchymal stem/progenitor cells. Hum Mol Genet. 15(19):2837-45.

APPENDIX:

Note: Full copy of the submitted manuscript to MOL ENDO that includes details for materials and methods used to generate the data described is appended.

Molecular Endocrinology

Genome-wide mapping and interrogation of the Nmp4 anti-anabolic bone axis

--Manuscript Draft--

Manuscript Number:	ME-14-1406R1
Article Type:	Research Paper
Full Title:	Genome-wide mapping and interrogation of the Nmp4 anti-anabolic bone axis
Order of Authors:	Paul Childress, MS
	Ketih Stayrook, BS
	Marta B Alvarez, DDS, PhD
	Zhiping Wang, PhD
	Yu Shao, BS
	Selene Hernandez-Buquer, MS
	Justin K Mack, BS
	Zachary R Grese, BS
	Yongzheng He, PhD
	Daniel Horan, BS
	Fredrick M Pavalko, PhD
	Stuart J Warden, PhD
	Alexander G Robling, PhD
	Feng-chun Yang, MD, PhD
	Matthew R Allen, PhD
	Venkatesh Krishnan, PhD
	Yunlong Liu, PhD
	Joseph Bidwell, PhD
Author Comments:	Disclosure statement: PC, MBA, ZW, YS, SHB, YH, DH, FMP, AGR, SJW, FCY, YL have nothing to disclose. Eli Lilly and Company has awarded research funds to JPB and MRA. Eli Lilly and Company funded part of this work. VK is an employee of Eli Lilly & Co and owns stock in this company. KS, JKM, and ZRG are employees of Eli Lilly & Co
Abstract:	Parathyroid hormone (PTH) is an osteoanabolic for treating osteoporosis but its potency wanes. Disabling the transcription factor Nmp4 in healthy, ovary-intact mice enhances bone response to PTH and BMP2 and protects from unloading-induced osteopenia. These Nmp4-/- mice exhibit expanded bone marrow (BM) populations of osteoprogenitors and supporting CD8+ T cells. To determine whether the Nmp4-/- phenotype persists in an osteoporosis model we compared PTH response in ovariectomized (ovx) wild type (WT) and Nmp4-/- mice. To identify potential Nmp4 target genes we performed bioinformatic/pathway profiling on Nmp4 ChIP-seq data. Mice (12wks) were ovx or sham-operated 4wks before the initiation of PTH therapy. Skeletal phenotype analysis included μCT, histomorphometry, serum profiles, FACS sorting and the growth/mineralization of cultured WT and Nmp4-/- BM mesenchymal stem progenitor cells (MSPCs). ChIP-seq data were derived using MC3T3-E1 pre-osteoblasts, murine embryonic stem cells, and two blood cell lines. Ovx Nmp4-/- mice exhibited an improved response to PTH coupled with elevated numbers of osteoprogenitors and CD8+ T cells, but were not protected from ovx-induced bone loss. Cultured Nmp4-/- MSPCs displayed enhanced proliferation and accelerated mineralization. ChIP-seq/gene ontology analyses identified target genes likely under Nmp4 control as enriched for negative regulators of biosynthetic processes. Interrogation of mRNA transcripts in non-differentiating and osteogenic differentiating

	WT and Nmp4-/- MSPCs was performed on 90 Nmp4 target genes and differentiation markers. These data suggest that Nmp4 suppresses bone anabolism, in part, by regulating insulin-like growth factor binding protein expression. Changes in Nmp4 status may lead to improvements in osteoprogenitor response to therapeutic cues.
Additional Information:	
Question	**Response**
Do you confirm that your submission meets the standards described in the Instructions to Authors, Cell Line Authentication? as follow-up to "CELL LINES: Does your submission include cell lines? (If you have questions, please contact the editorial staff at molendo@endocrine.org) "	Yes
FUNDING SOURCES: Please list all sources of funding for this manuscript. This should be included on the title page of your manuscript as well. If no funding, then respond NOT APPLICABLE.	DOD and Eli Lilly
STEROID HORMONE ASSAYS: Does your submission include steroid hormone assays? (If you have questions, please contact the editorial staff at molendo@endocrine.org)	No
CELL LINES: Does your submission include cell lines? (If you have questions, please contact the editorial staff at molendo@endocrine.org)	No

Cover Letter

INDIANA UNIVERSITY
DEPARTMENT OF ANATOMY AND CELL BIOLOGY
School of Medicine

07/06/15
Stephen R. Hammes, M.D., Ph.D.
Editor-in-Chief, Molecular Endocrinology

Dear Dr Hammes;
We are pleased to submit our revised manuscript Ref.: Ms. No. ME-14-1406 "*Genome-wide mapping and interrogation of the Nmp4 anti-anabolic bone axis*" for your consideration. We thank the reviewers for their insightful and helpful comments. We have made a substantial effort to comprehensively address their concerns (see separate file RESPONSE TO REVIEWERS). This includes the addition of a study to evaluate gene expression in non-differentiating and in osteogenic-differentiating WT and *Nmp4*$^{-/-}$ MPSCs during a 16-day culture period at five time-points using a custom Taqman Low-Density Array system designed for *96 genes* including Nmp4 target genes identified by our genome-wide ChIP-seq profiling, non-target genes that drive osteogenic differentiation and marker genes of this process. These results provide considerable new information on how Nmp4 may suppress the anabolic response to PTH. Additionally, these new data strengthen our assertion that further interrogation of the Nmp4 anti-anabolic network will identify pharmacologically accessible pathways for adding new bone to the old skeleton. The supplemental files are intended for online publication. Note that the revised/new text is in red font with a **black line** in the right margin. Finally, there is no requirement for a PDB number and we are not reporting a new structure or compounds.

Sincerely,

Joseph Bidwell
Professor

Medical Science Building 5035 635 Barnhill Drive Indianapolis, IN 46202-5120 (317) 274-7494 tel (317) 278-2040 fax

RESPONSE TO REVIEWERS

Ms. No. ME-14-1406 "*Genome-wide mapping and interrogation of the Nmp4 anti-anabolic bone axis*"

We thank the reviewers for the helpful and insightful comments. We believe that following their advice has made this a more powerful and informative study. Please note that the revised/new text is in red font with a **black line** in the right margin.

Comment: The phenotypic studies in the current work are merely confirmative

Response: The reviewers raise an important issue and we clearly failed to emphasize the significance of the questions addressed by these experiments.

- Our data are a key and obligatory *preclinical extension* of the *Nmp4*$^{-/-}$ phenotype. An overriding objective of the Nmp4 studies is to determine if this network of pathways harbor potential targets for treating postmenopausal osteoporosis. Therefore we addressed two central phenotype questions in the present study:
  (i) Does disabling Nmp4 protect mice from ovariectomy-induced bone loss as it does in disuse-induced osteopenia?
  (ii) Does the exaggerated response to PTH therapy in *Nmp4*$^{-/-}$ mice persist after ovariectomy?

Our findings that the null mice are not protected from ovarectomy-induced bone loss yet maintain the amplified response to PTH therapy is an important discovery. These data begin to demarcate the potential Nmp4-based therapeutic strategies. We have revised both the Introduction and Discussion to emphasize these points.

Comment: If Nmp4 suppresses Igf1 and Bmp2, and cellular synthetic process, why there is no difference between WT vs. *Nmp4*$^{-/-}$ mice under either basal or OVX-challenged conditions? Why is there only enhanced response to PTH treatment?

Response: The reviewer raises a significant question about features of the *Nmp4*$^{-/-}$ phenomenon. Although a definitive answer requires further study, we address this query in the Discussion. The key concepts of our response follow:

- The Nmp4 phenomenon differs from the results of recent clinical trials in which neutralizing sclerostin, an inhibitor of the Wnt signaling pathway and osteoblast differentiation, significantly increases baseline bone mineral density.
- Apparently disabling Nmp4 is not sufficient for driving excess bone formation but instead enlarges the number of osteoprogenitors that can be recruited once activated by an anabolic cue. The downregulation of *Cxcl12* in the *Nmp4*$^{-/-}$ cells may contribute to the increased number of CFU-F$^{alk\ phos+}$ osteoprogenitors (see low-density array data below).
- Once activated by an anabolic cue, e.g. PTH, the *Nmp4*$^{-/-}$ cells produce autocrine/paracrine factors that enhance the replication and differentiation of neighboring osteoprogenitors, a key early event driving the PTH anabolic response (see below).
- The occasionally observed elevated trabecular volume in untreated *Nmp4*$^{-/-}$ mice may be due to the sporadic local release of growth factors, e.g., Igf1 and/or Bmp2.
- However exogenous pharmacological doses of PTH provide a stronger stimulus for triggering the response leading to an enhanced bone formation.
- The enhanced mineralization in *Nmp4*$^{-/-}$ MSPC culture is only observed upon the addition of the anabolic cue dexamethasone, an Nmp4 target pathway.

Comment: Table 1, why didn't the CTX bone resorption marker and P1NP bone formation marker show significant differences between the pre-op and post-op group, even in WT mice?

Response:

- Surgery-induced changes in serum bone markers took longer than 4wks to be detected. Our mice showed the appropriate ovx-induced significant increases in body weight, decreases in uterine weight, and significant bone loss during the first 4wks post-op. Nevertheless, our study was not a longitudinal design in which repeated measures on each animal at numerous time points were obtained, thus the typical small increases in serum CTX seen in other ovx mouse studies may have been obscured. A more extensive time course for harvesting histomorphometry and serum samples is required to more fully characterize the anticipated differences in WT and *Nmp4*$^{-/-}$ dynamic bone remodeling. However, removal of a single outlier in the serum P1NP data indicated there was a 21% decline in serum P1NP in the *Nmp4*$^{-/-}$ mice during the first 4wks post-op but no significant change in the WT animals (Genotype p=0.37; Treatment p=0.16; GxT p=0.05, 2W ANOVA, see Results and Table 1 [revised]). Additionally, from pre-op to post-op 12wks (*vehicle-treated mice*) there was an approximately 50% decline in P1NP (genotype p=0.95; treatment p<0.0001; GxT p=0.36) and an approximate 20% decline in serum CTX (genotype p=0.14; treatment p=0.0003; GxT p=0.18). This suggests a decrease in bone remodeling in the untreated mice predominantly in the bone formation arm. We further address this issue in the revised Discussion.

Comment: Figures 1 and 2, The *Nmp4*$^{-/-}$ mice without PTH seems to lose more bone at 12wks compared to the WT without PTH treatment. Why does this happen?
Comment: The difference of FEMUR BV/TV between WT and *Nmp4*$^{-/-}$ at 12 wks seems to be smaller (or the same) comparing to the difference of FEMUR BV/TV between WT and *Nmp4*$^{-/-}$ at 8wks. This phenomenon also can be found for the L5 BV/TV. Can authors explain this?

Response:

- We agree that the graphical data suggest the vehicle-treated *Nmp4*$^{-/-}$ mice lose more bone between 8-12wks and that the difference between BV/TV in the two genotypes is smaller at the later time point, however stringent statistical analysis does not support this interpretation. Comparison of the femoral BV/TV data derived from the vehicle-treated mice at the 8wk and 12wk time points indicates a significant decline in both genotypes but no genotype or genotype x time interaction (Genotype p=0.44; Time p= 0.03; G x T 0.06, 2W ANOVA). A similar result is obtained with the L5 BV/TV data. This indicates that the modest enhanced bone loss in the *Nmp4*$^{-/-}$ mice observed 4wks post-op was stabilized or stabilizing by 8wks post-op.

Comment: I wonder if the difference of the PTH treatment between *Nmp4*$^{-/-}$ and WT will be less when the follow-up time is longer than 12 weeks?

Response:

- The reviewer's query whether the enhanced PTH-induced bone formation in the *Nmp4*$^{-/-}$ mice will decline after 12wks is very interesting. Although the elevated number of *Nmp4*$^{-/-}$osteoprogenitors declined at 12wks post-op, the higher number of *Nmp4*$^{-/-}$ CD8+ T cells did not decrease. Therefore, although the augmented response to PTH might be weakened in these mice, it may not disappear since the persistent increased lymphocyte number would provide extra Wnt10b. We have revised the Discussion to incorporate this talking point.

Comment: The identification of Nmp4 target genes relied solely on ChIP-seq analysis. As binding to the promoter may lead to either gene activation or repression, this approach can only reveal the binding properties, but does not reveal functional outcome. Gene expression analysis by either microarray or RNA-seq in parallel would be more informative.
Comment: The findings from ChIP-seq and bioinformatics analysis should be more extensively validated by ChIP-QPCR, mutagenesis and functional analysis, followed by rescuing experiments to determine whether the potential targets are truly functionally significant.
Comment: Although authors spent a great effort to create chip-seq data and the data is very interesting, but, regarding the specific genes/pathways that Nmp4 may be involved in PTH treatment, findings from chip-seq data seem to fall short and is inconclusive. I am wondering if there are Nmp4 targeted genes that are relevant to osteogenesis, bone mineralization, PTH and/or PTH treatment relevant pathways? In addition, have authors performed transcriptome profiling in relevant cells/tissues on those four experiment groups of animals? Did IGF1 or BMP express differently?

Response:

- We have added significantly more functional data to the revised manuscript. To evaluate gene expression in non-differentiating and in osteogenic-differentiating WT and *Nmp4*$^{-/-}$ MPSCs, RNA was isolated at five time points from both genotypes over the 16-day culture period. Individual cDNAs were quantified by qRT-PCR using a custom Taqman Low-Density Array system (Format 96a, Applied Biosystems, Foster City, CA) designed for 96 genes including Nmp4 target genes identified by our genome-wide ChIP-seq profiling, non-target genes that drive osteogenic differentiation and marker genes of this process. Our results are presented in Figures 9, 10 and Supplemental Figure 2A-2E. These data are very informative and suggest a mechanism underlying the enhanced PTH-induced anabolism in the *Nmp4*$^{-/-}$ mice. Briefly, the *Nmp4*$^{-/-}$ cells showed a dramatic surge in the expression of *Igfbp2* and downregulation of *Igfbp4* during the early stages of differentiation, both Nmp4 target genes. *Igfbp2* is a strong autocrine/paracrine anabolic signal and a recent study demonstrated that over-expression of this gene accelerated mineralization and enhanced osteocalcin (*Bglap*) expression in bone cells [Xi et al., 2014], strikingly similar to the phenotype of our null osteoprogenitors. *Igfbp4* is a potent inhibitor of osteogenesis [Miyakoshi et al., 1999]. Interestingly, disabling Nmp4 had no impact on the mRNA expression of the target genes *Igf1*and *Igfr1* but did elevate expression of *Pdk1*, a key component of the Igf1/insulin signaling pathway. Near the end of the 16-day differentiation period the *Nmp4*$^{-/-}$ cells exhibited an enhanced anabolic profile and expressed elevated levels of the non-target genes *Bmp2*, *Pth1r*, and *Bglap*. We also described the markedly downregulation of *Cxcl12* in the *Nmp4*$^{-/-}$ cells, a gene that plays a significant role in MSPC osteolineage commitment. Other differences between the WT and *Nmp4*$^{-/-}$ mRNA expression profiles are described. We agree that mutagenesis and rescuing experiments are the next step in analyzing the Nmp4 network but we respectfully contend that they are beyond the scope of the present study.
- Our Nmp4 ChIP-seq-derived map is the vital first step for deciphering the gene regulatory networks underlying the biological processes of this novel anti-anabolic axis. Our low-density array results are the first step in validating the reliability of this map.

Comment: Tables 1 and 2: It would be great to know the number of animals in each group.
Response: We have placed this information in Tables 1 and 2.

Genome-wide mapping and interrogation of the Nmp4 anti-anabolic bone axis

Paul Childress[1], Keith R. Stayrook[2], Marta B Alvarez[3], Zhiping Wang[4, 5], Yu Shao[4], Selene Hernandez-Buquer[1], Justin K Mack[2], Zachary R Grese[2], Yongzheng He[6, 7], Daniel Horan[1], Fredrick M Pavalko[8] Stuart J Warden[9, 10], Alexander G Robling[1], Feng-Chun Yang[6, 7] Matthew R Allen[1], Venkatesh Krishnan[2], Yunlong Liu[4, 5], Joseph P Bidwell[1, 4¶]

1. Department of Anatomy & Cell Biology, Indiana University School of Medicine (IUSM), Indianapolis, IN, 46202
2. Lilly Research Laboratories, Eli Lilly and Company, Indianapolis, Indiana, USA.
3. Orthopaedic Surgery IUSM
4. Department of Medical and Molecular Genetics, IUSM
5. Center for Computational Biology and Bioinformatics, IUSM
6. Department of Pediatrics, IUSM
7. Herman B Wells Center for Pediatric Research
8. Cellular & Integrative Physiology
9. Center for Translational Musculoskeletal Research, School of Health and Rehabilitation Sciences, IN University
10. Department of Physical Therapy, School of Health and Rehabilitation Sciences, IN University

Abbreviated title: The Nmp4 anti-anabolic axis

Key terms: bioinformatics, ChIP-seq, gene ontology, low-density arrays, osteoporosis, osteoprogenitors, ovariectomy

Word count: Main text: 8,075; Abstract 250; References 2203; Figure legends 1193; Supplemental legends 516]

Number of figures and tables: Ten figures + Two supplementary figures, Five tables + Three supplementary tables

¶Corresponding Author:
Joseph P. Bidwell
Department of Anatomy & Cell Biology
Indiana University School of Medicine
Medical Science Bldg 5035, 635 Barnhill Drive
Indianapolis, IN 46202
E-mail: jbidwell@iupui.edu

Disclosure statement: PC, MBA, ZW, YS, SHB, YH, DH, FMP, AGR, SJW, FCY, YL have nothing to disclose. Eli Lilly and Company has awarded research funds to JPB and MRA. Eli Lilly and Company funded part of this work. VK is an employee of Eli Lilly & Co and owns stock in this company. KS, JKM, and ZRG are employees of Eli Lilly & Co

ABSTRACT:

Parathyroid hormone (PTH) is an osteoanabolic for treating osteoporosis but its potency wanes. Disabling the transcription factor Nmp4 in healthy, ovary-intact mice enhances bone response to PTH and BMP2 and protects from unloading-induced osteopenia. These *Nmp4*$^{-/-}$ mice exhibit expanded bone marrow (BM) populations of osteoprogenitors and supporting CD8^{+} T cells. To determine whether the *Nmp4*$^{-/-}$ phenotype persists in an osteoporosis model we compared PTH response in ovariectomized (ovx) wild type (WT) and *Nmp4*$^{-/-}$ mice. To identify potential Nmp4 target genes we performed bioinformatic/pathway profiling on Nmp4 ChIP-seq data. Mice (12wks) were ovx or sham-operated 4wks before the initiation of PTH therapy. Skeletal phenotype analysis included μCT, histomorphometry, serum profiles, FACS sorting and the growth/mineralization of cultured WT and *Nmp4*$^{-/-}$ BM mesenchymal stem progenitor cells (MSPCs). ChIP-seq data were derived using MC3T3-E1 pre-osteoblasts, murine embryonic stem cells, and two blood cell lines. Ovx *Nmp4*$^{-/-}$ mice exhibited an improved response to PTH coupled with elevated numbers of osteoprogenitors and CD8^{+} T cells, but were not protected from ovx-induced bone loss. Cultured *Nmp4*$^{-/-}$ MSPCs displayed enhanced proliferation and accelerated mineralization. ChIP-seq/gene ontology analyses identified target genes likely under Nmp4 control as enriched for negative regulators of biosynthetic processes. Interrogation of mRNA transcripts in non-differentiating and osteogenic differentiating WT and *Nmp4*$^{-/-}$ MSPCs was performed on 90 Nmp4 target genes and differentiation markers. These data suggest that Nmp4 suppresses bone anabolism, in part, by regulating insulin-like growth factor binding protein expression. Changes in Nmp4 status may lead to improvements in osteoprogenitor response to therapeutic cues.

250 words

INTRODUCTION:

Patients with severe osteoporosis are often treated with parathyroid hormone (PTH), a potent osteoanabolic agent [Kraenzlin & Meier, 2011], however, the bone-building ability of this drug or its 'anabolic window' wanes, likely due to latent increases in bone resorption. [Cipriani et al., 2012; Baron & Hesse, 2012; Yu et al., 2011]. This limits its effectiveness to treat a chronic degenerative disease. Recent advances in bone-forming agents have shown that one can increase the extent of bone mass accrual with anti-SOST treatment compared to PTH (McClung et al., 2014). However, there may be unique pathways triggered by PTH, which allows for sustained targeting of early osteogenesis as evidenced by serum markers of bone formation such as N-terminal propeptide of type 1 procollagen (P1NP) and osteocalcin (OCN, Padhi et al., 2011; Saag et al., 2009). In contrast to PTH, anti-SOST antibodies may have a limited capacity for targeting osteoprogenitors as evidenced by a relatively transient up-regulation of collagen-based markers such as P1NP (McClung et al., 2014). Therefore given PTH's unique mode of action, therapies that could enhance PTH-mediated recruitment of osteoprogenitors may add value to some patients. How to achieve this enhancement is not clear. For example, attempts to extend and enhance PTH efficacy by combining treatment with anti-resorptive medications have met with mixed success and have generally been underwhelming [Cosman et al., 2011; Finkelstein et al., 2010; Black et al., 2003].

Blocking the activity of Nmp4/CIZ (nuclear matrix protein 4/cas interacting zinc finger protein, 'Nmp4') in mice dramatically enhanced their response to anabolic doses of PTH [He et al., 2013; Childress et al., 2011; Robling et al., 2009], suggesting a potential strategy for an adjuvant therapy [Krane, 2005]. Intermittent exogenous doses of hormone stimulated equivalent new bone formation in wild type (WT) and *Nmp4*$^{-/-}$ mice during the first 2wks of challenge, but at 3wks of treatment the null mice exhibited greater than a 2-fold increase in new trabecular bone compared to their WT littermates [Childress et al., 2011]. This augmented skeletogenesis in the *Nmp4*$^{-/-}$ mice was extended to 7wks of treatment and was observed in the femur, tibia, and vertebra. Serum osteocalcin continued to rise at this time point in the *Nmp4*$^{-/-}$ mice but had decreased in the WT animals [Childress et al., 2011]. However, the PTH response of the cortical compartment was equivalent throughout treatment in the WT and null mice

[Robling et al., 2009]. This suggests that disabling Nmp4 accelerates and enhances the response of bone to intermittent PTH [Childress et al., 2011].

Nmp4$^{-/-}$ bone may have a generalized accelerated and heightened response to systemic or local anabolic cues. For example, these mice also exhibited augmented BMP2-induced ectopic bone formation compared to their WT littermates [Morinobu et al., 2005]. The *Nmp4*-null mice showed an accelerated osseous regeneration after marrow ablation [Morinobu et al., 2005] and did not lose bone during hind limb unloading, which appeared to derive from an enhanced osteoblast activity [Hino et al., 2007].

Prerequisite for an adjuvant therapy target, disabling Nmp4 has little impact on the health, longevity, or global baseline phenotype of the mouse, with a few exceptions. The *Nmp4*$^{-/-}$ baseline skeletal phenotype (i.e., bone mineral density and/or content and trabecular architecture) is generally equivalent compared to WT animals], although we have occasionally observed an unprovoked increase in bone properties in *Nmp4*$^{-/-}$ mice [He et al., 2013, Childress et al., 2011; Robling et al., 2009; Morinobu et al., 2005]. Similarly, male *Nmp4*$^{-/-}$ mice exhibit variable degrees of spermatogenic cell degeneration resembling germinal-cell aplasia with focal spermatogenesis resulting in *sporadic* infertility [Nakamoto et al, 2004].

Our recent work suggests that the cellular basis of the osteoanabolic repressor function of Nmp4 is due to its effect on the bone marrow derived stromal stem/progenitor cells aka mesenchymal stem progenitor cells (MSPCs) [He et al., 2013]. *Nmp4*$^{-/-}$ mice have significantly more osteoprogenitor cells in their marrow, which lie in wait to be quickly mobilized to differentiate into active osteoblasts upon stimulation with various osteoanabolic stimuli [He et al., 2013]. There was no difference between WT and *Nmp4*$^{-/-}$ BM cellularity or profiles of several blood elements however, the null mouse exhibited a 4-fold increase in CD45^{-}/CD105^{+}/nestin^{+}/CD146^{+} BM osteoprogenitor cells. These markers are a common hallmark to CFU-F cells with osteogenic potential [Isern et al., 2013; Méndez-Ferrer et al., 2010] and indeed 4-fold more CFU-F$^{\text{Alk phos+}}$ and CFU-F$^{\text{Ob}}$ cells have been recovered from these mice compared to the WT animals [He et al., 2013; Morinobu et al., 2005]. A second, related phenomenon we have observed in *Nmp4*$^{-/-}$ mice is a 2-fold increase in the prevalence of CD8^{+} T-cells in the femoral marrow—

the lymphocyte population that provides potent input to induce MSPCs down the osteoblast differentiation pathway [He et al., 2013; Bedi et al., 2012; Terauchi et al., 2009; Li et al., 2014]. These blood cells express the PTHR1 receptor and support the PTH anabolic response via the release of Wnt10b upon hormone challenge, which drives osteoprogenitor differentiation to pre-osteoblasts and mature matrix-producing bone cells [Bedi et al., 2012; Terauchi et al., 2009; Li et al., 2014].

There is little information on the molecular mechanisms and cellular pathways that mediate the anti-anabolic action of Nmp4. This transcription factor is a Cys_2His_2 zinc finger protein that primarily localizes to the nucleus although there is evidence for cytoplasmic activity [Bidwell et al., 2012; Nakamoto et al., 2000]. The zinc fingers recognize the DNA minor groove of an AT-rich consensus sequence and two transactivation domains can suppress or activate transcription depending on the cellular context [Shah et al., 2004; Torrungruang et al., 2002; Thunyakitpisal et al., 2001; Nakamoto et al., 2000; Alvarez et al., 1998]. The amino terminus of the rodent protein contains an SH3-binding domain that associates with the adaptor signaling protein p130Cas [Nakaomoto et al., 2000], but the functional significance of this interaction remains unknown.

The *Nmp4*$^{-/-}$ progenitor cells and their progeny have an exaggerated stimulus response at the levels of transcription and cell signaling [Alvarez et al., 2012; Yang et al., 2010; Shen et al., 2002]. *Nmp4*-null bone marrow stromal cells (BMSCs) show an enhanced transcriptional response to PTH and BMP2 [Alvarez et al., 2012; Shah et al., 2004; Shen et al., 2002]. The *Nmp4*$^{-/-}$ derived calvarial cells exhibit an increased load-induced phosphorylation of Pi3k and Akt and beta-catenin nuclear translocation [Yang et al., 2010]. Analogous to heightened response to anabolic signals in *Nmp4*$^{-/-}$ osteolineage cells, osteoclast preparations from the null mice exhibited a heightened response to the remodeling signals of RANKL and M-CSF (Childress et al., 2011).

Two essential genotype-phenotype questions remaining to be addressed are (i) whether the *Nmp4*-null mouse is resistant to ovariectomy (ovx)-induced bone loss and (ii) if disabling Nmp4 improves PTH-based bone therapy in the OVX model. This is a focal preclinical extension of the *Nmp4*$^{-/-}$ phenotype necessary before this gene and its associated pathways can be considered potential targets for an adjuvant

therapy. Additionally, we used expanded cultures of WT and *Nmp4*$^{-/-}$ mesenchymal stem/progenitor cells (MSPCs) to probe the cell autonomous proliferative and mineralization activities of this cell population. To delineate the framework of the Nmp4 anti-anabolic network we performed genome-wide chromatin immunoprecipitation sequencing (ChIP-seq) on MC3T3-E1 cells and combined these data with the data available for Nmp4 (a.k.a. Znf384) from the Mouse Encyclopedia of DNA Elements (ENCODE) Consortium for transcription factors [Stamatoyannopoulos et al., 2012]. Bioinformatic profiling, gene ontology (GO), and pathway analysis were performed on these data sets to infer a map of the negative regulation of bone anabolism under Nmp4 control. Interrogation of mRNA transcripts in non-differentiating and osteogenic differentiating WT and *Nmp4*$^{-/-}$ MSPCs was performed on 90 Nmp4 target genes and differentiation markers to inaugurate validation of the Nmp4 anti-anabolic network.

MATERIALS AND METHODS:

Mice: Male and female *Nmp4*$^{-/-}$ mice, backcrossed onto a C57BL/6J background for 7 generations [He et al., 2013, Childress et al., 2011; Robling et al., 2009], and their WT littermates were produced and maintained in our colony at Indiana University Bioresearch Facility, Indiana University School of Dentistry. Our local Institutional Animal Care and Use Committee approved all husbandry practices and experimental procedures and regimens described in this investigation.

Bilateral ovariectomy surgery: 12wk-old virgin mice were anesthetized using isoflurane inhalation followed by a mixture of xylazine and ketamine administered intraperitoneally. A 1-2cm dorsal incision was made in the midline below the level of the last rib and the skin bluntly dissected from the muscle on either side of the incision. Through the skin incision, the muscle wall was incised 1cm lateral to the midline 1-2cm below the last rib to enter the abdominal cavity. The periovarian fat pad was located and gently grasped and exteriorized. Care was taken not to directly handle the ovary to avoid abdominal implantation of ovarian tissue. While holding the periovarian fat pad with forceps, the fallopian tube between the fat pad and uterus was clamped and crushed using mosquito hemostats. The crushed area was

cut with scissors and the fat pad with ovary removed. The procedure was repeated on the contralateral side. The skin incision was closed with one or two surgical wound clips. The sham surgeries involved all the outlined steps except the crushing the fallopian tubes and the actual removal of the ovaries. To confirm the efficacy of OVX, uteri were weighed following euthanasia.

PTH treatment: At 16 wks of age, ovx animals were sorted into four treatment groups based on equivalent mean-group-body weight. These four groups included 1) vehicle-treated WT; 2) PTH-treated WT; 3) vehicle-treated *Nmp4*$^{-/-}$ and 4) PTH-treated *Nmp4*$^{-/-}$ mice. Mice were injected subcutaneously (sc) with synthetic human PTH 1-34 acetate salt (Bachem Bioscience Inc, PA) at 30µg/kg/day, daily or vehicle control (0.2% BSA/1.0µN HCl in saline, Abbott Laboratory, North Chicago, IL) for the length of time indicated.

Cell culture: Cells from ATCC (MC3T3-E1 subclone 4) were maintained in α-MEM medium supplemented with 100 IU/ml penicillin, 100 µg/ml streptomycin, 25 µg/ml amphotericin, 2 mM L-glutamine (Gibco BRL, Grand Island, NY), ascorbic acid (50µg/ml, Sigma-Aldrich, St Louis, MO), and 10% fetal bovine serum (FBS; Sigma-Aldrich, St Louis, MO). Expanded mesenchymal stem/progenitor cell (MSPC) cultures were established as previously described [Wu et al., 2006]. Briefly, long bone BM was isolated from euthanized mice 6-8wks of age and the mononuclear cells (BMMNCs) were isolated using a Ficoll gradient. These cells were plated in Mesencult™ Media + Mesencult™ Stimulatory Supplement (StemCell™ Technologies, Vancouver BC, Canada) and maintained in culture for 3-4wks without passage and fed every 5-7 days by removing 50% of the old media and adding 50% fresh media, very gently so as not to disturb the cells. At approximately 80% confluence, the cells were passaged at 1:3 dilution for two more passages before use or were frozen for storage. Cells were used for experiments between passages 5-10. For comparing cell proliferation rates between WT and *Nmp4*$^{-/-}$ MSPCs, the cells were transferred to α-MEM medium without the ascorbic acid in 12-well plates at 5,000 cells/well (Day

193 0). Cells were counted on Day 2, 4, and 6 post-seeding prior to refreshing the medium for the remaining
194 cells. To evaluate mineralizing capacity cells were transferred to osteogenic differentiation medium and
195 after 48hrs (Day 0), which was comprised of α-MEM supplemented with ascorbic acid (5-50µg/ml,
196 Sigma Aldrich), dexamethasone (0-10nM, Sigma-Aldrich), and 10mM glycerol 2-phosphate disodium
197 salt hydrate (BGP, Sigma-Aldrich). For controls, cells were passaged into fresh MesenCult medium
198 without the osteogenic/mineralization supplements. Cells were stained for alkaline phosphatase activity
199 using naphthol AS-MX phosphate and fast red violet B salt following the manufacturer's instructions
200 (Sigma cat# 85L3R-1KT) or for mineralization using alizarin red.
201 To compare mRNA expression profiles of select genes in non-differentiating and osteogenic-
202 differentiating WT and *Nmp4*$^{-/-}$ MSPCs, cells were seeded into 12-well plates at either 10,000 or 25,000
203 cells/well in Mesencult™ Media + Mesencult™ Stimulatory Supplement. Those cells at the lower seeding
204 density were harvested on Day 3 post-seeding (non-differentiating). The remaining cells were transferred
205 to osteogenic differentiation medium 48hrs post-seeding and harvested on Days 5, 7, 9, and 16.
206
207 *Flow cytometry*: Cellular surface marker profiles from BM and peripheral blood (PBL) were assessed as
208 previously described [He et al., 2013]. The antibodies employed for flow cytometry were obtained from
209 BD Biosciences (San Jose, CA). Stained cells were analyzed on an FACS Calibur (BD Biosciences) and
210 results were quantified using FlowJo Version 8.8.6 software (TreeStar Inc, Ashland OR).
211
212 *Micro computed tomography (µCT)*: Trabecular bone architecture was analyzed as we have previously
213 described [He et al., 2013; Childress et al., 2011]. Briefly, femurs and L5 vertebra were excised from the
214 WT and *Nmp4*$^{-/-}$ mice after euthanasia, the muscle and connective tissue removed, and the bones
215 transferred to 10% buffered formalin, 4°C for 48 hr, after which the bones were placed in 70% ethanol
216 (4°C) until analyzed. For femur analysis a 2.6-mm span (~5 mm^3 of medullary space) of the excised distal
217 femoral metaphysis was scanned in 70% ethanol on a desktop µCT (µCT 35; Scanco Medical AG,
218 Bassersdorf, Switzerland) at 10 µm resolution using 55-kVp tube potential and 400-msec integration time,

to measure three-dimensional morphometric properties. The entire vertebra (L5) were scanned using standard methods (Skyscan 1172). Bones were reconstructed and analyzed using the manufacturer's software. The trabecular bone between the two growth plates was isolated from the cortical shell via manual tracing and assessed for trabecular architecture. From the three dimensional reconstructions the following parameters were obtained using the Scanco and Skyscan software analyses: trabecular bone volume per total volume (BV/TV, %), connectivity density (Conn.D, mm^{-3}), structure model index (SMI), trabecular number (Tb.N, mm^{-1}), trabecular thickness (Tb.Th, mm), and spacing (Tb.Sp, mm) [Bouxsein et al., 2010].

Bone histomorphometry: All histomorphometric parameters were obtained as previously described [Childress et al., 2011] following the ASBMR guidelines [Dempster et al., 2013]. Briefly, mice were administered intraperitoneal injections of calcein green (20 mg/kg; Sigma-Aldrich) and alizarin red (25 mg/kg, Sigma-Aldrich) 6 and 3 days before euthanasia, respectively. The femur marrow cavity was exposed via cutting the anterior face of the epiphyseal plate. Bones were embedded in methyl-methacrylate subsequent to dehydration with graded alcohols, sectioned (4μm) with a Leica RM2255 microtome (Leica Microsystems, Wetzlar, Germany), and mounted unstained on microscope slides and imaged under fluorescent light with a microscope system [Childress et al., 2011]. Bone formation rate (BFR), mineral apposition rate (MAR), and mineralizing surface (MS/BS) were obtained from a $0.03mm^2$ metaphyseal region of interest from 250μm to 1750μm below the growth plate using ImagePro 3.1 software (Media Cybernetics, Bethesda, MD, USA).

Serum biochemistry: We analyzed serum N-terminal propeptide of type 1 procollagen (P1NP) to evaluate global bone formation in our experimental mice using the Rat/Mouse P1NP EIA from IDS Immunodiagnostic Systems (Scottsdale, AZ) following the manufacturer's instructions. To follow bone resorption we analyzed serum C-terminal telopeptides (CTX) with the RatLaps™ ELISA (Immunodiagnostic Systems Inc) [Childress et al., 2011].

Quantitative real-time PCR (qRT-PCR) analysis: ChIP-qPCR was used to authenticate select ChIP-seq profiles employing SYBR Green assays and SYBR Green Supermix (Bio-rad, Hercules, CA). qRT-PCR reactions were carried out in triplicate on specific genomic regions. The resulting signals were normalized for primer efficiency by carrying out qRT-PCR reactions for each primer pair using Input DNA.

To evaluate gene expression in non-differentiating and in osteogenic-differentiating WT and *Nmp4*$^{-/-}$ MPSCs, RNA was isolated with RNAeasy columns according to the manufacturer's instructions (Qiagen, Gaithersburg, MD). The RNA was reverse-transcribed via the High-Capacity cDNA Reverse Transcription Kit (Applied Biosystems, Foster City, CA**)**. RNA expression profiling was performed on three-four replicates per time point for both genotypes over the 16-day culture period. Individual cDNAs were quantified by qRT-PCR using a custom TLDA system (Format 96a, Applied Biosystems, Foster City, CA) designed for 96 genes including Nmp4 target genes identified by our genome-wide ChIP-seq profiling, osteogenic differentiation marker genes, and candidate normalizer genes. All experiments were performed in biological quadruplicate or triplicate with TaqMan fast advanced master mix (Applied Biosystems) on a QuantStudio™ 7 Flex Real-Time PCR System. The probes used are listed in Supplemental Table 1. We used the ExpressionSuite v1.0.4™ analysis software (Applied Biosystems) to analyze these data. This software utilizes the comparative threshold cycle (ΔΔCT) method to quantify relative gene expression across a large number of genes and samples. The software provides options to normalize expression data using either global normalization or endogenous controls and calculates fold changes with P values. Gene expression data were normalized to five endogenous controls (*18S*, *Gusb*, *Rplp2*, *B2m*, and *Hprt*) although we report *Gusb* and *Rplp2* data here. In all experiments, the CT upper limit was set to 40, meaning that all mRNA detectors with a CT value greater than or equal to 40 were excluded. The multiple-comparisons correction (Benjamini-Hochberg method for false-discovery rate) was applied to the data and a P value of ≤0.05 was considered significant. Additionally, individual qRT-PCR reactions were performed to monitor the expressions of *Sp7* (osterix, Mm00504574_m1) and *Bglap* (osteocalcin, Mm03413826_mH) using Rplp2 as the normalizer (Mm03059047_gH). The prepared

cDNA was used to set up qRT-PCR reactions using FastStart Universal Probe Master mix (Rox) (Roche Life Science, Indianapolis, IN).

Chromatin immunoprecipitation sequencing (ChIP-seq) and ChIP analysis: Cells from ATCC (MC3T3-E1 subclone 4) were seeded into twenty-one 150mm plates at an initial density of 50,000 cells/plate (320 cells/cm^2) and maintained in αMEM complete medium + ascorbic acid. On Day 14 post-seeding, cells were treated with 25nM hPTH(1-34) or vehicle control for 1hr before harvest. Subsequent to treatment cells were fixed with 1% formaldehyde for 15min and quenched with 0.125M glycine. Cell pellets were frozen in an ethanol dry ice bath and shipped to Active Motif for FactorPath™ analysis. The chromatin was isolated from the pellets by adding lysis buffer followed by disruption with a Dounce homogenizer. Lysates were sonicated and the DNA sheared to an average length of 300-500 bp. Genomic DNA (Input) was prepared by treating aliquots of chromatin with RNase, proteinase K and heat for de-crosslinking, followed by ethanol precipitation. Pellets were resuspended and the resulting DNA was quantified on a NanoDrop spectrophotometer. Extrapolation to the original chromatin volume allowed quantitation of the total chromatin yield. An aliquot of chromatin (30µg) was precleared with protein A agarose beads (Invitrogen, ThermoFisher Scientific, Waltham, MA). Genomic DNA regions of interest were isolated using 4µg antibody against ZNF384 (Sigma HPA004051, Lot A57874). Complexes were washed, eluted from the beads with SDS buffer, and subjected to RNase and proteinase K treatment. Crosslinks were reversed by incubation overnight at 65°C, and ChIP DNA was purified by phenol-chloroform extraction and ethanol precipitation.

ChIP Sequencing (Illumina): ChIP and Input DNAs were prepared for amplification by converting overhangs into phosphorylated blunt ends and adding an adenine to the 3'-ends. Illumina genomic adapters were ligated and the sample was size-fractionated (200-300 bp) on an agarose gel. After a final PCR amplification step (18 cycles), the resulting DNA libraries were quantified and sequenced on HiSeq 2000. Sequences (50nt reads, single end) were aligned to the mouse genome (mm10) using the BWA

297 algorithm. Alignments were extended in silico at their 3'-ends to a length of 150 bp, which is the average
298 genomic fragment length in the size-selected library, and assigned to 32-nt bins along the genome. The
299 resulting histograms (genomic "signal maps") were stored in BAR and bigWig files. ZNF384 peak
300 locations were determined using the MACS algorithm (v1.4.2) with a cutoff of pvalue = 1e-7 [Li and
301 Durbin, 2009].
302
303 *Bioinformatic profiling*: In addition to generating our own Nmp4 ChIP-seq data from the MC3T3-E1 cells
304 we used Nmp4 (Znf384) ChIP-seq data from murine embryonic stem cell line (ES-E14) and the B-cell
305 lymphoma cell lines Ch12 and MEL from the ENCODE Consortium for transcription factors 2011 Freeze
306 data sets in NarrowPeak format (Rosenbloom et al., 2013). To assign an Nmp4 peak to a promoter region
307 it had to be within -5kb to +2kb from a transcription start site (TSS). To assign a peak to an intragenic
308 region it had to be located within the range defined by the TSS and the transcription end site (TES), and
309 not within the promoter range of the same gene. To assign a peak to an intergenic region it had to be -
310 10,000kb from the TSS and +10,000kb from the TES, and not within the promoter range of the same gene.
311 A peak could be assigned to multiple functional regions in an area of the genome harboring multiple
312 genes. A common example of this is an area with genes on both strands. A peak may not fit any of these
313 definitions and was assigned to the classification "other". This methodology yielded 34,317 functional
314 assignments for the peaks in the MC3T3-E1 cells.
315 *GEM analysis*: Genome wide Event finding and Motif discovery (GEM) [Guo et al., 2012] was used to
316 derive the Nmp4 consensus sequence. The latest mouse genome build (mm10) was employed together
317 with the GEM default ChIP-seq read distribution file and a minimal k-mer width of 6 and maximum of 20.
318 *Gene Ontology*: Gene ontology analysis was conducted using DAVID [Huang et al., 2009], and terms
319 summarized using REVIGO [Supek et al., 2011]. The ENCODE ChIP-Seq Significance Tool was
320 employed to identify enriched transcription factors in our Nmp4 gene target list [Auerbach et al., 2013].
321 Additionally some functional analysis was also generated through the use of QIAGEN's Ingenuity
322 Pathway Analysis (IPA®, QIAGEN Redwood City, www.qiagen.com/ingenuity).

Bone phenotype statistical analysis: Statistical evaluations were processed using the program JMP version 7.0.1 (SAS Institute, Cary, NC). The animal studies employed a two-way ANOVA using genotype and treatment as the independent variables followed by either a Tukey HSD or LS Means post hoc test if a genotype x treatment interaction was indicated. Statistical significance was set at $p \leq 0.05$. To compare growth rates of the WT and *Nmp4*$^{-/-}$ MSPCs derived from various experimental mice, we evaluated the slopes of log-transformed cell counts regressed onto experimental day using a t-test. The numbers of mice per treatment group and replicates/treatment for the cell studies are indicated in the appropriate figures and tables.

RESULTS:

Nmp4$^{-/-}$ *mice are not protected from ovx-induced bone loss*

To determine whether genetically disabling Nmp4 activity protects mice from ovx-induced bone loss as it does from unloading-associated osteopenia [Hino et al., 2007], we removed the ovaries or performed sham operations on both WT and *Nmp4*$^{-/-}$ mice (Figure 1). Both the ovx WT and ovx *Nmp4*$^{-/-}$ mice experienced significant weight gain at 4wks post-op (Table 1) consistent with previous mouse studies [Vieira Potter et al., 2012]. Additionally, ovx resulted in a significant decrease in uterine weight in both genotypes (Table 1). There was no genotype x treatment interaction in either of these parameters.

Both WT and *Nmp4*$^{-/-}$ mice exhibited significant bone loss 4wks after ovx surgery as measured in the trabecular bone compartment of the distal femur and the L5 vertebra (Table 1). The *Nmp4*$^{-/-}$ mice exhibited a trend towards enhanced loss of bone that neared significance in the distal femur (BV/TV, genotype x treatment interaction = 0.06, Table 1) and reached significance in the L5 vertebra (BV/TV, genotype x treatment interaction <0.05, Table 1). Despite this enhanced (or nearly enhanced) rate of bone loss the *Nmp4*$^{-/-}$ animals maintained more trabecular bone compared to WT mice during the first 4wks after ovariectomy. The *Nmp4*$^{-/-}$ mice exhibited a decrease in the serum bone formation marker P1NP at 4wks post-op and both genotypes showed significant decreases in this marker at 12wks post-op in the

vehicle-treated mice. A small decrease in the serum bone resorption marker CTX was observed at 12wks post-op in the vehicle-treated mice.

Ovx Nmp4$^{-/-}$ mice show an enhanced bone gain response to PTH therapy

With a separate group of ovx mice we initiated treatment of both WT and *Nmp4*-null ovx animals with PTH (30µg/kg/day) or vehicle control 4wks after surgery. The duration of hormone therapy lasted 4wks (8wks post-op) and 8wks (12wks post-op). The ovx *Nmp4*$^{-/-}$ mice showed an enhanced PTH-induced gain in femoral BV/TV and Conn D at 4wks and 8wks of therapy compared to their ovx WT littermates as well as an augmented gain in trabecular thickness at 8wks (Figure 2, Table 2). The null mice also showed an enhanced PTH response at the L5 vertebra at 8wks of treatment (Figure 3, Table 2). Specifically the 2-way ANOVA indicated strong genotype x treatment effects for the distal femur for both 4wks and 8wks therapy and for the L5 vertebra for 8wks therapy (see Figures 2A and 3A); the post-hoc tests concluded that the difference between the genotypes was within the hormone-treated groups. The vehicle-treated ovx WT and ovx *Nmp4*$^{-/-}$ groups showed no difference in BV/TV (Figures 2 and 3) at the end of the treatment regimens indicating that the modest enhanced loss in bone in the *Nmp4*$^{-/-}$ mice was stabilized by 4wks therapy. PTH significantly elevated MAR, MS/BS, and BFR at the end of 4wks treatment as shown by strong treatment effects (Table 3). However, there was no genotype effect or genotype x treatment interaction for any of these parameters (Table 3). Hormone significantly elevated serum levels of the bone formation marker P1NP and the resorption marker CTX at 8wks of therapy, but there was no treatment x genotype interaction for either of these parameters (Table 3).

FACS analysis of the BM CD45^{-}/CD105^{+}/CD146^{+}/nestin^{+} osteoprogenitors revealed a significant elevation in the number of these cells in the BM obtained from the *Nmp4*$^{-/-}$ mice at the end of 4wk therapy, irrespective of treatment (Figure 4A). This is consistent with our previous observation in the ovary-intact null mice [He et al., 2013]. By the end of 8wks treatment (12wks post-op) the observed increase in the number of these *Nmp4*$^{-/-}$ cells in the BM failed to reach statistical significance, but there was a significant elevation in the number of the PBL *Nmp4*$^{-/-}$ osteoprogenitors in the vehicle-treated mice (Figure 4D). The

Nmp4$^{-/-}$ mice showed a significant elevation in CD8^{+} T cells in both the BM and the PBL throughout the entire therapy regimen (Figure 4B and 4E). PTH significantly decreased the numbers of these cells in the BM at 8wks therapy in both genotypes (Figure 4B) but had no impact on the number of these cells in the PBL (Figure 4E). Disabling Nmp4 had little to no effect on CD4^{+} T cells, nor did treatment with PTH (Figure 4C and 4F). The modest increase in BM CD4^{+} T cells approached significance ($p<0.06$) but this was not reflected in the PBL, just as we previously observed in the ovary-intact mice [He et al., 2013].

To determine if the enhanced osteogenic potential of the BM could be reliably and reproducibly maintained in vitro in MSPC cultures over several passages and in the absence of supporting cells (e.g. T-cells) we established expanded WT and *Nmp4*$^{-/-}$ MSPCs from ovary-intact mice. The expanded *Nmp4*$^{-/-}$ MSPCs from ovary-intact mice exhibited modest but significantly enhanced proliferation compared to the WT cells (Figure 5A). Both the null and WT expanded MSPCs showed strong alkaline phosphatase expression (Figure 5B). However, the expanded *Nmp4*$^{-/-}$ MSPCs typically showed an accelerated and enhanced mineralization compared to WT cells under various concentrations of dexamethasone and ascorbic acid (Figure 5B). Finally, the expanded *Nmp4*$^{-/-}$ and WT MSPCs exhibited varying degrees of alkaline phosphatase staining while maintained in MesenCult medium, depending on the confluence of the cells and time in culture (3-9 days), however no mineralization was observed in these control cultures (data not shown).

Genome-wide ChIP-seq/gene ontology analysis reveals Nmp4 target genes and potential pathways of the anti-anabolic axis.

Nmp4 is expressed in nearly all cells, yet the most singular consequence of globally disabling this protein is the enhanced mobilization of bone cells upon osteoanabolic induction [He et al., 2013; Childress et al., 2011; Robling et al., 2009; Morinobu et al., 2005]. As a first step in understanding the origins of this phenotype, which may have clinical significance, we needed the following information: (1) the identity of the Nmp4 target genes including 'core' target genes common to multiple cell types; (2) identify common functions of these core genes to distinguish pathways that make osteoprogenitors

particularly vulnerable to the effects of Nmp4 and (3) experimental confirmation of some of these pathways. To begin to understand how Nmp4 works we set out to understand (4) whether Nmp4 targets functional regions of the genome, (5) if it binds directly to DNA or via other proteins, and (6) whether osteoanabolic agents, e.g. PTH, alter Nmp4 DNA-binding along target genes.

The potential Nmp4 target genes identified by ChIP-seq in the MC3T3-E1 (vehicle-treated) cells and those established in the three ENCODE cell lines were compared using those genes that had one or more peaks associated with the TSS. A Venn diagram of these genes showed that 2114 Nmp4 'core' target genes were common to the four cell lines (Figure 6A, and Supplemental Table 1). These core target genes were classified into functionally related categories using gene ontology (GO) analysis with the Database for Annotation, Visualization, and Integrated Discovery (DAVID) tool [Huang et al, 2009]. The functional annotation-clustering algorithm was applied to the target list, which is able to give a more insightful view of the relationships between annotation categories and terms compared to other analytic modules [Huang et al., 2009]. The significance of group classification was defined by enrichment scores based on Fisher exact statistics (false discovery rate, FDR $p<0.05$). The DAVID-derived biological profile was further summarized using REVIGO [Supek et al., 2011]. GO analysis of the core target genes designated Nmp4 as a negative regulator of cellular biosynthetic processes showing significant enrichment for genes involved in the regulation of transcription, chromatin modification, protein catabolic processes, regulation of the cell cycle, and mRNA processing/splicing (Figure 6B). Interestingly, the genes *specific* to any one particular cell line or specific to vehicle-treated or PTH-treated MC3T3-E1 cells did not yield a distinct biological process profile that reached statistical significance as obtained with the core target genes (data not shown). However, peak-associated genes common to the vehicle- and PTH-treated MC3T3-E1 cells yielded a profile nearly identical to that obtained with the core target genes.

Next we probed existing datasets for enriched transcription factors within our Nmp4 core target gene list using the ENCODE ChIP-seq Significance Tool [Auerbach et al., 2013] (Table 4). This profile shows that Nmp4 binding in the promoter regions of its target genes predominantly co-occurs with proteins that regulate chromatin organization and with proteins that contribute to maintaining

stem/progenitor pluripotency/multipotency and the poised gene state, e.g. CHD2, SIN3a, and GCN5 [Harada et al., 2012; Nascimento et al., 2011; Lin et al., 2007].

In an effort to gain further understanding of how Nmp4 regulates gene expression we prepared a genome-wide functional region map of the Nmp4 binding sites for all four cell types as described in Materials and Methods. The majority of the occupancy peaks were located in or near the TSS or in intragenic regions, areas typically associated with regulatory functions (Figure 7A). To determine if Nmp4 binds directly to DNA or can associate with the genome via other proteins we used the discovery algorithm GEM to derive the Nmp4 consensus-binding site from the MC3T3-E1 data. In support of previous studies by our lab and others the derived binding site matched the unusual homopolymeric (dA·dT) consensus sequence previously derived by cyclic amplification and electrophoretic mobility shift assay [Alvarez et al., 1998; Nakamoto et al., 2000] (Figure 7B). No other consensus sequences were identified suggesting a single and direct mode of genome association, mediated by the Cys2His2 DNA-binding domain [Torrungruang et al., 2002]. To determine whether PTH challenge altered Nmp4 DNA-binding along target genes we generated genome-wide Nmp4 ChIP-seq profiles using the pre-osteoblast cell line MC3T3-E1 treated with hPTH(1-34) or vehicle control for 1hr. We used the 1hr time point because we observed the most significant differences in femoral mRNA expression profiles between WT and *Nmp4*$^{-/-}$ mice 1hr after injection [Childress et al., 2011]. Hormone reduced Nmp4 genome-wide occupancy from a total of 15,446 to 13,109 binding sites. However, at the level of the single gene there was a diversity of changes in Nmp4 occupancy, i.e. PTH was observed to remove (e.g. Nid2), induce (e.g. Ccdc53) or have no effect on Nmp4-DNA association (e.g. Akt2, Arrb2) (Figure 8; also see ChIP-qPCR confirmation of Nmp4 binding, Figure S1).

As a first step in the validation of the ChIP-seq-derived anti-anabolic map we interrogated 90 mRNA transcripts in non-differentiating and osteogenic differentiating WT and *Nmp4*$^{-/-}$ expanded MSPCs at five different time points. The accelerated and enhanced mineralization of the *Nmp4*$^{-/-}$ MSPCs (Figure 5) is consistent with our previous observation that in response to PTH *Nmp4*$^{-/-}$ mice add more bone and add it faster than WT mice [Childress et al., 2011]. Our choice of Nmp4 target genes (Supplemental Table

1) was based on our DAVID analysis. We chose both core target genes and Nmp4 target genes identified in the MC3T3-E1 pre-osteoblasts. DAVID also uses KEGG (Kyoto Encyclopedia of Genes and Genomes) database to map large gene lists to signaling pathways [Huang et al., 2009]. For example the DAVID/KEGG profile of the Nmp4 core target genes included the TOR and insulin/IGF1 signaling pathways (Table 5) and indeed the insulin/IGF1->IRS1->PI3K->PDK1->Akt signaling response limb is common to many of the pathways listed. This is also consistent with our IPA analysis (Supplemental Table 3). Also included were Nmp4 target genes coding for proteins involved in the ubiquitin-proteasome system, chromatin remodeling, transcription regulation, and RNA processing. Finally we analyzed the expression of osteogenic differentiation markers.

Volcano plots (Supplemental Figure 2) identify genes that were statistically significantly upregulated or downregulated by at least 2-fold in the *Nmp4*$^{-/-}$ cells compared to the WT cohort on the same day of culture. Figures 9 and 10 compare the relative mRNA expression of select genes to the level of the transcript in WT cells on Day 3 of culture thus providing a time course view. The *Nmp4*$^{-/-}$ cells showed a strikingly elevated expression of the Nmp4 target gene *Igfbp2* mRNA and downregulation of the target gene *Igfbp4* mRNA during the early differentiation period (Figures 9A and 9B). Igfbp2 stimulates osteoblast differentiation whereas the Igfbp4 is a potent inhibitor of Igf actions [Xi et al., 2014; Miyakoshi et al., 1999]. Phosphoinositide-dependent kinase 1 (*Pdk1*, target gene) a key component of the Igf1/insulin signaling pathway [Calleja et al., 2014] was upregulated in the *Nmp4*$^{-/-}$ cells throughout the developmental time course (Figure 9C). Interestingly, neither the target genes *Igf1* nor its receptor *Igf1r* exhibited striking differences in gene expression between the two genotypes (data not shown). The *Nmp4*$^{-/-}$ cells exhibited an enhanced anabolic profile during the latter differentiation period as evidenced by elevated expression levels of the non-target genes *Bmp2* (Figure 9D), *Pth1r* (Figure 9E), and *Bglap* (osteocalcin, Figure 9F).

Cxcl12 expression (target gene), also known as stromal derived factor 1, was dramatically downregulated in the *Nmp4*$^{-/-}$ cells throughout development (Figure 10A) and the target gene *Plaur* (*uPAR*, urokinase plasminogen activator receptor) was upregulated in the null cells (Figure 10B). Both

genes play roles in MSPC osteogenic lineage commitment (Shahnazari et al., 2013; Sugiyama et al., 2006; Furlan et al., 2007; Kalbasi et al., 2014). *Spp1* (osteopontin, target gene) and *Thbs2* (thrombospondin 2, target gene) regulate aspects of mineralization [Hunter 2013; Alford et al., 2010] and the former was upregulated in our null cell whereas the latter was downregulated (Figures 10C and 10D). Type I collagen (*Col1a1*, target gene) expression was elevated in the *Nmp4*$^{-/-}$ cells throughout the developmental period (Figure 10E). Interestingly, we observed no substantial difference in the expression profiles of *Sp7* (osterix, Figure 10F) or the target gene Runx2 (data not shown), essential transcription factors for osteoblast differentiation (Komori, 2011).

DISCUSSION:

Our findings that the *Nmp4*$^{-/-}$ mice are not protected from ovarectomy-induced bone loss yet maintain the amplified response to PTH therapy is a key advance necessary for further consideration of Nmp4-based treatment strategies. The ovx *Nmp4*$^{-/-}$ mice displayed an enhanced hormone-induced recovery of femoral and L5 trabecular BV/TV despite delaying treatment until 4wks post-op to allow for significant bone loss. Both the ovx WT and ovx *Nmp4*$^{-/-}$ mice showed strong responses to PTH therapy. After 4wks and 8wks of treatment the WT mice displayed a 3.2-fold and 4.6-fold increase in femoral BV/TV over vehicle-treated mice, respectively. However the *Nmp4*$^{-/-}$ mice showed a 3.6-fold and 8.8-fold increase over the same time period resulting in a very strong genotype x treatment interaction. Differences in PTH-mediated BV/TV restoration efficacy between the WT and *Nmp4*$^{-/-}$ mice in the L5 vertebra and was less striking although statistically significant (1.3-fold vs 1.6-fold at 8wks in the WT and *Nmp4*$^{-/-}$ mice, respectively). We observed similar PTH-responsive femoral and L5 profiles between younger, ovary-intact WT and *Nmp4*-null mice [Robling et al., 2009; Childress et al., 2011; He et al., 2013]. The histomorphometry and serum data reported here tracked the PTH-induced increases in bone mass in the ovx animals showing strong treatment effects for bone formation parameters MAR, BFR, and MS/BS (at 4wks treatment) as well as strong increases in bone remodeling serum P1NP and CTX (at 8wks treatment). However, these parameters did not distinguish the genotypes in regards to the amount of bone formed

505 over this time period as was achieved with the μCT data. Interestingly, the histomorphometry data did not
506 distinguish the differences in PTH-induced bone formation in ovary-intact WT and *Nmp4*$^{-/-}$ mice
507 [Childress et al., 2011]. Our present observation that *Nmp4*$^{-/-}$ MSPCs exhibit an accelerated and enhanced
508 mineralization in response to anabolic cues, i.e. osteogenic medium suggests that the augmented bone
509 formation is an early event. Similarly, we did not observe the expected ovx-induced small increase in
510 serum CTX. Instead, the serum data of the vehicle-treated mice showed a large decrease in P1NP and a
511 smaller decrease in CTX over the time course of the entire experiment, i.e. pre-op vs 12wks post-op. This
512 suggests a decrease in bone remodeling in the untreated mice predominantly in the bone formation arm. A
513 more extensive time course with earlier harvest points for histomorphometry and serum samples is
514 required to more fully characterize the anticipated differences in WT and *Nmp4*$^{-/-}$ dynamic bone
515 remodeling.

516 The most robust phenotypic characteristic of Nmp4 ablation is the exaggerated bone formation
517 response to PTH or BMP2, which suggests that the adult mice harbor an increased number of BM MSPCs
518 with heightened sensitivity to osteoanabolic signals. Disabling Nmp4 has no observable impact on
519 embryonic or perinatal skeletal development. Adult MSPCs are a heterogeneous population of
520 multipotent stem, progenitor, and stromal cells that contribute to BM homeostasis [Mizoguchi et al.,
521 2014]. In mouse bone marrow much of the CFU-F activity is in the nestin^{+} cell population and in the
522 human marrow the CD146^{+} population [Mizoguchi et al., 2014; Sacchetti et al., 2007]. In ovary-intact,
523 *Nmp4*$^{-/-}$ mice we observed a 4-fold increase in the frequency of CD45^{-}/CD105^{+}/CD146^{+}/nestin^{+} cells
524 irrespective of treatment (PTH vs vehicle control), which paralleled the magnitude increase in CFU-F and
525 CFU-F$^{\text{alk phos}+}$ cell number in culture [He et al., 2013]. Similarly, the ovx *Nmp4*$^{-/-}$ mice exhibited an
526 approximate 3-fold increase in the CD45^{-}/CD105^{+}/CD146^{+}/nestin^{+} cells at 8wks post-op compared to the
527 ovx WT animals.

528 The enhanced osteogenic potential of the *Nmp4*$^{-/-}$ BM as measured by the frequency of cells
529 capable of becoming osteoprogenitors persists in expanded *Nmp4*$^{-/-}$ MSPC cultures over 5-10 passages
530 and removed from the supporting CD8^{+} T cells. In culture these cells displayed a modest increase in

proliferative activity and perhaps this aspect of the phenotype contributes to the observed expanded pool of osteoprogenitors in vivo. In an earlier study, Noda and colleagues demonstrated that *Nmp4*$^{-/-}$ BM yielded significantly more CFU-F^{Ob} mineralizing colonies at passage P_0 than WT BM [Morinobu et al., 2005]. Our present data extend these observations and show that the serially passaged Nmp4-/- MSPCs maintain a strikingly enhanced capacity for mineralization compared to the capacity of the WT cultures. Taken together these observations suggest that there is a cell autonomous role of Nmp4 for regulating MSPC osteogenesis.

Our -omics data combined with our low-density array results suggest that upon challenge with an anabolic cue *Nmp4*$^{-/-}$ MSPCs produce autocrine/paracrine factors that enhance the replication and differentiation of neighboring osteoprogenitors, a key early event driving the PTH anabolic response [Jilka, 2007]. We observed that once *Nmp4*$^{-/-}$ cells were transferred to osteogenic medium they expressed strikingly elevated levels of the Nmp4 target gene *Igfbp2*, a strong autocrine/paracrine factor that enhances osteogenesis (Xi et al., 2014). Consistent with our observations, overexpression of Igfbp2 in MC3T3-E1 cells accelerated the time course of differentiation and mineralization as well as increased the total number of differentiating cells. By Day 6 in this previous study, Igfbp2-overexpressing cells expressed twice as much osteocalcin as control cultures and this difference persisted [Xi et al., 2014]. This is a strikingly similar phenotype to the *Nmp4*$^{-/-}$ cells. Interestingly, the expression of the Nmp4 target gene *Igfbp4* was decreased in the *null* cells. This binding protein is a strong inhibitor of osteoblast differentiation [Miyakoshi et al., 1999] and thus its suppression may further accelerate and enhance the differentiation of the null cells. Igf1 is a key mediator of the PTH anabolic response [Bikle & Wang, 2012; Elis et al., 2010] and although there was no notable alteration in the expression profiles of *Igf1* or *Igf1r* in the null cells, the expression of *Pdk1*, a target of Nmp4 and a key kinase component of the Igf1/insulin signaling pathway was elevated. This may enhance the sensitivity of the *Nmp4*$^{-/-}$ cells to this growth factor. At the end of the 16-day culture period the *Nmp4*$^{-/-}$ cells exhibited an enhanced anabolic profile as evidenced by the elevated expressions of the non-target Nmp4 genes *Bmp2*, *Pth1r*, and *Bglap*. Perhaps this is an autocrine/paracrine response to the earlier surge in *Igfbp2* expression. Indeed the Igf1

pathway plays a significant role in MSPC proliferation and mineralization [Kumar and Ponnazhagan, 2012; Xian et al., 2012] and the null cells exhibited alterations in the expression not only of *Bglap* but the Nmp4 target extracelluar matrix proteins *Col1a1*, *Spp1*, and *Thbs2*. Although the molecular mechanisms underlying mineralization remain to be elucidated, *Spp1* is an anionic phosphoprotein expressed in mineralizing tissues that appears to regulate crystal size, shape, and location [Hunter, 2013]. *Thbs2* is an extracellular matrix glycoprotein that has pleiotropic effects on bone phenotype. This protein appears to suppress the MSPC osteoprogenitor pool but also supports mineralization [Alford et al., 2010; Hankenson et al., 2002; Hankenson et al., 2000]. Therefore whether the decrease in *Thbs2* expression in the *Nmp4*$^{-/-}$ cells impacts the observed alteration in the number of osteoprogenitors, alterations in mineralization or impacts cell phenotype in other ways remains to be determined. Finally, we observed no striking differences in the expression of the transcription regulators *Sp7* and *Runx2* between the genotypes. This suggests that disabling Nmp4 alters select aspects of the developing osteoblast phenotype.

The dramatic decrease in *Cxcl12* expression in the *Nmp4*$^{-/-}$ cells raises the question as to whether this plays a role in the observed increase in CFU-F$^{alk\ phos+}$ osteoprogenitors in the null mice [He et al., 2013; Morinobu et al., 2005 and the present work]. Cxcl12 and its receptor Cxcr4 play key roles in maintaining the bone marrow niche and Cxcl12 is expressed by bone marrow stromal cells and cells of the osteoblast lineage [Jung et al., 2006; Sugiyama et al., 2006]. Ablation of the receptor Cxcr4 in mature osteoblasts increased the number of CFU-F$^{alk\ phos+}$ osteoprogenitors recovered from these mice although the phenotype also included a decrease in BV/TV [Shahnazari et al., 2013]. Our results suggest that suppressing the expression of the Cxcr4 ligand Cxcl12 results in a similar impact on osteoprogenitor number but a different bone phenotype. The upregulation of *Plaur* expression in the *Nmp4*$^{-/-}$ MSPCs may potentially contribute to the increased number of CFU-F$^{alk\ phos+}$ cells since abrogating the activity of this GPI-anchored receptor suppressed MSPC osteogenic differentiation [Kalbasi et al., 2014]. Finally mutagenesis and rescuing experiments to determine whether the potential targets are truly functionally significant is the next required step for authenticating this new anti-anabolic network.

582 Further parsing of the enhanced *Nmp4*$^{-/-}$ BM osteogenic potential implicates the elevated
583 frequency of CD8^{+} T cells in both ovary-intact and ovx *Nmp4*$^{-/-}$ mice, although this requires functional
584 confirmation in these models. The ovx null animals exhibited elevated numbers of CD8^{+} T cells in both
585 BM and PBL compartments throughout the entire treatment regimen, similar to what we previously
586 observed in the younger ovary-intact *Nmp4*$^{-/-}$ mice, although this increase was limited to the BM [He et al.,
587 2013]. The elevated number of CD8^{+} T cells is intriguing since these cells are documented to amplify the
588 PTH anabolic response [Bedi et al., 2012; Terauchi et al., 2009]. MSPCs regulate T cell proliferation and
589 survival [Wang et al., 2012] and perhaps disabling Nmp4 de-represses this aspect of the cell-cell
590 interaction, although this apparent alteration in proliferation/survival may be a cell autonomous feature of
591 the *Nmp4*$^{-/-}$ T cell phenotype. Although the elevated number of *Nmp4*$^{-/-}$osteoprogenitors declined at 12wks
592 post-op, the higher number of *Nmp4*$^{-/-}$ CD8^{+} T cells did not decrease. Therefore, although the augmented
593 response to PTH might be weakened in the Nmp4$^{-/-}$ mice, it may not disappear since the persistent
594 increased lymphocyte number might provide extra Wnt10b as a potent osteoprogenitor differentiation
595 factor.
596 Why is there typically no difference between the amount of baseline trabecular bone in WT and
597 *Nmp4*$^{-/-}$ mice despite the presence of an expanded pool of osteoprogenitors and CD8^{+} T cells in the null
598 bone marrow? This phenomenon differs from the results of recent clinical trials in which neutralizing
599 sclerostin, an inhibitor of the Wnt signaling pathway and osteoblast differentiation, significantly increases
600 baseline bone mineral density [reviewed in Becker, 2014]. Apparently disabling Nmp4 is not sufficient
601 for driving excess bone formation but instead primes the aforementioned cells for activation by an
602 anabolic cue. The occasionally observed elevated trabecular volume in untreated *Nmp4*$^{-/-}$ mice may be
603 due to the sporadic local release of growth factors, e.g., Igf1, Igfbp2 or Bmp2. However exogenous
604 pharmacological doses of PTH provide a strong stimulus for triggering the response leading to the
605 enhanced bone formation. Once activated by the anabolic cue, the *Nmp4*$^{-/-}$ cells produce the
606 autocrine/paracrine factors that enhance the anabolic response.

607 Consistent with the requirement for a strong anabolic cue to trigger enhanced bone formation in
608 the *Nmp4*$^{-/-}$ mice, disabling this transcription factor did not protect the animals from ovx-induced bone
609 loss, indeed the initial rate of loss during the first 4wks after ovariectomy was higher (L5) or nearly
610 higher (distal femur) in the *Nmp4*$^{-/-}$ mice. These animals harbor a modestly elevated number of osteoclast
611 progenitors (CFU-GM) [He et al., 2013] that upon differentiation exhibit an enhanced bone-resorbing
612 activity in vitro [Childress et al., 2011]. Therefore a decrease in estrogen might accentuate this aspect of
613 the phenotype. Moreover, differences in sex steroid levels may underlie why intact male *Nmp4*$^{-/-}$ mice did
614 not lose bone under hind limb suspension [Hino et al., 2007]. As mentioned, the *Nmp4*$^{-/-}$ baseline
615 phenotype includes an occasional unprovoked enhancement in trabecular architecture, which we observed
616 in the present study. That is to say, despite the elevated initial bone loss, the cohort of sham and ovx
617 *Nmp4*$^{-/-}$ mice had more femoral and L5 trabecular bone compared to WT at the time of harvest (Table 3).
618 However, there was no statistical difference between vehicle-treated animals in either the 4wk or 8wk
619 hormone therapy cohorts (Figures 2 and 3). Longitudinal studies for serum turnover markers coupled with
620 pQCT in live mice could be used to track the real-time dynamics of ovx-induced bone loss and
621 subsequent therapy-induced bone gain between the WT and *Nmp4*$^{-/-}$ mice. In lieu of this, we employed a
622 2-way ANOVA, which incorporates differences in control groups, to evaluate whether there is an
623 interaction between genotype and treatment.
624 The present data also contribute to our knowledge as to how Nmp4 works at the molecular level.
625 Nmp4 binds throughout the genome but is primarily localized to regions near the TSS and within the gene,
626 consistent with mediating a regulatory role. GEM analysis confirmed the AT-rich homopolymeric
627 binding-site and did not identify other consensus sequences expected only if Nmp4 also interacted with
628 the genome indirectly via other DNA-binding proteins. Nmp4 association with the genome is responsive
629 to PTH since hormone decreased genome-wide occupancy in the MC3T3-E1 cells after 1hr of exposure.
630 However, the impact of PTH on Nmp4 occupancy was gene and site-specific and hormone stimulation
631 was observed to induce, remove, or have no effect on Nmp4 genomic occupancy. This may further

augment the fine control that this transcription factor has over the regulation of osteoprogenitor and/or bone-forming capacity.

There is a critical need for osteoanabolic agents [Lewiecki, 2011]. We have taken a two-pronged approach in our research to serve this clinical demand: (1) identify molecular and cellular mechanisms that could be used, for example in an adjuvant setting to promote enhanced efficacy or less frequent dosing with current osteoanabolic agents; and (2) identify innovative approaches to identify new drug targets/pathways or mechanisms of action that would provide needed substrate for the future drug discovery initiatives in bone disease, including osteoporosis. Our discovery-driven approaches have mapped a global network of Nmp4-regulated pathways potentially comprising a bone anti-anabolic axis. Further functional studies charting the hierarchy and interactions of theses network pathways will provide a novel integrated mechanism underlying the natural constraints on bone formation. We postulate that the Nmp4 anti-anabolic network may constitute a novel strategy to identify and reveal pharmacologically accessible pathways for adding new bone to the old skeleton.

Acknowledgements:

This work was supported in part by the Department of Defense (PR120563, JPB); Eli Lilly (062079-00002B, JPB); NIH (CTSI pre-doctoral fellowship TL1 000162, PC)

650 **REFERENCES:**

651

652 Alford AI, Terkhorn SP, Reddy AB, Hankenson KD. 2010 Thrombospondin-2 regulates matrix
653 mineralization in MC3T3-E1 pre-osteoblasts. Bone. 46(2):464-71.

654

655 Alvarez MB, Childress P, Philip BK, Gerard-O'Riley R, Hanlon M, Herbert BS, Robling AG, Pavalko
656 FM, Bidwell JP. 2012 Immortalization and characterization of osteoblast cell lines generated from wild-
657 type and Nmp4-null mouse BM stromal cells using murine telomerase reverse transcriptase (mTERT). J
658 Cell Physiol. 227(5):1873-82.

659

660 Alvarez M, Thunyakitpisal P, Morrison P, Onyia J, Hock J, Bidwell JP. 1998 PTH-responsive osteoblast
661 nuclear matrix architectural transcription factor binds to the rat type I collagen promoter. J Cell Biochem.
662 69(3):336-52

663

664 Auerbach RK, Chen B, Butte AJ. 2013 Relating genes to function: identifying enriched transcription
665 factors using the ENCODE ChIP-Seq significance tool. Bioinformatics. 29(15):1922-4.

666

667 Baron R, Hesse E. 2012 Update on bone anabolics in osteoporosis treatment: rationale, current status, and
668 perspectives. J Clin Endocrinol Metab. 97(2):311-25.

669

670 Becker CB 2014 Sclerostin inhibition for osteoporosis--a new approach. N Engl J Med. 370(5):476-7.

671

672 Bedi B, Li JY, Tawfeek H, Baek KH, Adams J, Vangara SS, Chang MK, Kneissel M, Weitzmann MN,
673 Pacifici R. 2012 Silencing of parathyroid hormone (PTH) receptor 1 in T cells blunts the bone anabolic
674 activity of PTH. Proc Natl Acad Sci U S A. 109(12):E725-33.

675

676 Bidwell JP, Childress P, Alvarez MB, Hood M Jr, He Y, Pavalko FM, Kacena MA, Yang FC. 2012
677 Nmp4/CIZ closes the parathyroid hormone anabolic window. Crit Rev Eukaryot Gene Expr. 22(3):205-18.
678
679 Bikle DD, Wang Y. 2012 Insulin like growth factor-I: a critical mediator of the skeletal response to
680 parathyroid hormone. Curr Mol Pharmacol. 5(2):135-42.
681
682 Black DM, Greenspan SL, Ensrud KE, Palermo L, McGowan JA, Lang TF, Garnero P, Bouxsein ML,
683 Bilezikian JP, Rosen CJ 2003 The effects of parathyroid hormone and alendronate alone or in
684 combination in postmenopausal osteoporosis. N Engl J Med 349: 1207–1215
685
686 Bouxsein ML, Boyd SK, Christiansen BA, Guldberg RE, Jepsen KJ, Müller R. 2010 Guidelines for
687 assessment of bone microstructure in rodents using micro-computed tomography. J Bone Miner Res
688 25:1468–86
689
690 Calleja V, Laguerre M, de Las Heras-Martinez G, Parker PJ, Requejo-Isidro J, Larijani B 2014 Acute
691 regulation of PDK1 by a complex interplay of molecular switches. Biochem Soc Trans. 42(5):1435-40.
692
693 Childress P, Philip BK, Robling AG, Bruzzaniti A, Kacena MA, Bivi N, Plotkin LI, Heller A, Bidwell JP.
694 2011 Nmp4/CIZ suppresses the response of bone to anabolic parathyroid hormone by regulating both
695 osteoblasts and osteoclasts. Calcif Tissue Int. 89(1):74-89.
696
697 Cipriani C, Irani D, Bilezikian JP. 2012 Safety of osteoanabolic therapy: a decade of experience. J Bone
698 Miner Res. 27(12):2419-28.
699

Cosman F, Eriksen EF, Recknor C, Miller PD, Guan˜ abens N, Kasperk C, Papanastasiou P, Readie A, Rao H, Gasser JA, Bucci-Rechtweg C, Boonen S 2011 Effects of intravenous zoledronic acid plus subcutaneous teriparatide [rhPTH(1–34)] in postmenopausal osteoporosis. J Bone Miner Res 26:503–511

Dempster DW, Compston JE, Drezner MK, Glorieux FH, Kanis JA, Malluche H, Meunier PJ, Ott SM, Recker RR, Parfitt AM. 2013 Standardized nomenclature, symbols, and units for bone histomorphometry: a 2012 update of the report of the ASBMR Histomorphometry Nomenclature Committee. J Bone Miner Res. 28(1):2-17. doi: 10.1002/jbmr.1805.

Elis S, Courtland HW, Wu Y, Fritton JC, Sun H, Rosen CJ, Yakar S. 2010 Elevated serum IGF-1 levels synergize PTH action on the skeleton only when the tissue IGF-1 axis is intact. J Bone Miner Res. 25(9):2051-8.

Finkelstein JS, Wyland JJ, Lee H, Neer RM 2010 Effects of teriparatide, alendronate, or both in women with postmenopausal osteoporosis. J Clin Endocrinol Metab 95:1838–1845

Furlan F, Galbiati C, Jorgensen NR, Jensen JE, Mrak E, Rubinacci A, Talotta F, Verde P, Blasi F. 2007 Urokinase plasminogen activator receptor affects bone homeostasis by regulating osteoblast and osteoclast function. J Bone Miner Res. 22(9):1387-96.

Guo Y, Mahony S, Gifford DK 2012 High resolution genome wide binding event finding and motif discovery reveals transcription factor spatial binding constraints. PLoS Computational Biology 8(8): e1002638.

Hankenson KD, Bornstein P 2002 The secreted protein thrombospondin 2 is an autocrine inhibitor of marrow stromal cell proliferation. J Bone Miner Res 17:415–25.

726

727 Hankenson KD, Bain SD, Kyriakides TR, Smith EA, Goldstein SA, Bornstein P 2000 Increased marrow-
728 derived osteoprogenitor cells and endosteal bone formation in mice lacking thrombospondin 2. J Bone
729 Miner Res 15:851–62.

730

731 Harada A, Okada S, Konno D, Odawara J, Yoshimi T, Yoshimura S, Kumamaru H, Saiwai H, Tsubota T,
732 Kurumizaka H, Akashi K, Tachibana T, Imbalzano AN, Ohkawa Y. 2012 Chd2 interacts with H3.3 to
733 determine myogenic cell fate. EMBO J. 31(13):2994-3007.

734

735 He Y, Childress P, Hood M Jr, Alvarez M, Kacena MA, Hanlon M, McKee B, Bidwell JP, Yang FC.
736 2013 Nmp4/CIZ suppresses the parathyroid hormone anabolic window by restricting mesenchymal stem
737 cell and osteoprogenitor frequency. Stem Cells Dev. 22(3):492-500.

738

739 Hino K, Nakamoto T, Nifuji A, Morinobu M, Yamamoto H, Ezura Y, Noda M. 2007 Deficiency of CIZ,
740 a nucleocytoplasmic shuttling protein, prevents unloading-induced bone loss through the enhancement of
741 osteoblastic bone formation in vivo. Bone. 40(4):852-60.

742

743 Huang da W, Sherman BT, Lempicki RA. 2009 Systematic and integrative analysis of large gene lists
744 using DAVID bioinformatics resources. Nat Protoc. 4(1):44-57.

745

746 Hunter GK 2013 Role of osteopontin in modulation of hydroxyapatite formation. Calcif Tissue Int.
747 93(4):348-54.

748

749 Isern J, Martín-Antonio B, Ghazanfari R, Martín AM, López JA, del Toro R, Sánchez-Aguilera A, Arranz
750 L, Martín-Pérez D, Suárez-Lledó M, Marín P, Van Pel M, Fibbe WE, Vázquez J, Scheding S, Urbano-

751 Ispizúa Á, Méndez-Ferrer S. 2013 Self-renewing human bone marrow mesenspheres promote
752 hematopoietic stem cell expansion. Cell Rep. 3(5):1714-24.
753
754 Jilka RL 2007 Molecular and cellular mechanisms of the anabolic effect of intermittent PTH. Bone. 2007
755 40(6):1434-46.
756 Kalbasi Anaraki P, Patecki M, Larmann J, Tkachuk S, Jurk K, Haller H, Theilmeier G, Dumler I. 2014
757 Urokinase receptor mediates osteogenic differentiation of mesenchymal stem cells and vascular
758 calcification via the complement C5a receptor. Stem Cells Dev. 23(4):352-62.
759
760 Jung Y, Wang J, Schneider A, Sun YX, Koh-Paige AJ, Osman NI, McCauley LK, Taichman RS 2006
761 Regulation of SDF-1 (CXCL12) production by osteoblasts; a possible mechanism for stem cell homing.
762 Bone 38: 497–508
763
764 Komori T. 2011 Signaling networks in RUNX2-dependent bone development. J Cell Biochem.
765 112(3):750-5.
766
767 Kraenzlin ME, Meier C. 2011 Parathyroid hormone analogues in the treatment of osteoporosis. Nat Rev
768 Endocrinol. 7(11):647-56.
769
770 Krane SM. 2005 Identifying genes that regulate bone remodeling as potential therapeutic targets. J Exp
771 Med. 201(6):841-3.
772
773 Kumar S, Ponnazhagan S. 2012 Mobilization of bone marrow mesenchymal stem cells in vivo augments
774 bone healing in a mouse model of segmental bone defect. Bone 50(4):1012-8.
775

776 Lewiecki EM 2011 New targets for intervention in the treatment of postmenopausal osteoporosis Nature
777 Reviews Rheumatology 7:631-638
778
779 Li H and Durbin R 2009 Fast and accurate short read alignment with Burrows-Wheeler Transform.
780 Bioinformatics, 25:1754-60.
781
782 Li JY, Walker LD, Tyagi AM, Adams J, Weitzmann MN, Pacifici R. 2014 The sclerostin-independent
783 bone anabolic activity of intermittent PTH treatment is mediated by T-cell-produced Wnt10b. J Bone
784 Miner Res. 29(1):43-54.
785
786 Lin W, Srajer G, Evrard YA, Phan HM, Furuta Y, Dent SY. 2007 Developmental potential of Gcn5(−/−)
787 embryonic stem cells in vivo and in vitro. Dev Dyn. 236:1547–1557.
788
789 McClung MR, Grauer A, Boonen S, Bolognese MA, Brown JP, Diez-Perez A, Langdahl BL, Reginster
790 JY, Zanchetta JR, Wasserman SM, Katz L, Maddox J, Yang YC, Libanati C, Bone HG. 2014
791 Romosozumab in postmenopausal women with low bone mineral density. N Engl J Med. 370(5):412-20.
792
793 Méndez-Ferrer S, Michurina TV, Ferraro F, Mazloom AR, Macarthur BD, Lira SA, Scadden DT,
794 Ma'ayan A, Enikolopov GN, Frenette PS. 2010 Mesenchymal and haematopoietic stem cells form a
795 unique bone marrow niche. Nature. 466(7308):829-34.
796
797 Miyakoshi N, Richman C, Qin X, Baylink DJ, Mohan S 1999 Effects of recombinant insulin-like growth
798 factor-binding protein-4 on bone formation parameters in mice. Endocrinology 140: 5719–5728
799

800 Mizoguchi T, Pinho S, Ahmed J, Kunisaki Y, Hanoun M, Mendelson A, Ono N, Kronenberg HM,
801 Frenette PS. 2014 Osterix marks distinct waves of primitive and definitive stromal progenitors during
802 bone marrow development. Dev Cell. 29(3):340-9.
803
804 Morinobu M, Nakamoto T, Hino K, Tsuji K, Shen ZJ, Nakashima K, Nifuji A, Yamamoto H, Hirai H,
805 Noda M. 2005 The nucleocytoplasmic shuttling protein CIZ reduces adult bone mass by inhibiting bone
806 morphogenetic protein-induced bone formation. J Exp Med. 201(6):961-70.
807
808 Nakamoto T, Shiratsuchi A, Oda H, Inoue K, Matsumura T, Ichikawa M, Saito T, Seo S, Maki K, Asai T,
809 Suzuki T, Hangaishi A, Yamagata T, Aizawa S, Noda M, Nakanishi Y, Hirai H. 2004 Impaired
810 spermatogenesis and male fertility defects in CIZ/Nmp4-disrupted mice. Genes Cells 9(6):575-89.
811
812 Nakamoto T, Yamagata T, Sakai R, Ogawa S, Honda H, Ueno H, Hirano N, Yazaki Y, Hirai H. 2000 CIZ,
813 a zinc finger protein that interacts with p130(cas) and activates the expression of matrix
814 metalloproteinases. Mol Cell Biol. 20(5):1649-58
815
816 Nascimento EM, Cox CL, MacArthur S, Hussain S, Trotter M, Blanco S, Suraj M, Nichols J, Kübler B,
817 Benitah SA, Hendrich B, Odom DT, Frye M. 2011 The opposing transcriptional functions of Sin3a and c-
818 Myc are required to maintain tissue homeostasis. Nat Cell Biol. 13(12):1395-405.
819
820 D. Padhi, G. Jang, B. Stouch, L. Fang, E. Posvar 2011 Single-dose, placebo-controlled, randomized study
821 of AMG 785, a sclerostin monoclonal antibody J Bone Miner Res, 26: 19–26
822
823 Robling AG, Childress P, Yu J, Cotte J, Heller A, Philip BK, Bidwell JP. 2009 Nmp4/CIZ suppresses
824 parathyroid hormone-induced increases in trabecular bone. J Cell Physiol. 219(3):734-43.
825

826 Rosenbloom KR, Sloan CA, Malladi VS, Dreszer TR, Learned K, Kirkup VM, Wong MC, Maddren M,
827 Fang R, Heitner SG, Lee BT, Barber GP, Harte RA, Diekhans M, Long JC, Wilder SP, Zweig AS,
828 Karolchik D, Kuhn RM, Haussler D, Kent WJ. 2013 ENCODE data in the UCSC Genome Browser: year
829 5 update. Nucleic Acids Res. 41(Database issue):D56-63.
830
831 Saag KG, Zanchetta JR, Devogelaer JP, Adler RA, Eastell R, See K, Krege JH, Krohn K, Warner MR.
832 2009 Effects of teriparatide versus alendronate for treating glucocorticoid-induced osteoporosis: thirty-
833 six-month results of a randomized, double-blind, controlled trial. Arthritis Rheum. 60(11):3346-55.
834
835 Sacchetti B, Funari A, Michienzi S, Di Cesare S, Piersanti S, Saggio I, Tagliafico E, Ferrari S, Robey PG,
836 Riminucci M, Bianco P. 2007 Self-renewing osteoprogenitors in bone marrow sinusoids can organize a
837 hematopoietic microenvironment. Cell. 131(2):324-36
838
839 Shah R, Alvarez M, Jones DR, Torrungruang K, Watt AJ, Selvamurugan N, Partridge NC, Quinn CO,
840 Pavalko FM, Rhodes SJ, Bidwell JP. 2004 Nmp4/CIZ regulation of matrix metalloproteinase 13 (MMP-
841 13) response to parathyroid hormone in osteoblasts. Am J Physiol Endocrinol Metab. 287(2):E289-96.
842
843 Shahnazari M, Chu V, Wronski TJ, Nissenson RA, Halloran BP 2013 CXCL12/CXCR4 signaling in the
844 osteoblast regulates the mesenchymal stem cell and osteoclast lineage populations. FASEB J. 27(9):3505-
845 13.
846
847 Shen ZJ, Nakamoto T, Tsuji K, Nifuji A, Miyazono K, Komori T, Hirai H, Noda M. 2002 Negative
848 regulation of bone morphogenetic protein/Smad signaling by Cas-interacting zinc finger protein in
849 osteoblasts. J Biol Chem. 277(33):29840-6.
850

851 Stamatoyannopoulos JA, et al., [Mouse ENCODE Consortium] 2012 An encyclopedia of mouse DNA
852 elements (Mouse ENCODE). Genome Biol. 13(8):418.
853
854 Sugiyama T., Kohara H., Noda M., Nagasawa T 2006 Maintenance of the hematopoietic stem cell pool by
855 CXCL12-CXCR4 chemokine signaling in bone marrow stromal cell niches. Immunity 25: 977–988
856
857 Supek F, Bošnjak M, Škunca N, Šmuc T. 2011 REVIGO summarizes and visualizes long lists of gene
858 ontology terms. PLoS One. 6(7):e21800.
859
860 Terauchi M, Li JY, Bedi B, Baek KH, Tawfeek H, Galley S, Gilbert L, Nanes MS, Zayzafoon M,
861 Guldberg R, Lamar DL, Singer MA, Lane TF, Kronenberg HM, Weitzmann MN, Pacifici R. 2009 T
862 lymphocytes amplify the anabolic activity of parathyroid hormone through Wnt10b signaling. Cell Metab.
863 10(3):229-40.
864
865 Thunyakitpisal P, Alvarez M, Tokunaga K, Onyia JE, Hock J, Ohashi N, Feister H, Rhodes SJ, Bidwell
866 JP. 2001 Cloning and functional analysis of a family of nuclear matrix transcription factors (NP/NMP4)
867 that regulate type I collagen expression in osteoblasts. J Bone Miner Res. 16(1):10-23
868
869 Torrungruang K, Alvarez M, Shah R, Onyia JE, Rhodes SJ, Bidwell JP. 2002 DNA binding and gene
870 activation properties of the Nmp4 nuclear matrix transcription factors. J Biol Chem. 277(18):16153-9.
871
872 Vieira Potter VJ, Strissel KJ, Xie C, Chang E, Bennett G, Defuria J, Obin MS, Greenberg AS. 2012
873 Adipose tissue inflammation and reduced insulin sensitivity in ovariectomized mice occurs in the absence
874 of increased adiposity. Endocrinology. 153(9):4266-77.
875

876 Wang L, Zhao Y, Shi S. 2012 Interplay between mesenchymal stem cells and lymphocytes: implications
877 for immunotherapy and tissue regeneration. J Dent Res. 91(11):1003-10.
878
879 Wu X, Estwick SA, Chen S, Yu M, Ming W, Nebesio TD, Li Y, Yuan J, Kapur R, Ingram D, Yoder MC,
880 Yang FC. 2006 Neurofibromin plays a critical role in modulating osteoblast differentiation of
881 mesenchymal stem/progenitor cells. Hum Mol Genet. 15(19):2837-45.
882
883 Xi G, Wai C, DeMambro V, Rosen CJ, Clemmons DR 2014 IGFBP-2 directly stimulates osteoblast
884 differentiation. J Bone Miner Res. 29(11):2427-38
885 Xian L, Wu X, Pang L, Lou M, Rosen CJ, Qiu T, Crane J, Frassica F, Zhang L, Rodriguez JP, Xiaofeng
886 Jia, Shoshana Yakar, Shouhong Xuan, Argiris Efstratiadis, Mei Wan, Xu Cao. 2012 Matrix IGF-1
887 maintains bone mass by activation of mTOR in mesenchymal stem cells. Nat Med. 18(7): 1095-101.
888
889 Yang Z, Bidwell JP, Young SR, Gerard-O'Riley R, Wang H, Pavalko FM. 2010 Nmp4/CIZ inhibits
890 mechanically induced beta-catenin signaling activity in osteoblasts. J Cell Physiol. 223(2):435-41.
891
892 Yu EW, Neer RM, Lee H, Wyland JJ, de la Paz AV, Davis MC, Okazaki M, Finkelstein JS. 2011 Time-
893 dependent changes in skeletal response to teriparatide: escalating vs. constant dose teriparatide (PTH 1-
894 34) in osteoporotic women. Bone. 48(4):713-9.
895
896

FIGURE LEGENDS

Figure 1: Schematic of treatment regimen for WT and *Nmp4*$^{-/-}$ mice; Group 1 mice were subjected to ovariectomy (ovx) or sham operation at 12wks of age and evaluated for bone loss 4wks post-op (16wks of age). Group 2 mice were ovx at 12wks of age and began PTH or vehicle therapy at 16wks of age for a duration of 4wks and 8wks. Endpoint analyses included micro–computed tomography μCT, serum analysis for N-terminal propeptide of type 1 procollagen (P1NP) and C-terminal telopeptides (CTX), and dynamic histomorphometry.

Figure 2: Disabling Nmp4 enhances PTH restorative therapy in the distal femur of ovx *Nmp4*$^{-/-}$ mice [A] Interaction plots of femoral trabecular bone volume/total volume (BV/TV) of ovx WT and ovx *Nmp4*$^{-/-}$ mice as determined by μCT at 4wks of treatment and 8wks of treatment. Data are average ± SD, number of mice/experimental group = 8-9). Statistical differences were determined using a 2-way ANOVA and significance was set at $p \leq 0.05$. The Tukey's HSD post hoc test was used to determine differences between the treatment groups. There were genotype, treatment and genotype x treatment interaction at both time points. There was no difference between the vehicle-treated WT and *Nmp4*$^{-/-}$ mice. [B] μCT images showing PTH-induced improvements in distal femur trabecular architecture in ovx WT and *Nmp4*$^{-/-}$ mice after 8 weeks of treatment (12wks post-op, 24wks of age).

Figure 3: The exaggerated response to anabolic PTH persists in the L5 vertebra of ovx *Nmp4*$^{-/-}$ mice. [A] Interaction plots of L5 vertebra bone volume/total volume (BV/TV) of ovx WT and ovx *Nmp4*$^{-/-}$ mice as determined by μCT at 4wks of treatment and 8wks of treatment. Data are average ± SD, number of mice/experimental group = 8-9). Statistical differences were determined using a 2-way ANOVA and significance was set at $p \leq 0.05$. The LS Means Student t post hoc test was used to determine differences between the treatment groups. There were genotype, treatment effects at both time points and a genotype x treatment interaction at 8wks therapy. There was no difference between the vehicle-treated WT and

Nmp4$^{-/-}$ mice. [B] µCT images showing PTH-induced improvements in L5 trabecular architecture in ovx WT and *Nmp4*$^{-/-}$ mice after 8 weeks of treatment (12wks post-op, 24wks of age).

Figure 4: Ovx does not abrogate the expanded population of osteoprogenitors and CD8+ T cells in *Nmp4*$^{-/-}$ mice. FACS analysis of BM and PBL osteoprogenitors, CD8+ T cells, and CD4+ T cells. [A, D] The frequency of femoral BM and PBL CD45-/CD105+/CD146+/CD105+/nestin+ osteoprogenitor cells in WT and *Nmp4*$^{-/-}$ mice at the end of 4wks and 8wks treatment with intermittent PTH or vehicle control; [B, E] the frequency of BM and PBL CD8+ T cells from the WT and *Nmp4*$^{-/-}$ mice; [C, F] the frequency of BM and PBL CD4+ T cells from the WT and null mice. Data are average ± SD, number of mice/experimental group = 8–9; Statistical differences were determined using a 2-way ANOVA and significance was set at $p \leq 0.05$.

Figure 5: Expanded *Nmp4*$^{-/-}$ MSPCs exhibit enhanced proliferation and mineralization in culture. [A] Comparative growth rates of expanded WT and *Nmp4*$^{-/-}$ MSPCs. Cell counts/day (n=4 lines per genotype log10 cells/well, 3 wells/sample, average ± SD, t test, $t<0.05$). Note: each 'line' is derived from a single mouse [B] Alkaline phosphatase (alk phos) and alizarin red staining of a WT and *Nmp4*$^{-/-}$ MSPC cultures from Day7-Day28. See text for details

Figure 6: Nmp4 associates with core target genes common to multiple cell types and acts as a *negative regulation of cellular biosynthetic processes* [A] Venn diagram illustrating the shared Nmp4 target genes in the MC3T3-E1 osteoblast-like cells (vehicle-treated), and the three ENCODE cells lines, ES-E14 (embryonic stem cells), MEL, and CH12 cells (B-cell lymphomas). [B] DAVID/REVIGO gene ontology (GO) profile of Nmp4 core target genes

Figure 7: Nmp4 binds to AT-rich DNA typically proximal to TSS sites or within intragenic regions. [A] Genome-wide mapping of the Nmp4 binding sites show that most sites are distributed in the TSS and

intragenic regions of the genome. ChIP-seq analysis included vehicle-treated and PTH-treated MC3T3-E1 osteoblast-like cells (vMC and pMC, respectively) and three murine cell lines from the ENCODE Consortium including ES-E14 (Es14), which are E14 undifferentiated mouse embryoinic stem cells, and two mouse erythroleukemia cell lines (Ch12 and MEL) derived from B-cell lymphomas. [B] GEM analysis for the Nmp4 consensus sequence derived from MC3T3-E1 cells. A minimal k-mer width of 6 and maximum of 20 were used. The optimal position weight matrix (PWM) score for the MC3T3-E1 data was 10.07. The hypergeometric P-value (hgp) was 1e-1466.1.

Figure 8: ChIP-seq reveals Nmp4 binding profiles at specific gene loci. Mouse MC3T3-E1 cells were seeded into twenty-one 150mm plates at an initial density of 50,000 cells/plate (320 cells/cm^2) and maintained in αMEM complete medium + ascorbic acid for 14 days. Prior to harvest cells were treated with 25nM hPTH(1-34) or vehicle control for 1hr. Processing for ChIP-seq analysis was performed as described in the Materials and Methods. Sequences (50nt reads, single end) were aligned to the mouse genome (mm10) using the BWA algorithm. Alignments were extended in silico at their 3'-ends to a length of 150bp, which is the average genomic fragment length in the size-selected library, and assigned to 32-nt bins along the genome. Nmp4 (Znf384) peak locations were determined using the MACS algorithm (v1.4.2) with a cutoff of pvalue = 1e-7. The genomic loci including the chromosome number and nucleotide interval are indicated. Read scales are indicated on the Y-axis. An arrow indicates the transcriptional start sites and direction of transcription for each of the genes; vertical boxes within the gene indicate exons. The Nmp4 ChIP-seq gene profiles include (A) *Nid2* (B) *Akt2*, (C) *Pdk1* (D) *ccdc53*, (E) *Arrb2* and (F) *Irs1*. The input DNA profiles were devoid of peaks.

Figure 9: Comparison of mRNA expression profiles derived from non-differentiating (Day 3) and osteogenic-differentiating (Days 5-16) WT and *Nmp4*$^{-/-}$ cells. All transcript levels are compared to WT Day 3 providing a time course of expression. mRNA profiles [A] *Igfbp2*; [B] *Igfbp4;* [C] *Pdk1*; [D] *Bmp2*; [E] *Pth1r* were derived from the TLDA system (Format 96a, Applied Biosystems, Foster City,

CA) performed on a QuantStudio™ 7 Flex Real-Time PCR System and normalized with GusB. Profile [F] *Bglap* mRNA profile qRT-PCR reactions were performed on an Eppendorf Mastercycler® RealPlex^2 using *Rplp2* as the normalizer as previously described [Robling et al, 2009]. Comparison of profiles using *GusB* and *Rplp2* as the normalizer showed no differences in the shape of the expression profiles

Figure 10: Comparison of mRNA expression profiles derived from non-differentiating (Day 3) and osteogenic-differentiating (Days 5-16) WT and *Nmp4*$^{-/-}$ cells. All transcript levels are compared to WT Day 3 providing a time course of expression. mRNA profiles [A] *Cxcl12*; [B] *Plaur;* [C] *Spp1*; [D] *Thbs2*; [E] *Col1a1* were derived from the TLDA system (Format 96a, Applied Biosystems, Foster City, CA) performed on a QuantStudio™ 7 Flex Real-Time PCR System and normalized with GusB. Profile [F] *Sp7* mRNA profile qRT-PCR reactions were performed on an Eppendorf Mastercycler® RealPlex^2 using *Rplp2* as the normalizer as previously described [Robling et al., 2009]. The Day 16 WT sample is the average of two replicates. Comparison of profiles using GusB and Rplp2 as the normalizer showed no differences in the shape of the expression profiles

Supplemental Figure S1: qRT-PCR validates the ChIP-seq profiles. [A] The Nmp4 ChIP-seq profile for the gene *Col1a1*. The genomic loci including the chromosome number and nucleotide interval are indicated. Read scale is indicated on the Y-axis. An arrow marks the transcriptional start site and direction of transcription; vertical boxes within the gene identify exons. [B] qRT-PCR was used to authenticate the ChIP-seq peaks as described in the Materials and Methods.

Supplemental Figure 2: Volcano plots derived from gene expression profiles of non-differentiating (Day 3) and osteogenic-differentiating (Days 5-16) WT and *Nmp4*$^{-/-}$ as described in the Materials and Methods. RNA expression profiling was performed on a QuantStudio™ 7 Flex Real-Time PCR System and data analyzed using the ExpressionSuite v1.0.4™ analysis software (Applied Biosystems) as described in the Materials and Methods. [A] WT vs *Nmp4*$^{-/-}$ cells at Day 3 post-seeding. mRNA transcript expression was

compared to WT cells (Day 3). Cells maintained in Mesencult™ Media + Mesencult™ Stimulatory Supplement. [B] WT vs *Nmp4*$^{-/-}$ cells at Day 5 post-seeding. mRNA transcript expression was compared to WT cells (Day 5). Cells maintained in differentiation medium for 48hrs [C] WT vs *Nmp4*$^{-/-}$ cells at Day 7 post-seeding. mRNA transcript expression was compared to WT cells (Day 7). Cells maintained in differentiation medium for 96hrs [D] WT vs *Nmp4*$^{-/-}$ cells at Day 9 post-seeding. mRNA transcript expression was compared to WT cells (Day 9). Cells maintained in differentiation medium for 144hrs [E] WT vs *Nmp4*$^{-/-}$ cells at Day 16 post-seeding. mRNA transcript expression was compared to WT cells (Day 16). Cells maintained in differentiation medium for 192hrs. Genes indicated with green dots (left of center) and above the X-axis exhibited a significant downregulation by over 2-fold. Genes indicated with the red dots (right of center) and above the X-axis exhibited a significant upregulation by over 2-fold.

Supplemental TABLE 1: 96 Nmp4 'core' target genes, non-core target genes, and non-target genes including 5 candidate normalizer genes. Individual cDNAs were quantified by qRT-PCR using a custom TLDA system (Format 96a, Applied Biosystems, Foster City, CA) as described in the Materials and Methods on a QuantStudio™ 7 Flex Real-Time PCR System. We used the ExpressionSuite v1.0.4™ analysis software (Applied Biosystems) to analyze these data.

Supplemental TABLE 2: 2114 Nmp4 'core' target genes common to the four cell lines MC3T3-E1 osteoblast-like cells, and three murine cell lines from the ENCODE Consortium including ES-E14 (Es14), which are E14 undifferentiated mouse embryoinic stem cells, and two mouse erythroleukemia cell lines (Ch12 and MEL) derived from B-cell lymphomas.

Supplemental TABLE 3: IPA analysis of 2114 Nmp4 'core' target genes common to the four cell lines MC3T3-E1 osteoblast-like cells, and three murine cell lines from the ENCODE Consortium including ES-E14 (Es14), which are E14 undifferentiated mouse embryoinic stem cells, and two mouse erythroleukemia cell lines (Ch12 and MEL) derived from B-cell lymphomas.

Table 1

Click here to download Table: TABLE 1 rev.docx

Table 1: Bone loss data.

	WT		*Nmp4*$^{-/-}$		2-WAY ANOVA p-values		
	SHAM	OVX	SHAM	OVX	Genotype	Treatment	Gene x Treat
%Δ Body weight	2.48±7.73	8.65±5.48	4.14±4.70	5.66±2.94	0.69	0.03	0.17
Uterine weight (g)	0.10±0.05	0.04±0.02	0.10±0.02	0.05±0.02	0.30	<0.0001	0.34
Distal Femur							
BV/TV	0.019±0.004	0.012±0.004	0.038±0.011	0.021±0.010	<0.0001	<0.0001	0.06
SMI	3.818±0.250	4.055±0.357	3.387±0.263	3.810±0.294	0.0008	0.0011	0.32
Tb.N (mm^{-1})	2.554±0.239	2.165±0.385	3.128±0.218	2.797±0.276	<0.0001	0.0004	0.76
Tb.Th (mm)	0.040±0.005	0.041±0.005	0.039±0.003	0.037±0.004	0.08	0.87	0.23
Tb.Sp (mm)	0.393±0.036	0.477±0.097	0.317±0.026	0.359±0.037	<0.0001	0.0012	0.25
L5 Vertebra							
BV/TV	0.189±0.028	0.177±0.013	0.253±0.019	0.212±0.019	<0.0001	0.0004	0.05
Tb.N (mm^{-1})	3.797±0.513	3.580±0.285	4.491±0.345	4.022±0.254	<0.0001	0.0091	0.32
Tb.Th (mm)	0.050±0.003	049±0.002	0.056±0.002	0.053±0.002	<0.0001	0.0032	0.02
Tb.Sp (mm)	0.227±0.023	0.229±0.013	0.202±0.020	0.214±0.012	0.0013	0.25	0.44

Serum P1NP	WT : *Nmp4*$^{-/-}$			p-values [G; T; G x T]^{4wks}	p-values [G; T; G x T]^{12wks}
	Pre-op	Post-op^{4wks}	Post-op^{12wks}		
	5.62±1.21 : 6.02±1.41	5.83±1.41 : 4.77±1.22	3.15±0.65 : 2.81±0.76	0.34; 0.16; 0.05	0.95; <0.0001; 0.36

Serum CTX	WT : *Nmp4*$^{-/-}$			p-values [G; T; G x T]^{4wks}	p-values [G; T; G x T]^{12wks}
	Pre-op	Post-op^{4wks}	Post-op^{12wks}		
	13.66±2.43 : 13.37±1.88	12.96±3.04 : 13.53±2.58	11.47±2.24 : 9.36±1.22	0.92; 0.46; 0.96	0.14; 0.0003; 0.18

The % change body weight, uterine weight, and microCT of distal femur and L5 vertebra from WT and *Nmp4*$^{-/-}$ mice after ovx or sham operation 4wks post-op. Serum bone formation [P1NP] and bone resorption [CTX] marker levels were compared in mice previous to the operation (Pre-op) and 4wks and 12wks subsequent to surgery (Post-op). The 12wks post-op data was obtained from the vehicle-control treatment groups. Data are average ± SD, number of mice/experimental group=8-14 [4 mice in WT SHAM uterine weight]). Statistical significance was set at $p \leq 0.05$ and differences were determined using a 2-way ANOVA.

Table 2

Click here to download Table: TABLE 2.docx

Table 2: PTH-induced bone gain data.

	WT		*Nmp4*$^{-/-}$		2-WAY ANOVA p-values		
Distal Femur							
4wks	VEH	PTH	VEH	PTH	Genotype	Treatment	Gene x Treat
Conn D (mm^{-3})	3.180±3.870	33.230±26.730	9.681±15.979	67.533±14.111	0.0018	<0.0001	0.03
SMI	3.752±0.437	3.013±0.384	3.472±0.327	2.514±0.113	0.0025	<0.0001	0.36
Tb.N (mm^{-1})	2.100±0.519	2.441±0.281	2.712±0.241	2.833±0.224	0.0002	0.06	0.36
Tb.Th (mm)	0.039±0.010	0.042±0.007	0.033±0.003	0.044±0.003	0.54	0.004	0.09
Tb.Sp (mm)	0.510±0.157	0.409±0.051	0.370±0.036	0.342±0.032	0.0019	0.04	0.24
8wks							
Conn D (mm^{-3})	3.123±5.307	38.658±14.910	0.982±1.103	58.128±13.570	0.03	<0.0001	0.0064
SMI	3.808±0.479	2.470±0.284	3.589±0.218	2.262±0.141	0.05	<0.0001	0.96
Tb.N (mm^{-1})	2.132±0.297	2.164±0.431	2.286±0.145	2.552±0.277	0.02	0.17	0.28
Tb.Th (mm)	0.037±0.006	0.048±0.005	0.030±0.004	0.049±0.003	0.12	<0.0001	0.02
Tb.Sp (mm)	0.476±0.072	0.471±0.109	0.438±0.033	0.378±0.045	0.01	0.20	0.27
L5 Vertebra							
4wks	VEH	PTH	VEH	PTH	Genotype	Treatment	Gene x Treat
Tb.N (mm^{-1})	3.453±0.451	4.875±0.587	3.891±0.504	5.518±0.381	0.0049	<0.0001	0.56
Tb.Th (mm)	0.051±0.002	0.049±0.002	0.054±0.004	0.051±0.001	0.04	0.03	0.60
Tb.Sp (mm)	0.246±0.021	0.224±0.030	0.229±0.021	0.197±0.021	0.02	0.0036	0.52
8wks							
Tb.N (mm^{-1})	4.046±0.917	5.648±1.191	3.627±0.235	5.906±0.754	0.79	<0.0001	0.26
Tb.Th (mm)	0.053±0.003	0.049±0.004	0.055±0.001	0.054±0.001	0.0018	0.0044	0.09
Tb.Sp (mm)	0.239±0.021	0.206±0.037	0.256±0.020	0.186±0.023	0.86	<0.0001	0.05

MicroCT (distal femur and L5 vertebra) from ovx WT and ovx *Nmp4*$^{-/-}$ mice after 4 wks and 8wks PTH/VEH therapy. Data are average ± SD, number of mice/experimental group = 8-9. Statistical significance was set at $p \leq 0.05$ and differences were determined using a 2-way ANOVA.

Table 3
Click here to download Table: TABLE 3.docx

Table 3: Histomorphometry and serum analyses.

	WT		*Nmp4*$^{-/-}$		2-WAY ANOVA p-values		
	VEH	PTH	VEH	PTH	Genotype	Treatment	Gene x Treat
Dynamic histo							
MAR (µm/day)	2.28±0.37	3.80±0.73	2.29±0.37	3.61±0.40	0.70	<0.0001	0.66
MS/BS (%)	0.41±0.09	0.55±0.05	0.44±0.10	0.52±0.06	0.98	0.01	0.45
BFR (µm^2/µm/day)	0.95±0.28	2.09±0.52	1.01±0.25	1.86±0.22	0.60	<0.0001	0.37

Serum	WT		*Nmp4*$^{-/-}$		2-WAY ANOVA p-values		
	VEH^{8wks}	PTH^{8wks}	VEH^{8wks}	PTH^{8wks}	Genotype	Treatment	Gene x Treat
P1NP (ng/ml)	3.147±0.653	10.066±2.659	2.806±0.760	8.042±3.304	0.19	<0.0001	0.34
CTX (ng/ml)	11.466±2.239	15.147±3.518	9.361±1.222	14.157±1.532	0.12	0.0002	0.56

Dynamic bone histomorphometry data of the distal femur from WT and *Nmp4*$^{-/-}$ mice treated with intermittent PTH or vehicle for 4wks (8wks post-op). Sera data were collected at the end of 8wks treatment (12wks post-op). The parameters include mineral apposition rate (MAR), mineralizing surface/bone surface (MS/BS), and bone formation rate (BFR). Data are average ± SD, number of mice/experimental group = 4-7. A 2-way ANOVA was used to determine statistical differences and significance was set at $p \leq 0.05$.

Table 4
Click here to download Table: TABLE 4.docx

Table 4: ENCODE ChIP-Seq Significance Tool profile for enriched transcription factors [TFs] within the Nmp4 target core gene list

Factor	Q-value*	Factor	Q-value
Nmp4	0.00E+00	Max	0.00E+00
CHD2	0.00E+00	Mxi1	0.00E+00
CTCF	0.00E+00	NELFe	0.00E+00
GCN5	0.00E+00	Pol2	0.00E+00
HCFC1	0.00E+00	SIN3A	0.00E+00
MAZ	0.00E+00	TBP	0.00E+00
p300	0.00E+00	c-Myc	7.352e-317

* Hypergeometric test; Benjamini-Hochberg; (select TFs from 72 entries).

Table 5
Click here to download Table: TABLE 5.docx

Table 5: DAVID profile of KEGG pathway mapping.

GO Term Pathways	FDR
TOR signaling pathway	0.003
Insulin signaling pathway	0.004
Chronic myeloid leukemia	0.026
JAK-STAT signaling pathway	0.026
Neurotrophin signaling pathway	0.034

Only pathways with an FDR of $p<0.05$ are listed

Figure 1
Click here to download Figure: FIGURE 1.tif

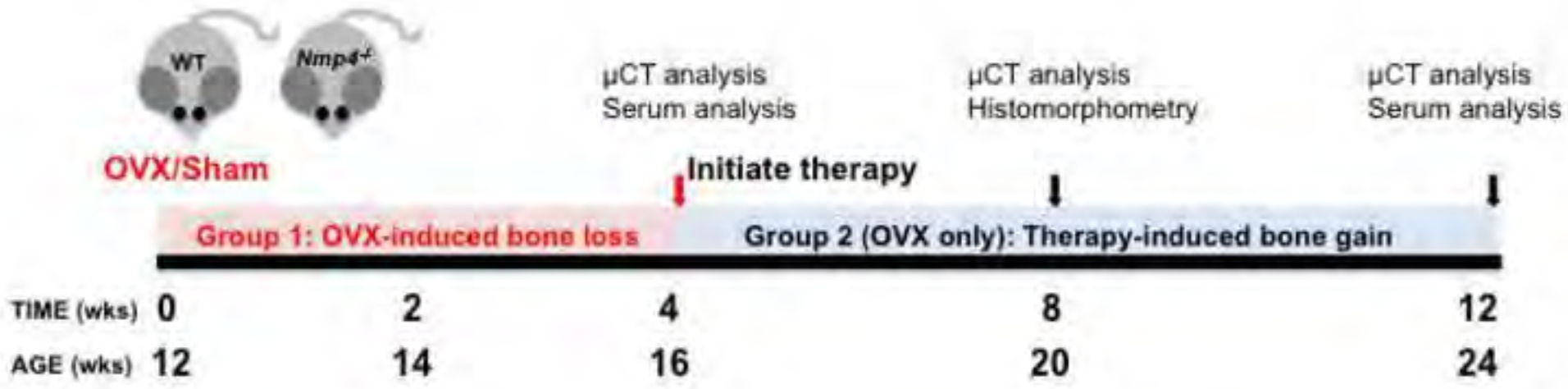

Figure 2
Click here to download Figure: FIGURE 2.tif

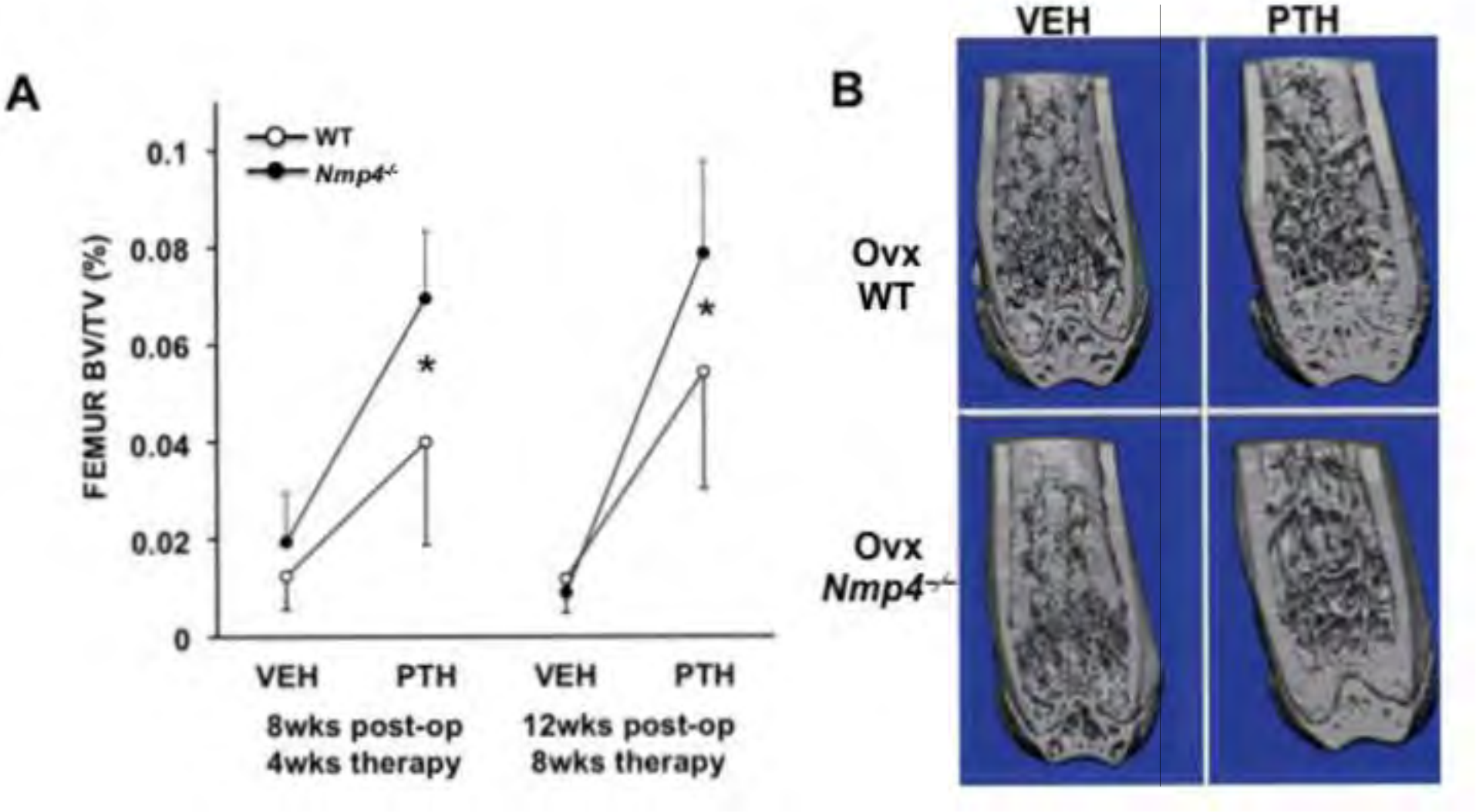

Figure 3
Click here to download Figure: FIGURE 3.tif

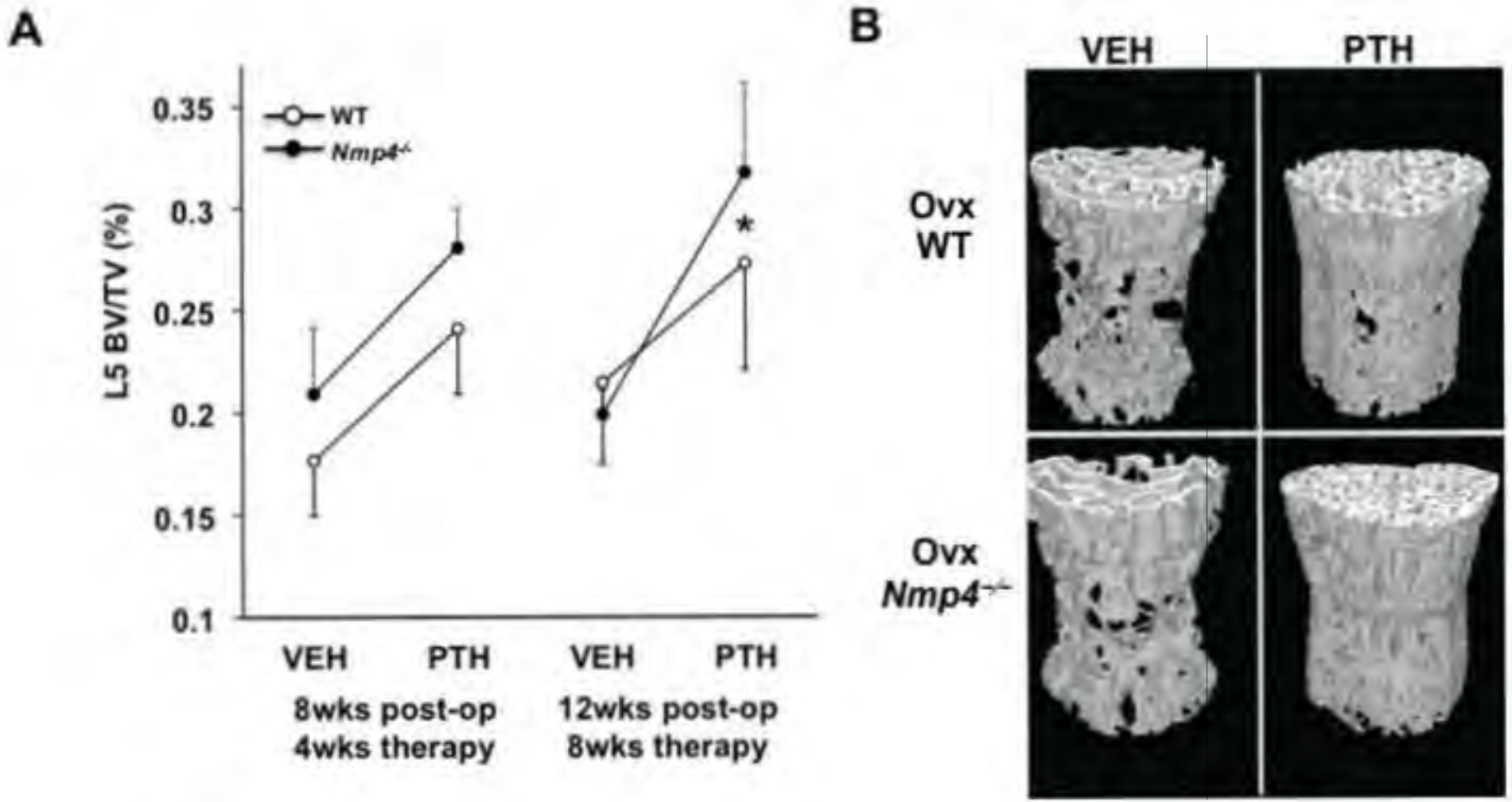

Figure 4

Click here to download Figure: FIGURE 4.tif

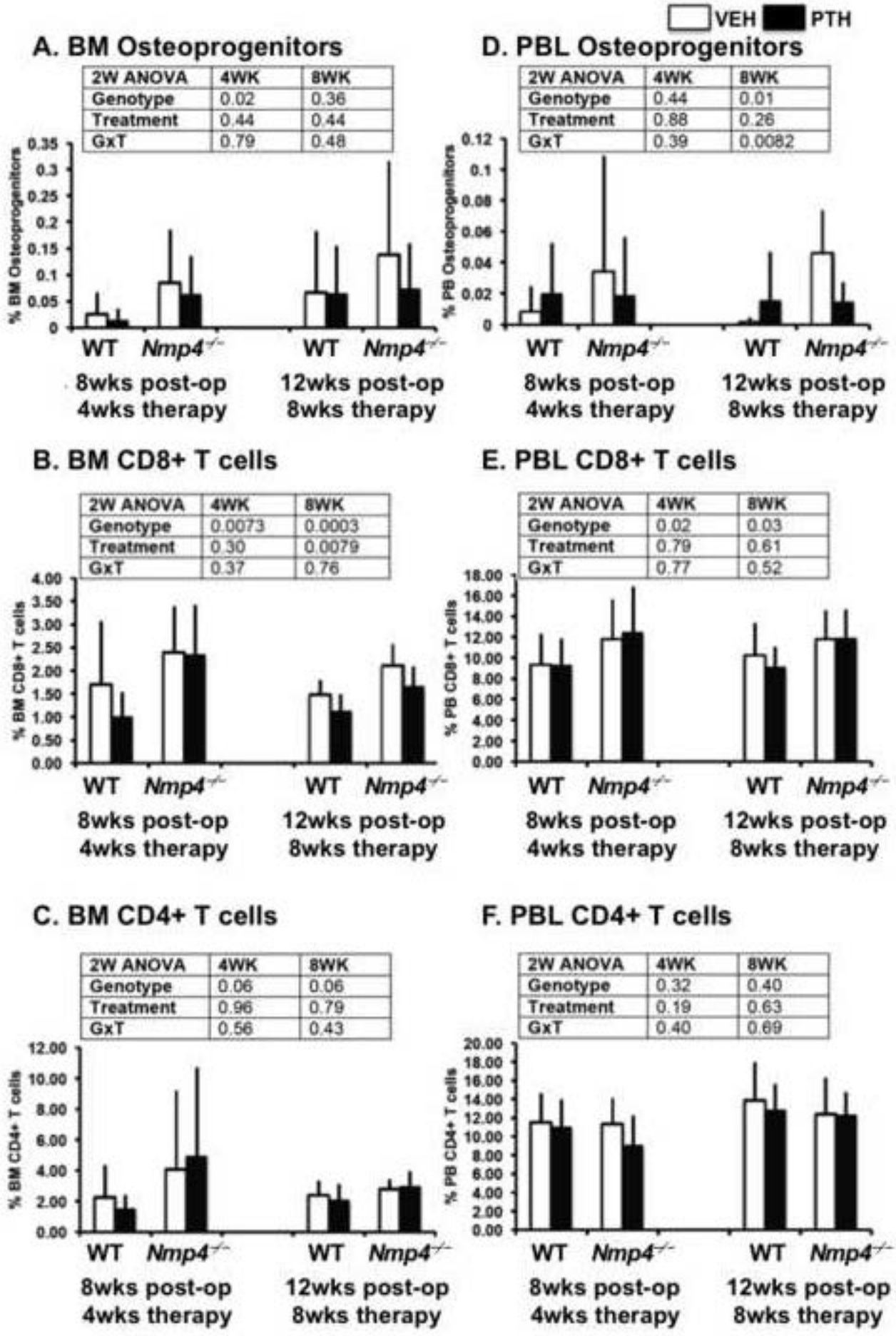

Figure 5
Click here to download Figure: FIGURE 5.tif

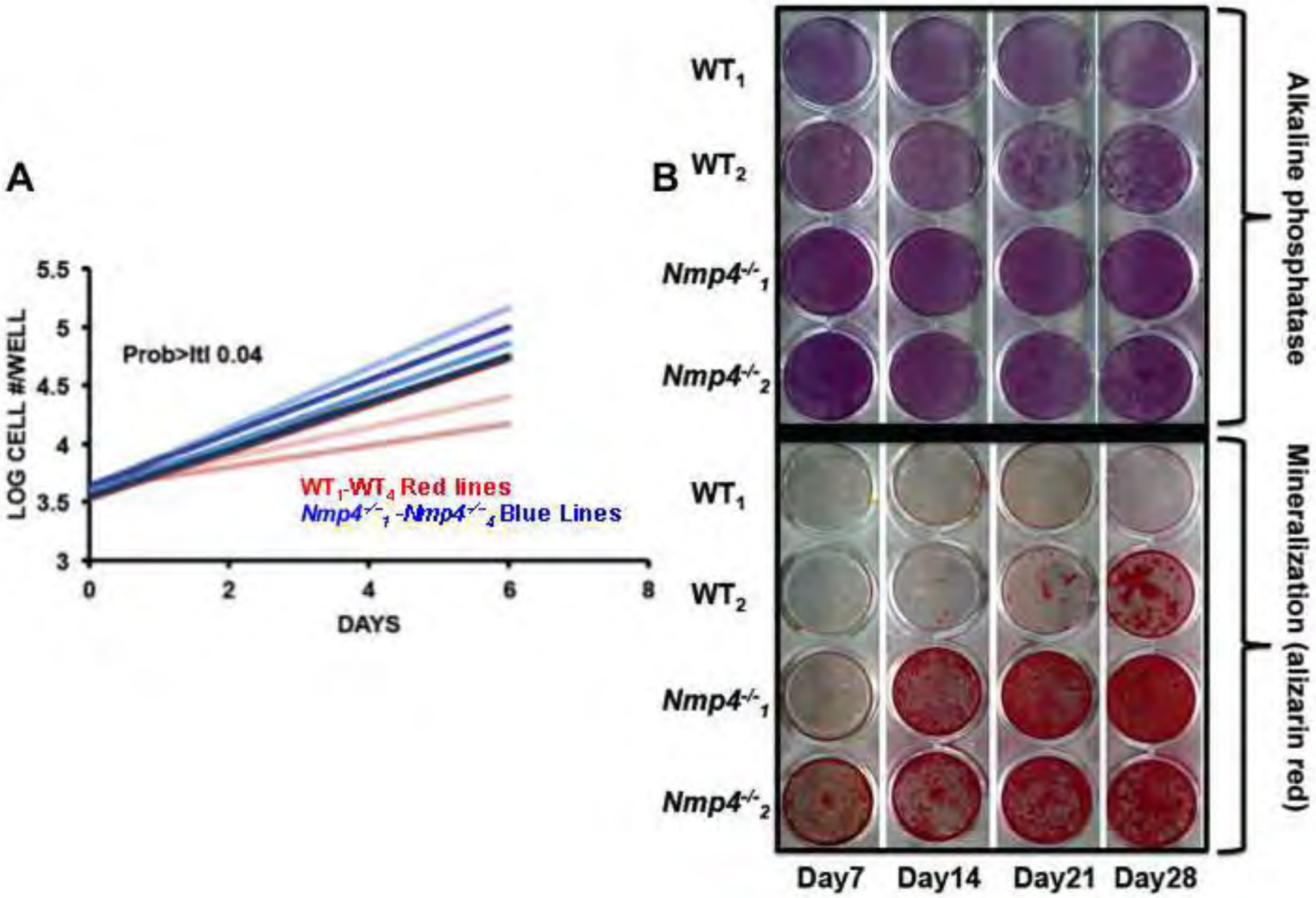

Figure 6
Click here to download Figure: FIGURE 6.tif

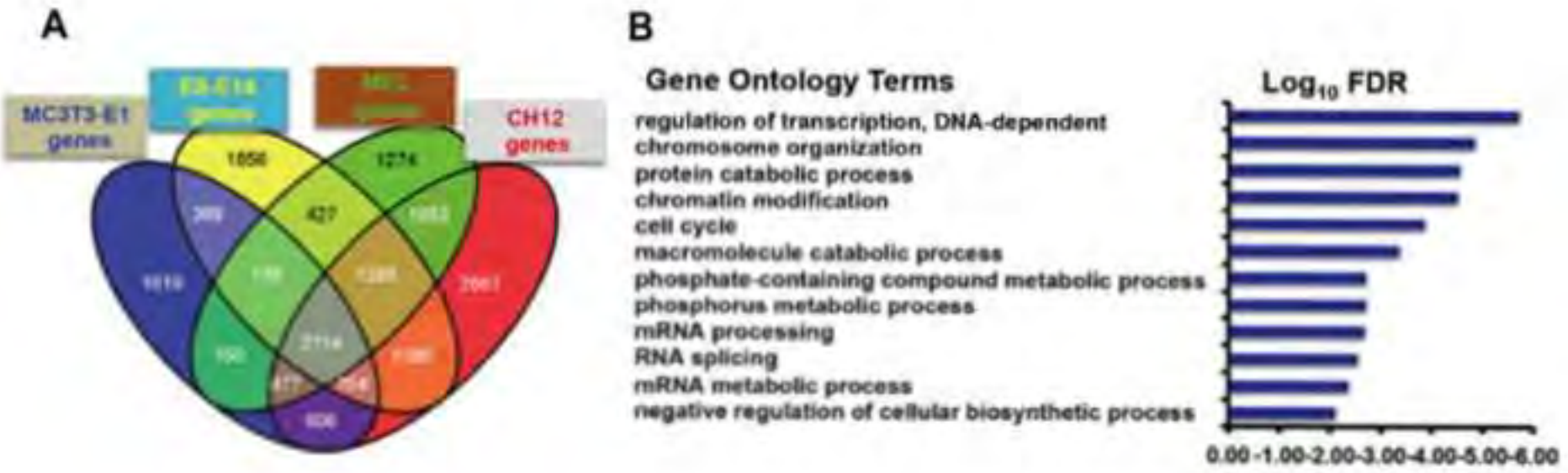

Figure 7
Click here to download Figure: FIGURE 7.tif

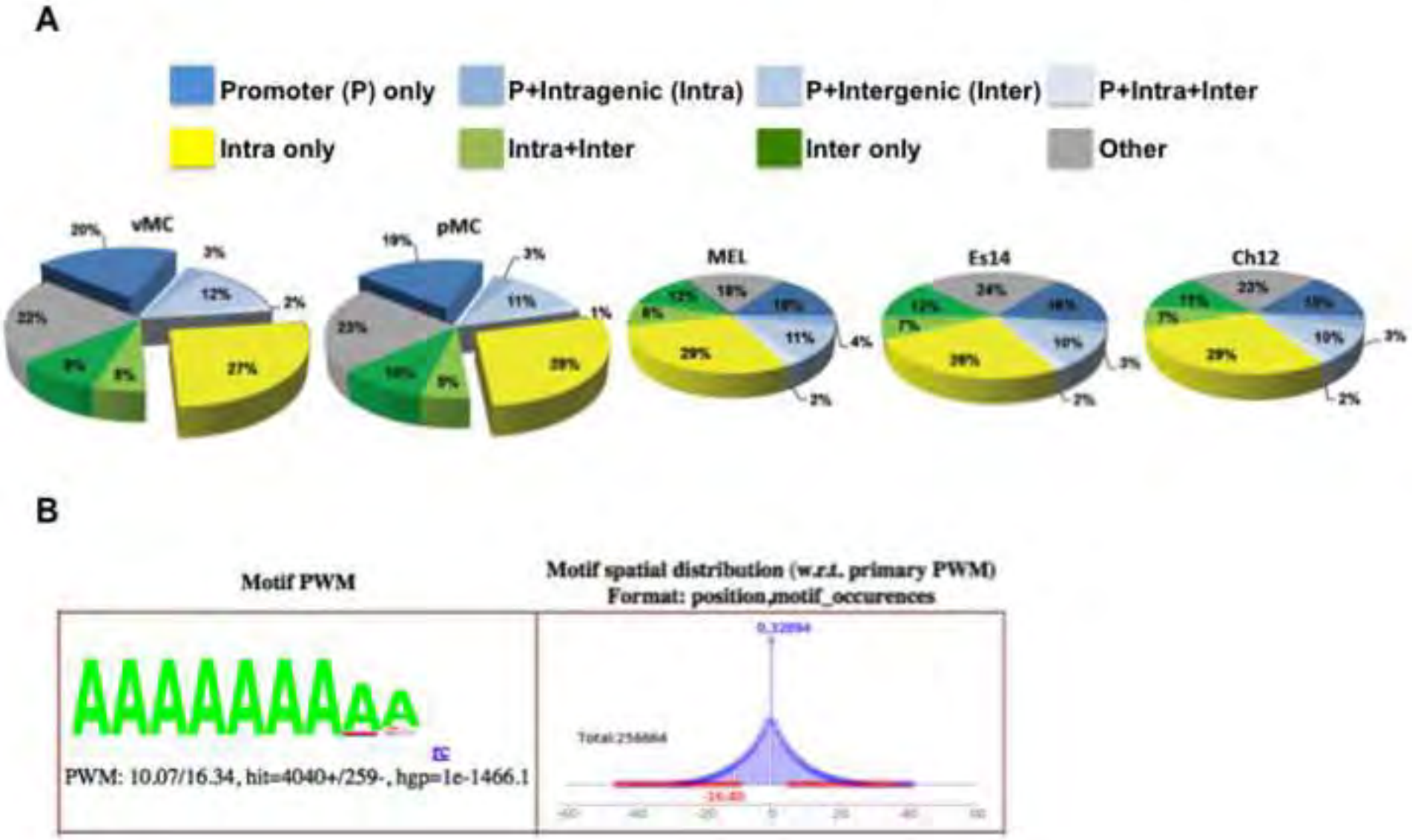

Figure 8

Click here to download Figure: FIGURE 8.tif

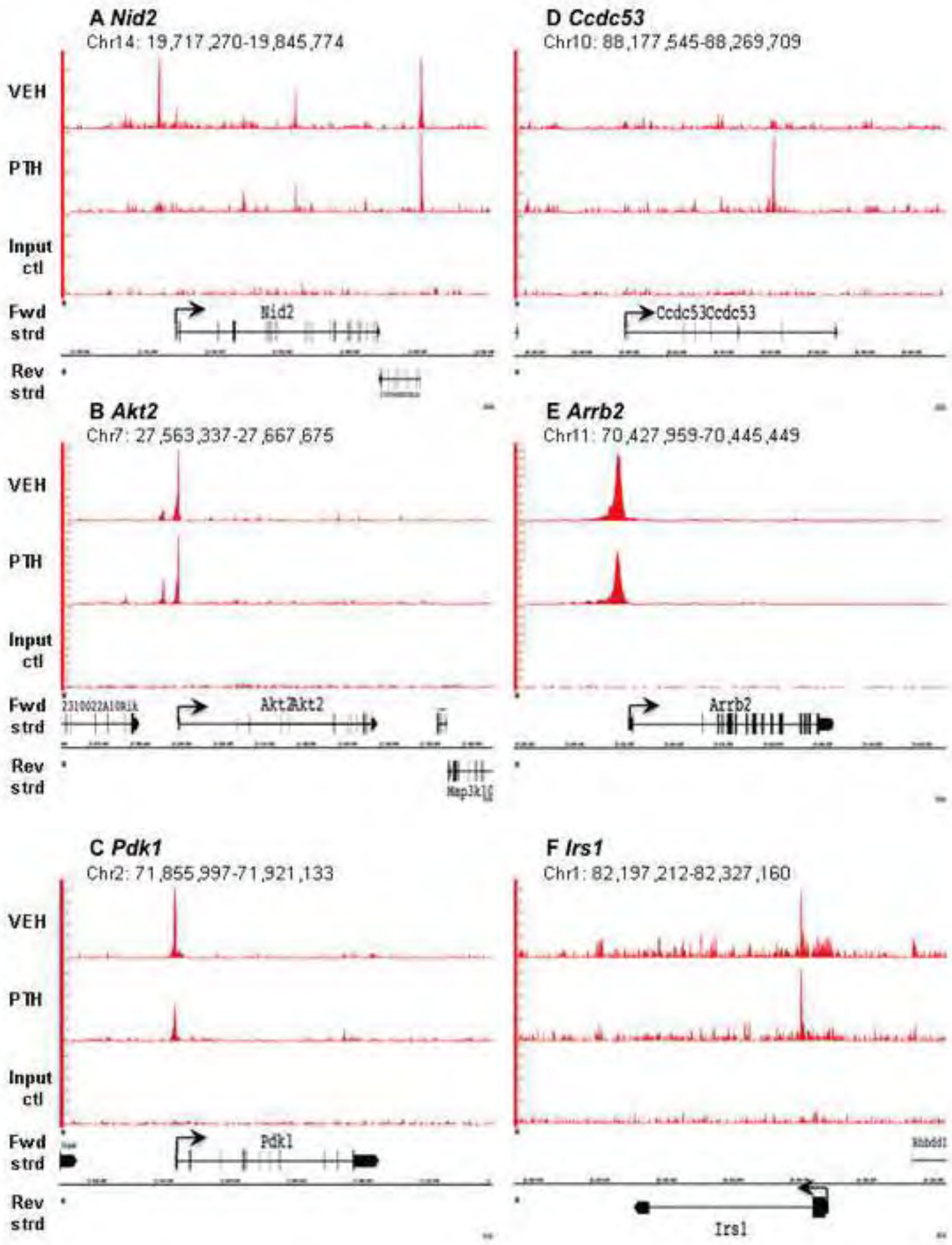

Figure 9
Click here to download Figure: FIGURE 9.tif

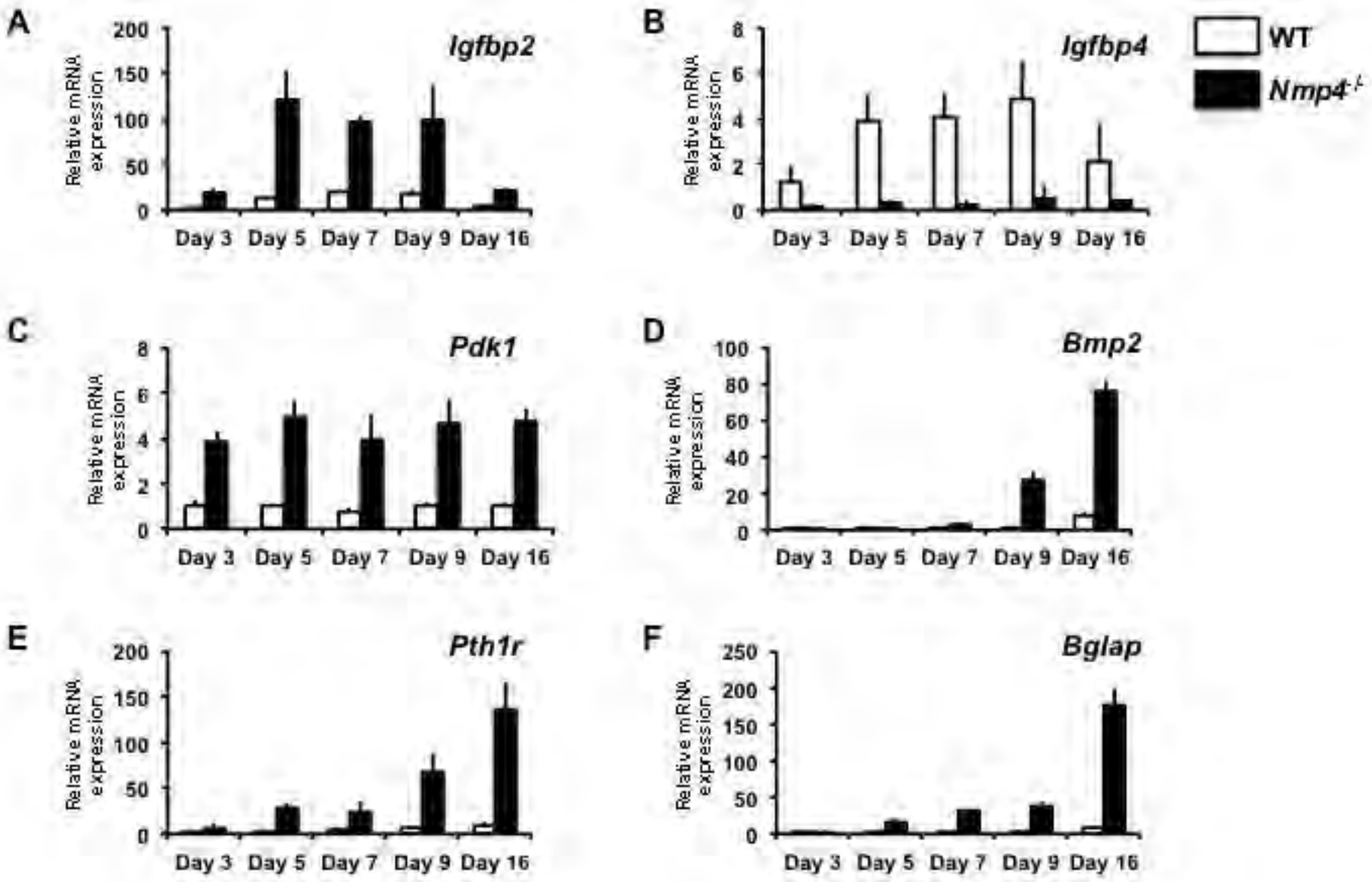

Figure 10
Click here to download Figure: FIGURE 10.tif

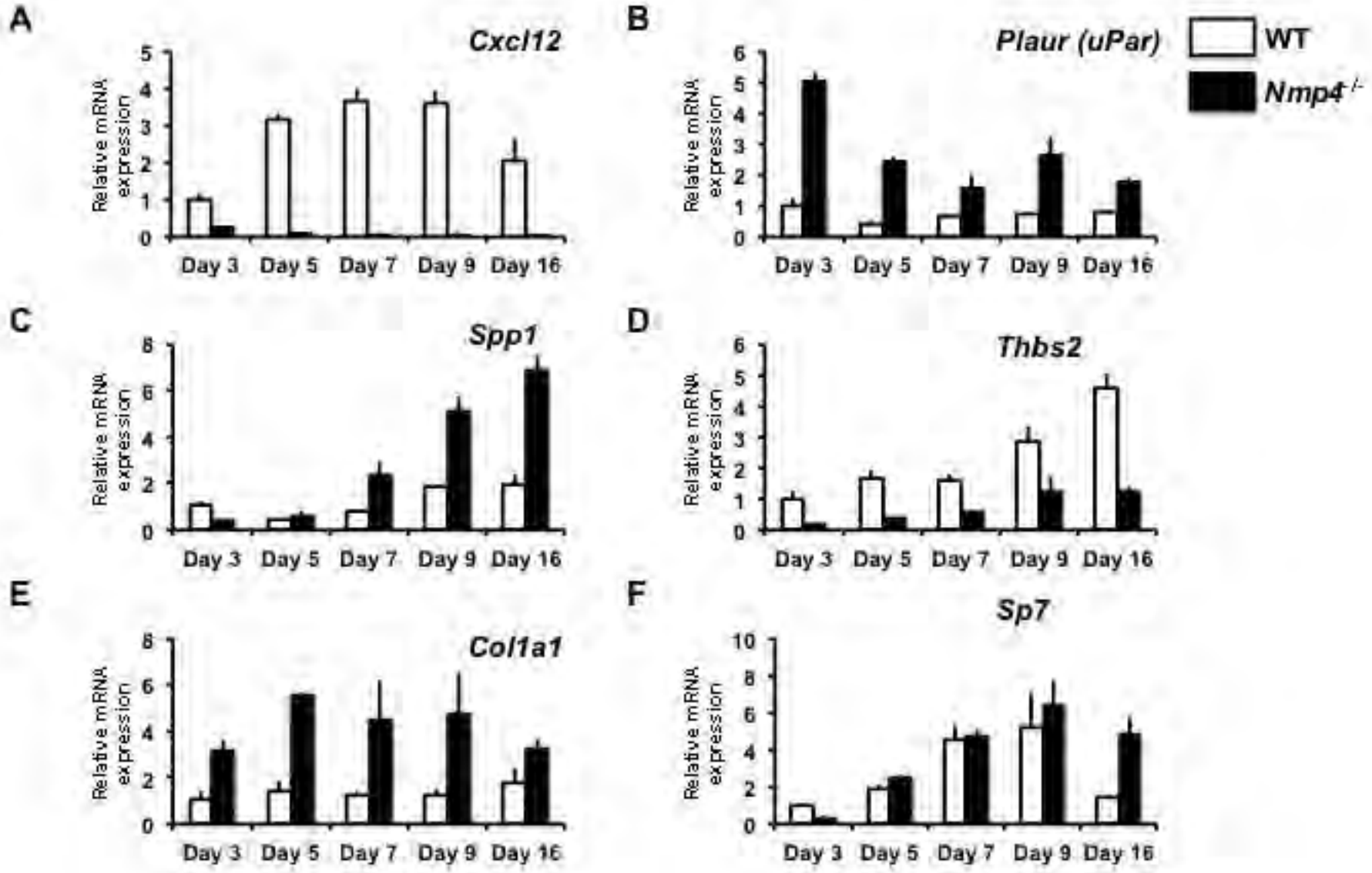

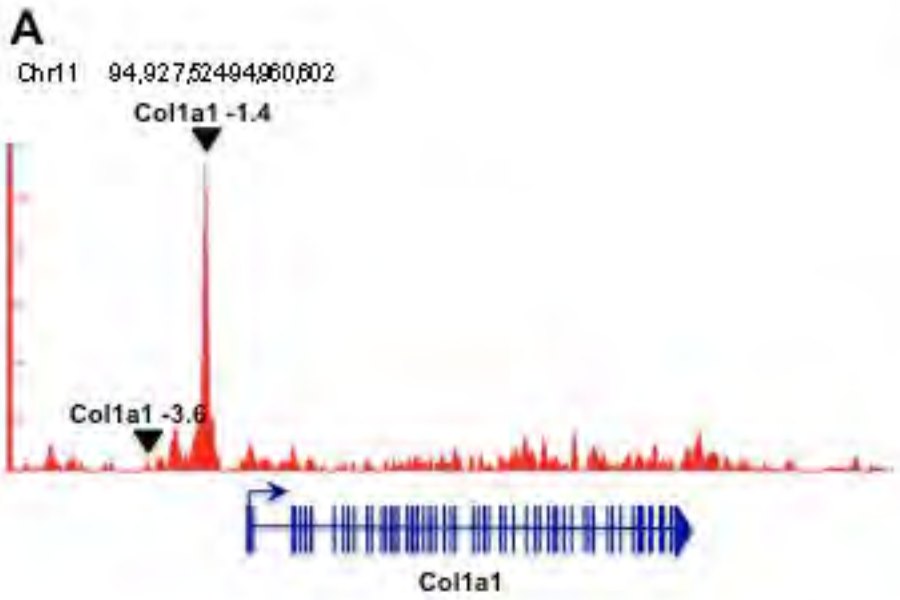
A
Chr11 94,927,524,94,960,602
Col1a1 -1.4
Col1a1 -3.6
Col1a1

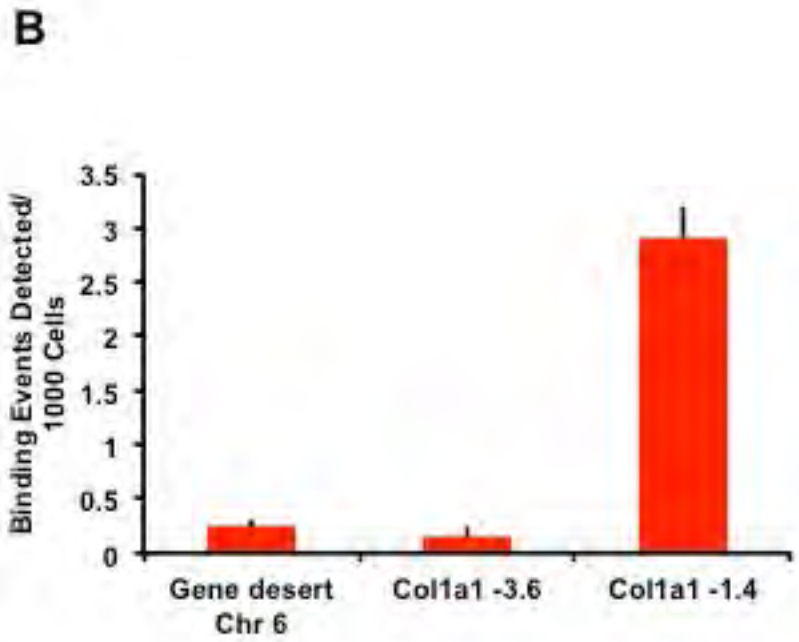
B
Binding Events Detected/ 1000 Cells
3.5
3
2.5
2
1.5
1
0.5
0
Gene desert Chr 6
Col1a1 -3.6
Col1a1 -1.4

Supplemental Figure 2A
Click here to download Supplemental Data: SUPPLEMENTAL FIGURE 2A.tif

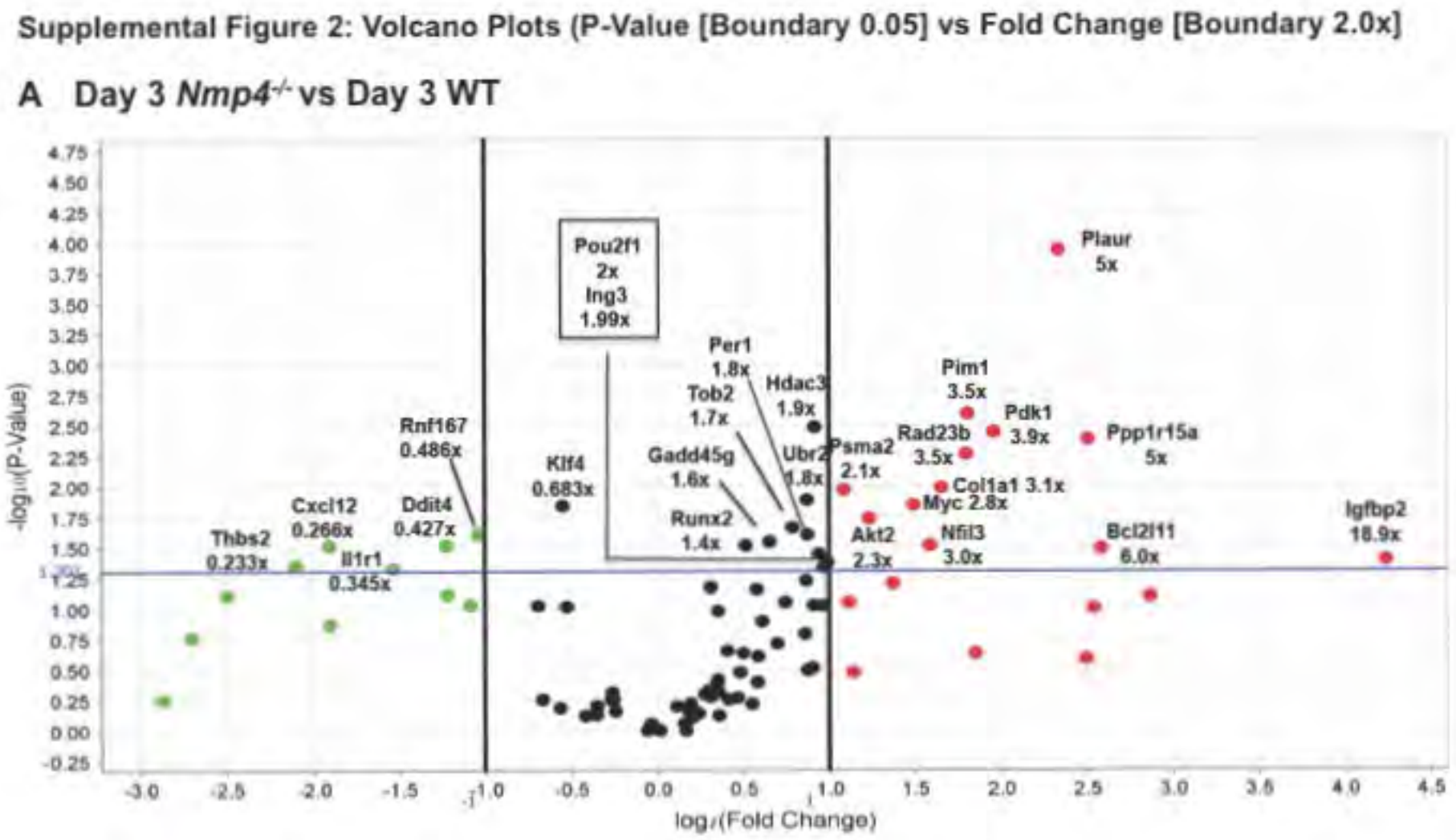

Supplemental Figure 2B
Click here to download Supplemental Data: SUPPLEMENTAL FIGURE 2B.tif

Supplemental Figure 2: Volcano Plots (P-Value [Boundary 0.05] vs Fold Change [Boundary 2.0x]

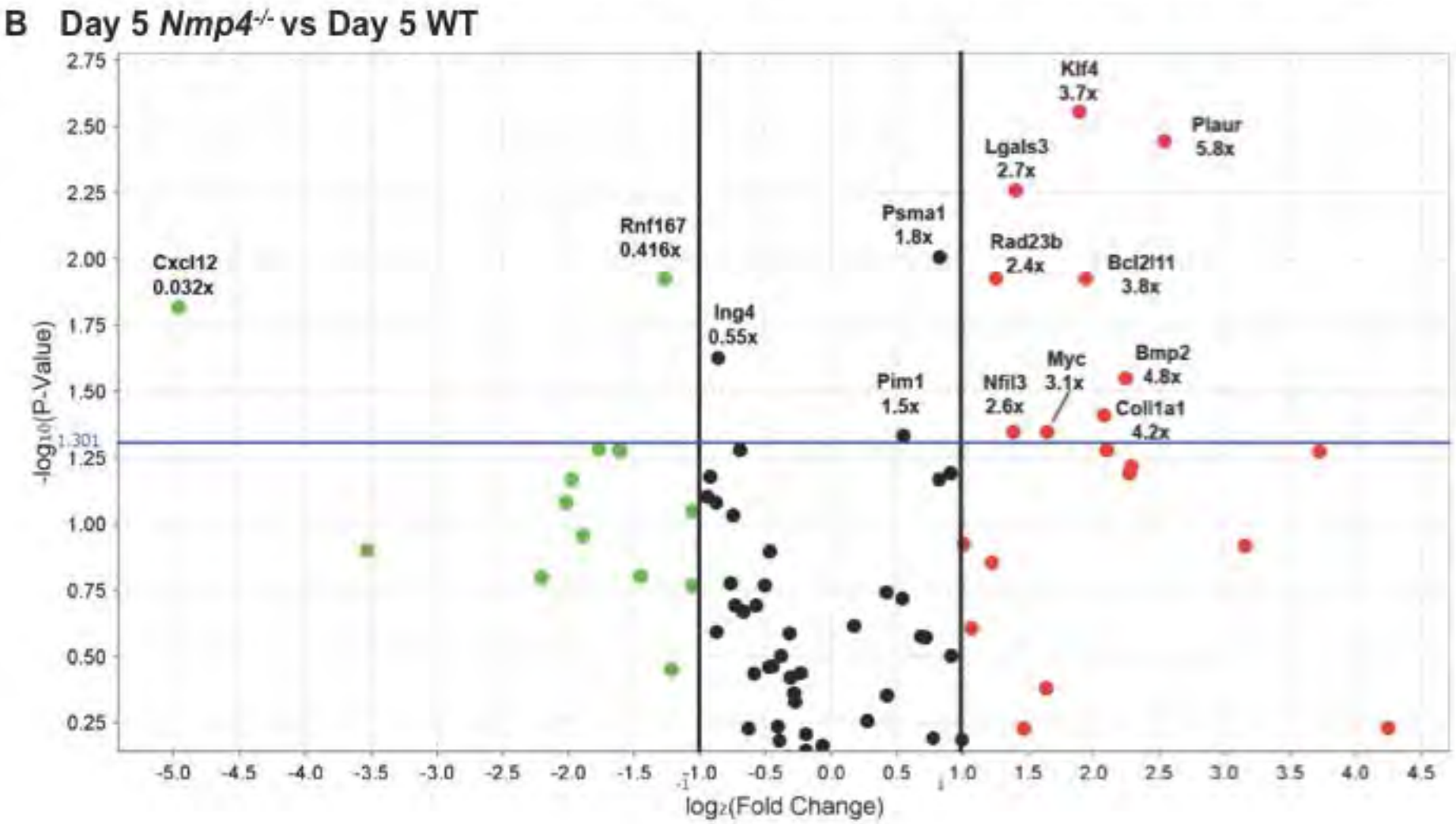

Supplemental Figure 2C
Click here to download Supplemental Data: SUPPLEMENTAL FIGURE 2C.tif

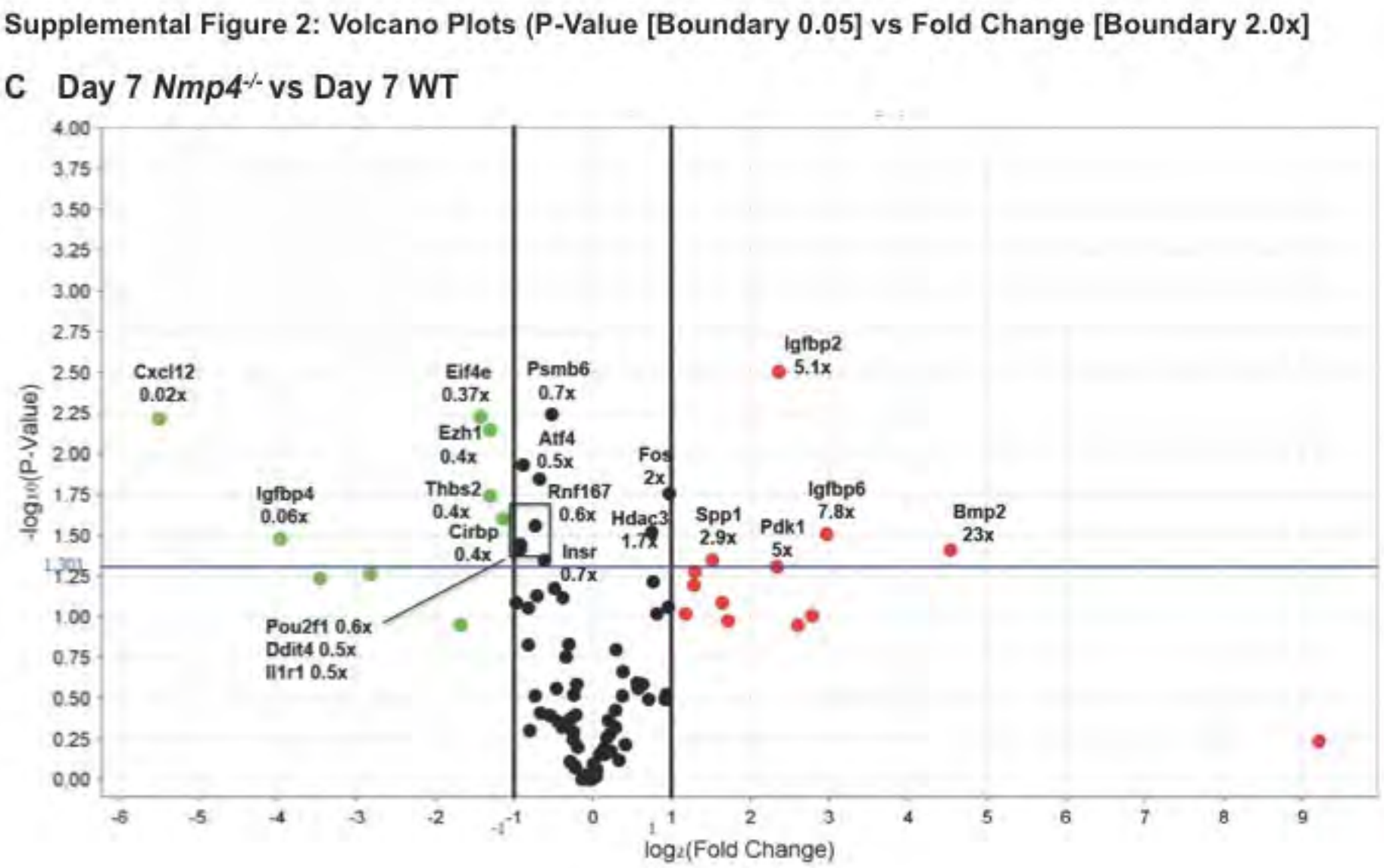

Supplemental Figure 2A

Click here to download Supplemental Data: SUPPLEMENTAL FIGURE 2A.tif

Supplemental Figure 2B

Click here to download Supplemental Data: SUPPLEMENTAL FIGURE 2B.tif

Supplemental Figure 2C

Click here to download Supplemental Data: SUPPLEMENTAL FIGURE 2C.tif

Supplemental Figure 2D
Click here to download Supplemental Data: SUPPLEMENTAL FIGURE 2D.tif

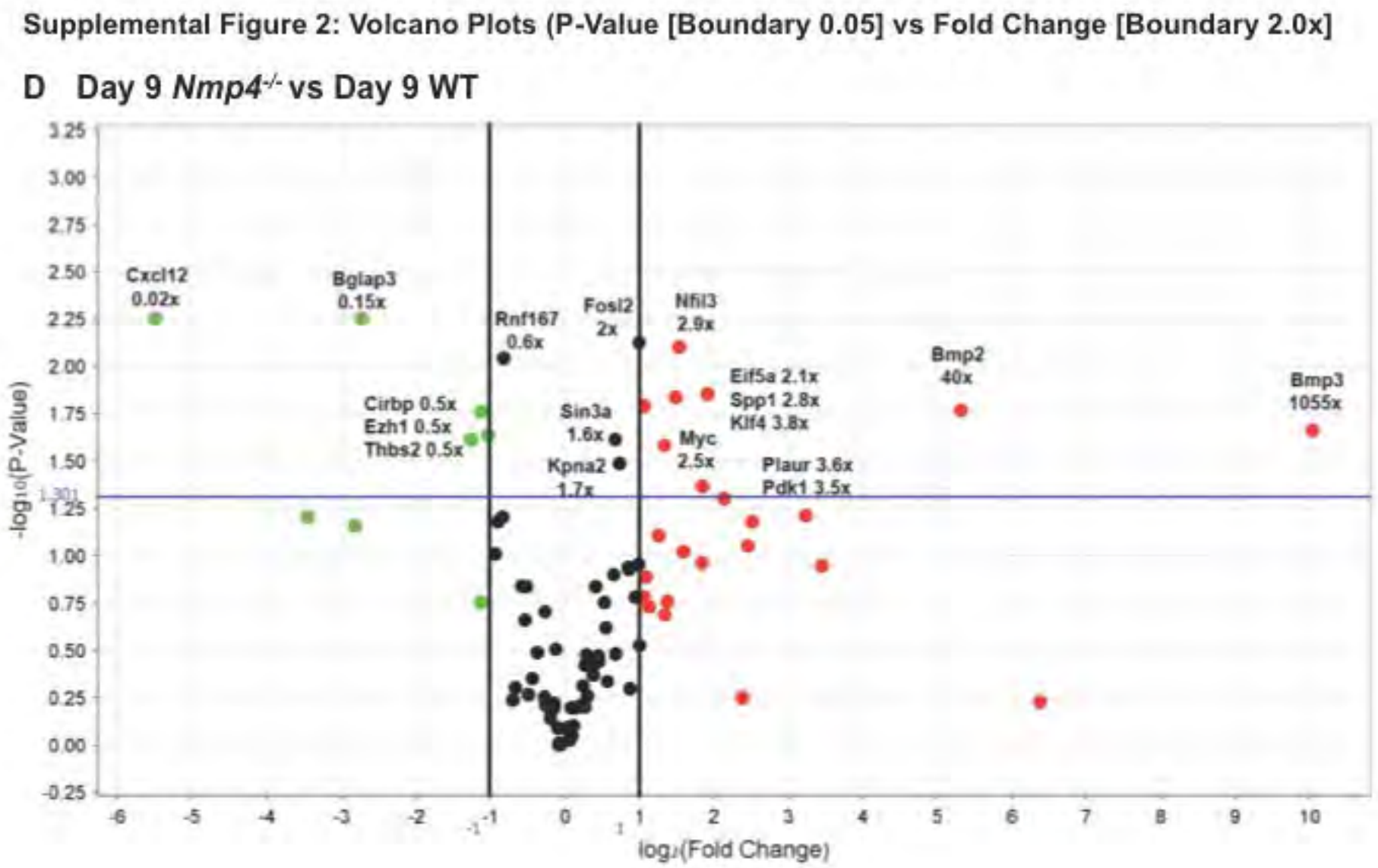

Supplemental Data Legends

Click here to download Supplemental Data Legends: FIGURE LEGENDS.docx

Supplemental Data Legends
Click here to download Supplemental Data Legends: FIGURE LEGENDS.docx

FIGURE LEGENDS

Figure 1: Schematic of treatment regimen for WT and *Nmp4*$^{-/-}$ mice; Group 1 mice were subjected to ovariectomy (ovx) or sham operation at 12wks of age and evaluated for bone loss 4wks post-op (16wks of age). Group 2 mice were ovx at 12wks of age and began PTH or vehicle therapy at 16wks of age for a duration of 4wks and 8wks. Endpoint analyses included micro–computed tomography μCT, serum analysis for N-terminal propeptide of type 1 procollagen (P1NP) and C-terminal telopeptides (CTX), and dynamic histomorphometry.

Figure 2: Disabling Nmp4 enhances PTH restorative therapy in the distal femur of ovx *Nmp4*$^{-/-}$ mice [A] Interaction plots of femoral trabecular bone volume/total volume (BV/TV) of ovx WT and ovx *Nmp4*$^{-/-}$ mice as determined by μCT at 4wks of treatment and 8wks of treatment. Data are average ± SD, number of mice/experimental group = 8-9). Statistical differences were determined using a 2-way ANOVA and significance was set at $p \leq 0.05$. The Tukey's HSD post hoc test was used to determine differences between the treatment groups. There were genotype, treatment and genotype x treatment interaction at both time points. There was no difference between the vehicle-treated WT and *Nmp4*$^{-/-}$ mice. [B] μCT images showing PTH-induced improvements in distal femur trabecular architecture in ovx WT and *Nmp4*$^{-/-}$ mice after 8 weeks of treatment (12wks post-op, 24wks of age).

Figure 3: The exaggerated response to anabolic PTH persists in the L5 vertebra of ovx *Nmp4*$^{-/-}$ mice. [A] Interaction plots of L5 vertebra bone volume/total volume (BV/TV) of ovx WT and ovx *Nmp4*$^{-/-}$ mice as determined by μCT at 4wks of treatment and 8wks of treatment. Data are average ± SD, number of mice/experimental group = 8-9). Statistical differences were determined using a 2-way ANOVA and significance was set at $p \leq 0.05$. The LS Means Student t post hoc test was used to determine differences between the treatment groups. There were genotype, treatment effects at both time points and a genotype x treatment interaction at 8wks therapy. There was no difference between the vehicle-treated WT and

Nmp4$^{-/-}$ mice. [B] µCT images showing PTH-induced improvements in L5 trabecular architecture in ovx WT and *Nmp4*$^{-/-}$ mice after 8 weeks of treatment (12wks post-op, 24wks of age).

Figure 4: Ovx does not abrogate the expanded population of osteoprogenitors and CD8+ T cells in *Nmp4*$^{-/-}$ mice. FACS analysis of BM and PBL osteoprogenitors, CD8+ T cells, and CD4+ T cells. [A, D] The frequency of femoral BM and PBL CD45-/CD105+/CD146+/CD105+/nestin+ osteoprogenitor cells in WT and *Nmp4*$^{-/-}$ mice at the end of 4wks and 8wks treatment with intermittent PTH or vehicle control; [B, E] the frequency of BM and PBL CD8+ T cells from the WT and *Nmp4*$^{-/-}$ mice; [C, F] the frequency of BM and PBL CD4+ T cells from the WT and null mice. Data are average ± SD, number of mice/experimental group = 8–9; Statistical differences were determined using a 2-way ANOVA and significance was set at $p \leq 0.05$.

Figure 5: Expanded *Nmp4*$^{-/-}$ MSPCs exhibit enhanced proliferation and mineralization in culture. [A] Comparative growth rates of expanded WT and *Nmp4*$^{-/-}$ MSPCs. Cell counts/day (n=4 lines per genotype log10 cells/well, 3 wells/sample, average ± SD, t test, $t<0.05$). Note: each 'line' is derived from a single mouse [B] Alkaline phosphatase (alk phos) and alizarin red staining of a WT and *Nmp4*$^{-/-}$ MSPC cultures from Day7-Day28. See text for details

Figure 6: Nmp4 associates with core target genes common to multiple cell types and acts as a *negative regulation of cellular biosynthetic processes* [A] Venn diagram illustrating the shared Nmp4 target genes in the MC3T3-E1 osteoblast-like cells (vehicle-treated), and the three ENCODE cells lines, ES-E14 (embryonic stem cells), MEL, and CH12 cells (B-cell lymphomas). [B] DAVID/REVIGO gene ontology (GO) profile of Nmp4 core target genes

Figure 7: Nmp4 binds to AT-rich DNA typically proximal to TSS sites or within intragenic regions. [A] Genome-wide mapping of the Nmp4 binding sites show that most sites are distributed in the TSS and

intragenic regions of the genome. ChIP-seq analysis included vehicle-treated and PTH-treated MC3T3-E1 osteoblast-like cells (vMC and pMC, respectively) and three murine cell lines from the ENCODE Consortium including ES-E14 (Es14), which are E14 undifferentiated mouse embryoinic stem cells, and two mouse erythroleukemia cell lines (Ch12 and MEL) derived from B-cell lymphomas. [B] GEM analysis for the Nmp4 consensus sequence derived from MC3T3-E1 cells. A minimal k-mer width of 6 and maximum of 20 were used. The optimal position weight matrix (PWM) score for the MC3T3-E1 data was 10.07. The hypergeometric P-value (hgp) was 1e-1466.1.

Figure 8: ChIP-seq reveals Nmp4 binding profiles at specific gene loci. Mouse MC3T3-E1 cells were seeded into twenty-one 150mm plates at an initial density of 50,000 cells/plate (320 cells/cm^2) and maintained in αMEM complete medium + ascorbic acid for 14 days. Prior to harvest cells were treated with 25nM hPTH(1-34) or vehicle control for 1hr. Processing for ChIP-seq analysis was performed as described in the Materials and Methods. Sequences (50nt reads, single end) were aligned to the mouse genome (mm10) using the BWA algorithm. Alignments were extended in silico at their 3'-ends to a length of 150bp, which is the average genomic fragment length in the size-selected library, and assigned to 32-nt bins along the genome. Nmp4 (Znf384) peak locations were determined using the MACS algorithm (v1.4.2) with a cutoff of pvalue = 1e-7. The genomic loci including the chromosome number and nucleotide interval are indicated. Read scales are indicated on the Y-axis. An arrow indicates the transcriptional start sites and direction of transcription for each of the genes; vertical boxes within the gene indicate exons. The Nmp4 ChIP-seq gene profiles include (A) *Nid2* (B) *Akt2*, (C) *Pdk1* (D) *ccdc53*, (E) *Arrb2* and (F) *Irs1*. The input DNA profiles were devoid of peaks.

Figure 9: Comparison of mRNA expression profiles derived from non-differentiating (Day 3) and osteogenic-differentiating (Days 5-16) WT and *Nmp4*$^{-/-}$ cells. All transcript levels are compared to WT Day 3 providing a time course of expression. mRNA profiles [A] *Igfbp2*; [B] *Igfbp4;* [C] *Pdk1*; [D] *Bmp2*; [E] *Pth1r* were derived from the TLDA system (Format 96a, Applied Biosystems, Foster City,

CA) performed on a QuantStudio™ 7 Flex Real-Time PCR System and normalized with GusB. Profile [F] *Bglap* mRNA profile qRT-PCR reactions were performed on an Eppendorf Mastercycler® RealPlex^2 using *Rplp2* Mm03059047_gH) as the normalizer as previously described [Robling et al, 2009]. Comparison of profiles using *GusB* and *Rplp2* as the normalizer showed no differences in the shape of the expression profiles

Figure 10: Comparison of mRNA expression profiles derived from non-differentiating (Day 3) and osteogenic-differentiating (Days 5-16) WT and *Nmp4*$^{-/-}$ cells. All transcript levels are compared to WT Day 3 providing a time course of expression. mRNA profiles [A] *Cxcl12*; [B] *Plaur;* [C] *Spp1*; [D] *Thbs2*; [E] *Col1a1* were derived from the TLDA system (Format 96a, Applied Biosystems, Foster City, CA) performed on a QuantStudio™ 7 Flex Real-Time PCR System and normalized with GusB. Profile [F] *Sp7* mRNA profile qRT-PCR reactions were performed on an Eppendorf Mastercycler® RealPlex^2 using *Rplp2* (Mm03059047_gH) as the normalizer as previously described [Robling et al., 2009]. The Day 16 WT sample is the average of two replicates. Comparison of profiles using GusB and Rplp2 as the normalizer showed no differences in the shape of the expression profiles

Supplemental Figure S1: qRT-PCR validates the ChIP-seq profiles. [A] The Nmp4 ChIP-seq profile for the gene *Col1a1*. The genomic loci including the chromosome number and nucleotide interval are indicated. Read scale is indicated on the Y-axis. An arrow marks the transcriptional start site and direction of transcription; vertical boxes within the gene identify exons. [B] qRT-PCR was used to authenticate the ChIP-seq peaks as described in the Materials and Methods.

Supplemental Figure 2: Volcano plots derived from gene expression profiles of non-differentiating (Day 3) and osteogenic-differentiating (Days 5-16) WT and *Nmp4*$^{-/-}$ as described in the Materials and Methods. RNA expression profiling was performed on a QuantStudio™ 7 Flex Real-Time PCR System and data analyzed using the ExpressionSuite v1.0.4™ analysis software (Applied Biosystems) as described in the

Materials and Methods. [A] WT vs *Nmp4*$^{-/-}$ cells at Day 3 post-seeding. mRNA transcript expression was compared to WT cells (Day 3). Cells maintained in Mesencult™ Media + Mesencult™ Stimulatory Supplement. [B] WT vs *Nmp4*$^{-/-}$ cells at Day 5 post-seeding. mRNA transcript expression was compared to WT cells (Day 5). Cells maintained in differentiation medium for 48hrs [C] WT vs *Nmp4*$^{-/-}$ cells at Day 7 post-seeding. mRNA transcript expression was compared to WT cells (Day 7). Cells maintained in differentiation medium for 96hrs [D] WT vs *Nmp4*$^{-/-}$ cells at Day 9 post-seeding. mRNA transcript expression was compared to WT cells (Day 9). Cells maintained in differentiation medium for 144hrs [E] WT vs *Nmp4*$^{-/-}$ cells at Day 16 post-seeding. mRNA transcript expression was compared to WT cells (Day 16). Cells maintained in differentiation medium for 192hrs. Genes indicated with green dots (left of center) and above the X-axis exhibited a significant downregulation by over 2-fold. Genes indicated with the red dots (right of center) and above the X-axis exhibited a significant upregulation by over 2-fold.

Supplemental TABLE 1: 96 Nmp4 'core' target genes, non-core target genes, and non-target genes including 5 candidate normalizer genes. Individual cDNAs were quantified by qRT-PCR using a custom TLDA system (Format 96a, Applied Biosystems, Foster City, CA) as described in the Materials and Methods on a QuantStudio™ 7 Flex Real-Time PCR System. We used the ExpressionSuite v1.0.4™ analysis software (Applied Biosystems) to analyze these data.

Supplemental TABLE 2: 2114 Nmp4 'core' target genes common to the four cell lines MC3T3-E1 osteoblast-like cells, and three murine cell lines from the ENCODE Consortium including ES-E14 (Es14), which are E14 undifferentiated mouse embryoinic stem cells, and two mouse erythroleukemia cell lines (Ch12 and MEL) derived from B-cell lymphomas.

Supplemental TABLE 3: IPA analysis of 2114 Nmp4 'core' target genes common to the four cell lines MC3T3-E1 osteoblast-like cells, and three murine cell lines from the ENCODE Consortium including

ES-E14 (Es14), which are E14 undifferentiated mouse embryoinic stem cells, and two mouse erythroleukemia cell lines (Ch12 and MEL) derived from B-cell lymphomas.

Supplemental Table 1

Click here to download Supplemental Data: NMP4 MS SUPPLEMENTAL TABLE 1.xlsx

Detector	Reporter	Quencher	Description	Comments	Sequence
18S-Hs99999901_s1	FAM	Non Fluorescent	Eukaryotic 18S rRNA		
Akt2-Mm02026778_g1	FAM	Non Fluorescent	thymoma viral proto-oncogene 2		
Alpl-Mm00475834_m1	FAM	Non Fluorescent	alkaline phosphatase, liver/bone/kidney		
Arrb2-Mm00520666_g1	FAM	Non Fluorescent	arrestin, beta 2		
Atf4-Mm00515325_g1	FAM	Non Fluorescent	activating transcription factor 4		
Bcl2l11-Mm00437796_m1	FAM	Non Fluorescent	BCL2-like 11 (apoptosis facilitator)		
Bglap3-Mm00649782_gH	FAM	Non Fluorescent	bone gamma-carboxyglutamate protein 3		
Bmp2-Mm01340178_m1	FAM	Non Fluorescent	bone morphogenetic protein 2		
Bmp3-Mm00557790_m1	FAM	Non Fluorescent	bone morphogenetic protein 3		
Bmp4-Mm00432087_m1	FAM	Non Fluorescent	bone morphogenetic protein 4		
Bmp6-Mm01332882_m1	FAM	Non Fluorescent	bone morphogenetic protein 6		
Bmpr1a-Mm00477650_m1	FAM	Non Fluorescent	bone morphogenetic protein receptor, type 1A		
Cbfb-Mm01251026_g1	FAM	Non Fluorescent	core binding factor beta		
Cbx4-Mm00483089_m1	FAM	Non Fluorescent	chromobox 4		
Cbx7-Mm00520006_m1	FAM	Non Fluorescent	chromobox 7		
Cdc6-Mm03048221_m1	FAM	Non Fluorescent	cell division cycle 6		
Cirbp-Mm00483336_g1	FAM	Non Fluorescent	cold inducible RNA binding protein		
Col1a1-Mm00801666_g1	FAM	Non Fluorescent	collagen, type I, alpha 1		
Crebbp-Mm01342452_m1	FAM	Non Fluorescent	CREB binding protein		
Cxcl12-Mm00445553_m1	FAM	Non Fluorescent	chemokine (C-X-C motif) ligand 12		
Ddit4-Mm00512504_g1	FAM	Non Fluorescent	DNA-damage-inducible transcript 4		
Dnm3os-Mm03455916_s1	FAM	Non Fluorescent	dynamin 3, opposite strand		
Ehmt2-Mm01132261_m1	FAM	Non Fluorescent	euchromatic histone lysine N-methyltransferase 2		
Eif4e-Mm00725633_s1	FAM	Non Fluorescent	eukaryotic translation initiation factor 4E		
Eif5a-Mm01971736_g1	FAM	Non Fluorescent	eukaryotic translation initiation factor 5A		
Ephb4-Mm01201157_m1	FAM	Non Fluorescent	Eph receptor B4		
Ezh1-Mm00468440_m1	FAM	Non Fluorescent	enhancer of zeste homolog 1 (Drosophila)		
Fos-Mm00487425_m1	FAM	Non Fluorescent	FBJ osteosarcoma oncogene		
Fosl2-Mm00484442_m1	FAM	Non Fluorescent	fos-like antigen 2		
Gadd45b-Mm00435121_g1	FAM	Non Fluorescent	growth arrest and DNA-damage-inducible 45 beta		
Gadd45g-Mm01352550_g1	FAM	Non Fluorescent	growth arrest and DNA-damage-inducible 45 gamma		
Gas1-Mm01700206_g1	FAM	Non Fluorescent	growth arrest specific 1		
Hdac3-Mm00515916_m1	FAM	Non Fluorescent	histone deacetylase 3		

Hif1a-Mm00468869_m1	FAM	Non Fluorescent	hypoxia inducible factor 1, alpha subunit
Igf1-Mm00439560_m1	FAM	Non Fluorescent	insulin-like growth factor 1
Igf1r-Mm00802831_m1	FAM	Non Fluorescent	insulin-like growth factor I receptor
Igfbp2-Mm00492632_m1	FAM	Non Fluorescent	insulin-like growth factor binding protein 2
Igfbp4-Mm00494922_m1	FAM	Non Fluorescent	insulin-like growth factor binding protein 4
Igfbp6-Mm00599696_m1	FAM	Non Fluorescent	insulin-like growth factor binding protein 6
Il1r1-Mm00434237_m1	FAM	Non Fluorescent	interleukin 1 receptor, type I
Ing3-Mm00458324_m1	FAM	Non Fluorescent	inhibitor of growth family, member 3
Ing4-Mm00460097_m1	FAM	Non Fluorescent	inhibitor of growth family, member 4
Insr-Mm01211875_m1	FAM	Non Fluorescent	insulin receptor
Irs1-Mm01278327_m1	FAM	Non Fluorescent	insulin receptor substrate 1
Klf4-Mm00516104_m1	FAM	Non Fluorescent	Kruppel-like factor 4 (gut)
Kpna2-Mm00834020_gH	FAM	Non Fluorescent	karyopherin (importin) alpha 2
Lgals3-Mm00802901_m1	FAM	Non Fluorescent	lectin, galactose binding, soluble 3
Lrp1-Mm00464608_m1	FAM	Non Fluorescent	low density lipoprotein receptor-related protein 1
Msx2-Mm00442992_m1	FAM	Non Fluorescent	msh homeobox 2
Myc-Mm00487804_m1	FAM	Non Fluorescent	myelocytomatosis oncogene
Nbr1-Mm01249798_m1	FAM	Non Fluorescent	neighbor of Brca1 gene 1
Ncor1-Mm01333102_m1	FAM	Non Fluorescent	nuclear receptor co-repressor 1
Ncor2-Mm00448796_m1	FAM	Non Fluorescent	nuclear receptor co-repressor 2
Nfil3-Mm00600292_s1	FAM	Non Fluorescent	nuclear factor, interleukin 3, regulated
Nr3c1-Mm00433832_m1	FAM	Non Fluorescent	nuclear receptor subfamily 3, group C, member 1
Pdk1-Mm00554306_m1	FAM	Non Fluorescent	pyruvate dehydrogenase kinase, isoenzyme 1
Per1-Mm00501813_m1	FAM	Non Fluorescent	period circadian clock 1
Phf12-Mm00663497_m1	FAM	Non Fluorescent	PHD finger protein 12
Pim1-Mm00435712_m1	FAM	Non Fluorescent	proviral integration site 1
Plaur-Mm00440911_m1	FAM	Non Fluorescent	plasminogen activator, urokinase receptor
Pou2f1-Mm00448332_m1	FAM	Non Fluorescent	POU domain, class 2, transcription factor 1
Ppp1r15a-Mm01205601_g1	FAM	Non Fluorescent	protein phosphatase 1, regulatory (inhibitor) subunit 15A
Prpf19-Mm00467298_m1	FAM	Non Fluorescent	PRP19/PSO4 pre-mRNA processing factor 19 homolog (S. cerevisiae)
Psma1-Mm00803741_m1	FAM	Non Fluorescent	proteasome (prosome, macropain) subunit, alpha type 1
Psma2-Mm00776364_mH	FAM	Non Fluorescent	proteasome (prosome, macropain) subunit, alpha type 2
Psma3-Mm00834115_g1	FAM	Non Fluorescent	proteasome (prosome, macropain) subunit, alpha type 3
Psmb6-Mm00599713_g1	FAM	Non Fluorescent	proteasome (prosome, macropain) subunit, beta type 6

Pth1r-Mm00441046_m1	FAM	Non Fluorescent	parathyroid hormone 1 receptor
Ptp4a1-Mm00850755_g1	FAM	Non Fluorescent	protein tyrosine phosphatase 4a1
Rad23b-Mm00772280_m1	FAM	Non Fluorescent	RAD23b homolog (S. cerevisiae)
Rffl-Mm00482724_m1	FAM	Non Fluorescent	ring finger and FYVE like domain containing protein
Rnf167-Mm00550967_g1	FAM	Non Fluorescent	ring finger protein 167
Rnf5-Mm01134793_g1	FAM	Non Fluorescent	ring finger protein 5
Rps6kb1-Mm01310033_m1	FAM	Non Fluorescent	ribosomal protein S6 kinase, polypeptide 1
Rptor-Mm00712676_m1	FAM	Non Fluorescent	regulatory associated protein of MTOR, complex 1
Runx2-Mm00501584_m1	FAM	Non Fluorescent	runt related transcription factor 2
Sin3a-Mm00488255_m1	FAM	Non Fluorescent	transcriptional regulator, SIN3A (yeast)
Smad7-Mm00484742_m1	FAM	Non Fluorescent	SMAD family member 7
Sp7-Mm04209856_m1	FAM	Non Fluorescent	Sp7 transcription factor 7
Sparc-Mm00486332_m1	FAM	Non Fluorescent	secreted acidic cysteine rich glycoprotein
Spp1-Mm00436767_m1	FAM	Non Fluorescent	secreted phosphoprotein 1
Suz12-Mm01304145_g1	FAM	Non Fluorescent	suppressor of zeste 12 homolog (Drosophila)
Thbs2-Mm01279240_m1	FAM	Non Fluorescent	thrombospondin 2
Tle3-Mm00437097_m1	FAM	Non Fluorescent	transducin-like enhancer of split 3, homolog of Drosophila E(spl)
Tob2-Mm00451524_s1	FAM	Non Fluorescent	transducer of ERBB2, 2
Ttc3-Mm00493917_m1	FAM	Non Fluorescent	tetratricopeptide repeat domain 3
Ubr2-Mm00524868_m1	FAM	Non Fluorescent	ubiquitin protein ligase E3 component n-recognin 2
Usp15-Mm00452856_m1	FAM	Non Fluorescent	ubiquitin specific peptidase 15
Usp2-Mm00497452_m1	FAM	Non Fluorescent	ubiquitin specific peptidase 2
Xiap-Mm01311594_mH	FAM	Non Fluorescent	X-linked inhibitor of apoptosis
Zbtb7a-Mm00657132_m1	FAM	Non Fluorescent	zinc finger and BTB domain containing 7a
Rplp2-Mm00782638_s1	FAM	Non Fluorescent	ribosomal protein, large P2
Gusb-Mm01197698_m1	FAM	Non Fluorescent	glucuronidase, beta
B2m-Mm00437762_m1	FAM	Non Fluorescent	beta-2 microglobulin
Hprt-Mm01545399_m1	FAM	Non Fluorescent	hypoxanthine guanine phosphoribosyl transferase
Dkk2-Mm01322146_m1	FAM	Non Fluorescent	dickkopf homolog 2 (Xenopus laevis)

Supplemental Table 2
Click here to download Supplemental Data: NMP4 MS SUPPLEMENTAL TABLE 2.xlsx

Common elements in "vMC3T3", "MEL", "Es14" and "Ch12": **Nmp4 'CORE' genes**

0610031O16Rik
0610043K17Rik
1110001J03Rik
1110002J07Rik
1110002L01Rik
1110037F02Rik
1110038B12Rik
1110051M20Rik
1190002F15Rik
1600002K03Rik
1600020E01Rik
1700001G11Rik
1700007K13Rik
1700007L15Rik
1700013F07Rik
1700016C15Rik
1700018L02Rik
1700018M17Rik
1700021A07Rik
1700022K14Rik
1700023H06Rik
1700030C12Rik
1700034H15Rik
1700052N19Rik
1700063D05Rik
1700064E03Rik
1700067K01Rik
1700095J07Rik

1700101I11Rik
1700110C19Rik
1700112E06Rik
1700120B22Rik
1810013L24Rik
1810019N24Rik
1810059C17Rik
2010204K13Rik
2210016F16Rik
2210408F21Rik
2210417K05Rik
2310011J03Rik
2310034G01Rik
2310068J16Rik
2410002F23Rik
2410022M11Rik
2500002B13Rik
2500004C02Rik
2510009E07Rik
2610301B20Rik
2610507B11Rik
2700029M09Rik
2700050L05Rik
2700060E02Rik
2810403A07Rik
2810403D21Rik
2810404F17Rik
2810408M09Rik
2810428I15Rik

2810454H06Rik
3010003L21Rik
3110009E18Rik
3110067C02Rik
3110082J24Rik
4732471J01Rik
4921530L18Rik
4921531C22Rik
4930402F06Rik
4930404I05Rik
4930412O13Rik
4930432B10Rik
4930447C04Rik
4930503L19Rik
4930509E16Rik
4930529M08Rik
4930546H06Rik
4930552N02Rik
4931406C07Rik
4933411K20Rik
4933433G15Rik
4933434E20Rik
5031434O11Rik
5330430P22Rik
5530601H04Rik
5730405O15Rik
5730420D15Rik
5730455P16Rik
5730508B09Rik

9030624J02Rik
9430008C03Rik
9430041J12Rik
9430083A17Rik
9530026F06Rik
9530027J09Rik
9530068E07Rik
9630014M24Rik
A330017A19Rik
A330050B17Rik
A330069E16Rik
A430018G15Rik
A630072M18Rik
A730036I17Rik
A830031A19Rik
A830035A12Rik
A930001C03Rik
A930007I19Rik
AA387883
AA415398
AA465934
Aaas
Aarsd1
AB041803
Abcb6
Abcc10
Abcc3
Abcf3
Abcg2

Abhd16a
Abi1
Abl1
Ablim1
Abr
Acaca
Acad11
Acat1
Acot8
Acp6
Acsl4
Actb
Actr8
Acyp1
Adam17
Adamts1
Adamts10
Adamts6
Adamtsl4
Adat1
Adc
Adcy3
Adcy7
Adk
Ado
Adora2b
Adpgk
Adrbk1
Adss

AF357374
AF357376
Afap1l1
Aff1
Aff4
Afmid
Aftph
Aga
Agbl5
Agpat1
Agt
Ahcyl2
Ahsa2
AI118078
AI450353
AI462493
AI597468
Aicda
Aifm1
AK006189
AK006245
AK007083
AK013187
AK015545
AK016837
AK018891
AK018967
AK019250
AK019365

AK031165
AK035829
AK037159
AK038627
AK040752
AK042136
AK043789
AK043804
AK043846
AK043958
AK044354
AK044623
AK045700
AK047520
AK048941
AK051804
AK053136
AK053772
AK054042
AK078466
AK079699
AK079730
AK079777
AK085438
AK087382
AK089118
AK131831
AK132720
AK134933

AK140370
AK141659
AK142999
AK154275
AK155149
AK155592
AK156477
AK158379
AK162774
AK163160
AK164218
AK165329
AK166079
AK167137
AK172386
AK188991
AK204212
AK212603
AK212710
Ak3
Akap1
Akap13
Akirin1
Akirin2
Akt2
Aldoa
Alg5
Alkbh5
Aloxe3

Ambra1
Ammecr1
Anapc1
Anapc5
Ang
Ank3
Ankrd24
Ankrd40
Ankrd52
Ankrd54
Antxr1
Anxa2
Anxa7
Ap1g1
Ap1s2
Ap3m1
Ap4s1
Aph1c
Appl1
Arf3
Arfgap1
Arhgap12
Arhgap18
Arhgap21
Arhgap26
Arhgap4
Arhgef10l
Arhgef25
Arhgef7

Arid1b
Arl15
Arl2bp
Arl3
Arl5a
Arl6ip5
Arpc3
Arrb2
Arrdc3
Arvcf
Asap1
Asb4
Ash2l
Asl
Asun
Asxl1
Asxl2
Atad2
Atat1
Atf7ip
Atg16l1
Atg16l2
Atg2a
Atg2b
Atl3
Atp13a1
Atp1b2
Atp2b1
Atp5a1

Atp5b
Atp6v0a1
Atp6v1a
Atp6v1b2
Atp6v1e1
Atpaf2
Atpif1
Atraid
Atrnl1
Atxn2
Atxn3
Atxn7l1
Atxn7l3
Avl9
AW209491
AW495222
B230217C12Rik
B230325K18Rik
B330016D10Rik
B3gnt2
B930003M22Rik
B930082K07Rik
Bach2
Banf1
Baz2b
BB019430
Bbc3
BC004004
BC024582

BC025920
BC030867
BC055111
BC055823
BC065397
BC099561
BC126883
Bcar1
Bcas2
Bcas3
Bcl11a
Bcl2l1
Bcl7a
Bdp1
Bend3
Bgn
Birc6
Blcap
Blmh
Bloc1s4
Bola2
Bptf
Brat1
Brca1
Brd3
Brf1
Bri3
Brwd3
Bscl2

Btaf1
Btd
Btf3l4
C030013C21Rik
C030034L19Rik
C030037D09Rik
C1ra
C1rb
C1rl
C2
C2cd2l
C2cd5
C330006A16Rik
C330007P06Rik
Cabin1
Cacna1f
Cad
Cage1
Calm2
Camk2d
Capn8
Capn9
Capns1
Car12
Carhsp1
Cask
Caskin2
Casp8
Cat

Catsper2
Catsperg1
Cbfb
Cbr1
Cbx4
Cbx7
Ccdc116
Ccdc136
Ccdc14
Ccdc146
Ccdc176
Ccdc22
Ccdc65
Ccdc77
Ccdc84
Ccdc92
Ccdc93
Ccnd2
Ccnh
Ccnk
Ccser2
Cct6a
Cd164
Cd164l2
Cd247
Cd276
Cd2ap
Cd300lh
Cdc14b

Cdc25a
Cdc26
Cdc6
Cdc73
Cdca5
Cdh12
Cdh16
Cdk11b
Cdk17
Cdk2ap1
Cdk5rap3
Cdkal1
Cdkl3
Cdkl5
Cdkn1b
Cdkn2c
Cdv3
Celf1
Cep128
Cfdp1
Cfi
Cflar
Chd2
Chd3
Chek1
Chfr
Chrac1
Chrna1
Chrnb4

Chst11
Chst3
Chsy1
Cic
Cirbp
Cisd3
Ciz1
Ckap5
Clasp1
Clca1
Clcf1
Clcn2
Clcn5
Cldn14
Clic4
Clint1
Clip1
Clk3
Clptm1
Clspn
Clta
Cltc
Cmah
Cmip
Cnn2
Cnot3
Cnot6
Cnot6l
Cnppd1

Cnpy3
Cnpy4
Cog4
Col8a2
Commd1
Commd7
Commd8
Comt
Cops7a
Cops8
Copz2
Coq10a
Coq5
Cox7b
Cpeb3
Cpm
Cpt1c
Cradd
Creb3
Crebbp
Crebl2
Creld1
Crem
Crk
Crlf3
Crnkl1
Crocc
Cryl1
Cryzl1

Cse1l
Csgalnact2
Csnk1a1
Csnk1g3
Cspp1
Csrnp1
Ctnna3
Ctnnd1
Ctsa
Ctse
Ctsl
Cttn
Cuedc1
Cux1
Cwc15
Cyb5
Cyb5d1
Cyb5r1
Cyp2t4
Cyth1
D030025P21Rik
D030028A08Rik
D14Abb1e
D17Wsu104e
D630003M21Rik
D6Wsu163e
D830025C05Rik
Dapk2
Dbi

Dbp
Dbr1
Dcaf17
Dcakd
Dck
Ddb2
Ddit4
Ddx20
Deb1
Def8
Dennd1b
Des
Desi1
Dgat1
Dgcr14
Dgka
Dhodh
Dhrs3
Dhx38
Dhx57
Dhx58
Dhx8
Dlat
Dleu2
Dmtf1
Dmtn
Dnajb14
Dnajc25
Dnajc3

Dnajc8
Dnm1
Dnmt1
Dnttip2
Dopey2
Dpagt1
Dpcd
Dpep1
Dpep2
Dph3
Dpy30
Dpysl2
Dpysl5
DQ544183
DQ548101
DQ552992
DQ553098
DQ565977
DQ566768
DQ692659
DQ694768
DQ695092
DQ695356
DQ703023
DQ704415
DQ704975
DQ705542
DQ712916
DQ713407

DQ716966
DQ725849
Dr1
Drg1
Drg2
Drp2
Dscr3
Dtd2
Dtnb
Dtx3
Dus1l
Dus2l
Dus3l
Dusp13
Dusp16
Dynll1
Dynll2
Dyrk1a
Dzip3
E030042O20Rik
E130102H24Rik
E130304I02Rik
E2f2
E530001K10Rik
Eapp
Ebf1
Ece1
Ech1
Ecsit

Edem1
Eed
Eef1b2
Eef2k
Efcab2
Ehbp1
Ehmt2
Eid1
Eif1ad
Eif3c
Eif3d
Eif3k
Eif3l
Eif4e
Eif4ebp2
Eif4g3
Eif4h
Eif5a
Eif5b
Elk3
Elk4
Ell
Elmsan1
Emp1
Entpd5
Epb4.1
Epb4.1l1
Epc1
Ephb4

Epo
Erbb2
Ercc6l
Ergic1
Erlin2
Ern1
Esyt2
Ets2
Etv5
Evi5
Ewsr1
Exd2
Exosc8
Extl2
Eya3
F420014N23Rik
Fam111a
Fam117a
Fam129b
Fam131a
Fam134a
Fam136a
Fam185a
Fam188a
Fam19a2
Fam214b
Fam216a
Fam35a
Fam49b

Fam57b
Fam63b
Fam73b
Fam98a
Fanca
Fancc
Fance
Fancg
Fars2
Fbxl16
Fbxl20
Fbxo30
Fbxo36
Fbxo42
Fbxo47
Fbxo9
Fchsd2
Fdps
Fes
Fgd2
Fgfr1op2
Fhl3
Fhl4
Fig4
Figf
Fignl1
Fis1
Fkbp10
Fkbp14

Fkbp1a
Fkbp5
Fkbp7
Fkbp8
Flna
Fmnl2
Fnbp1
Fndc3a
Fndc7
Fnip1
Fosl2
Foxh1
Foxj3
Foxn2
Foxn3
Foxo1
Foxp1
Frat1
Frat2
Frg1
Frmd4a
Frs2
Fry
Fstl1
Fus
Fut8
Fxr2
Fyttd1
Fzd7

G730013B05Rik
Gabarapl1
Gabarapl2
Gabpb1
Gabpb2
Gadd45b
Gadd45g
Gadd45gip1
Gak
Gapdh
Gapvd1
Gareml
Gast
Gata3
Gatad2a
Gatc
Gbas
Gbp3
Gcc2
Gclc
Gdf9
Gdi2
Gemin2
Gemin6
Gfpt2
Gga2
Ggnbp2
Ggt5
Gimap8

Gins1
Git2
Glg1
Glipr1
Glo1
Glud1
Gm10433
Gm10463
Gm10610
Gm10642
Gm10653
Gm10655
Gm10657
Gm10658
Gm10762
Gm10837
Gm11184
Gm11206
Gm11292
Gm11335
Gm11336
Gm11437
Gm11453
Gm11464
Gm11474
Gm11491
Gm11521
Gm11602
Gm11612

Gm11619
Gm11627
Gm11630
Gm11680
Gm11696
Gm11715
Gm11827
Gm12035
Gm12054
Gm12057
Gm12060
Gm12063
Gm12245
Gm12257
Gm12279
Gm12308
Gm12309
Gm12314
Gm12358
Gm12396
Gm12795
Gm12951
Gm12974
Gm12981
Gm13054
Gm13182
Gm13201
Gm13256
Gm13297

Gm13334
Gm13363
Gm13375
Gm13398
Gm13447
Gm13548
Gm13559
Gm13564
Gm13626
Gm13630
Gm13657
Gm13705
Gm13770
Gm13830
Gm13836
Gm13855
Gm13936
Gm14005
Gm14167
Gm14216
Gm14455
Gm14634
Gm15411
Gm15420
Gm15454
Gm15688
Gm15747
Gm15760
Gm15787

Gm15831
Gm15860
Gm15892
Gm15903
Gm15927
Gm15962
Gm16023
Gm16185
Gm16196
Gm16197
Gm16230
Gm16274
Gm16540
Gm16557
Gm16580
Gm16740
Gm16880
Gm17077
Gm17098
Gm17112
Gm17138
Gm17157
Gm17300
Gm17617
Gm17661
Gm17705
Gm19705
Gm20257
Gm20748

Gm4221
Gm4673
Gm4978
Gm5069
Gm5134
Gm5258
Gm5428
Gm5432
Gm5464
Gm5512
Gm608
Gm6225
Gm6297
Gm6444
Gm6471
Gm6525
Gm7598
Gm9812
Gm9850
Gm9900
Gm9959
Gm9985
Gna13
Gnb2
Gnb2l1
Gnl3
Golga3
Got2
Gpbar1

Gpn3
Gpr19
Gpr35
Gpr82
Gpr85
Gramd1a
Grb2
Grcc10
Grik4
Gse1
Gskip
Gstt3
Gtf2h2
Gtf2i
Gtf2ird2
Gyk
Gypc
Gys1
Gzmm
H1f0
H2afz
H2-D1
H2-DMb1
H2-DMb2
H2-L
Hacl1
Hbp1
Hdac7
Hdgfrp2

Heatr5a
Helb
Helz
Herc4
Hes1
Hes7
Hexim2
Hic1
Hic2
Hif1a
Hint2
Hip1r
Hira
Hirip3
Hist1h2ac
Hist1h2af
Hist1h2bb
Hist1h2bc
Hist1h3c
Hivep1
Hlcs
Hlx
Hmbs
Hmg20b
Hmox2
Hnrnpf
Hnrnph1
Hnrnph3
Hnrnpk

Hnrnpl
Hnrnpu
Hnrnpul1
Hnrnpul2
Homer1
Hoxb6
Hoxb8
Hoxc5
Hoxd10
Hoxd3
Hps3
Hsd17b12
Hsp90ab1
Hspa13
Hspa4
Hspb9
I830077J02Rik
Ica1
Icam1
Id3
Ifi35
Ift80
Igf1r
Igfbp6
Ik
Il1rap
Il3ra
Ilf2
Ilf3

Ilk
Immt
Impdh1
Ing1
Ing3
Ing4
Inip
Ino80
Ino80d
Ino80e
Inpp5b
Ints8
Ipo11
Iqce
Iqcg
Irf2bp2
Irf2bpl
Irs3
Itfg2
Itgb2
Itgb5
Itm2b
Itpkb
Izumo4
Jarid2
Kalrn
Kansl1
Kars
Kat2a

Kat2b
Kbtbd7
Kcnh3
Kctd19
Kctd20
Kdm3a
Kdm4d
Kdm5a
Kif11
Kif23
Kif24
Kif5b
Klc1
Klhdc10
Klhl11
Klhl18
Kmt2d
Kntc1
Kpna2
Kpnb1
Krt222
L3mbtl2
L3mbtl3
Lamp2
Lamtor3
Larp4
Lars2
Las1l
Lck

Lctl
Ldb1
Leo1
Leprel4
Leprotl1
Letm2
Lhb
Lias
Lipe
Lmf2
Lmna
Lmo2
Lmo4
Lmtk2
Lnx2
LOC100504608
LOC100504703
Loxl3
Lpar5
Lphn1
Lpin2
Lpxn
Lrch1
Lrg1
Lrig2
Lrp2bp
Lrrc1
Lrrc16a
Lrrc16b

Lrrc46
Lrrc49
Lrrc58
Lrrk1
Lrsam1
Lsmd1
Luc7l
Luc7l2
Luc7l3
Luzp1
Ly6g6f
Lyrm4
Lyrm7
Lysmd3
Lyzl6
Mad2l1
Mad2l1bp
Madd
Maea
Magt1
Malat1
Maml2
Manea
Map2k6
Map2k7
Map3k12
Map3k3
Map4k1
Map4k2

Map4k3
Mapk6
Mapkbp1
Mapt
March5
March6
March7
March8
Mark2
Marveld1
Mast4
Mbnl2
Mbnl3
Mbtps2
Mccc1
Mcm3
Mcm3ap
Mcm9
Mcts1
Mdp1
Med13
Med14
Med18
Med6
Melk
Memo1
Mettl1
Mettl14
Mettl17

Mettl8
Mga
Mical3
Midn
Mif4gd
Mir125a
Mir132
Mir152
Mir15b
Mir17
Mir17hg
Mir18
Mir1931
Mir1956
Mir199b
Mir19a
Mir19b-1
Mir20a
Mir212
Mir3058
Mir3109
Mir5122
Mir5135
Mir615
Mir670
Mir677
Mir702
Mir92-1
Mir99b

Mirlet7e
Mitd1
Mkks
Mlec
Mlf2
Mllt10
Mlxip
Mmp25
Mms19
Mob1a
Mob3a
Morc3
Morf4l1
Morf4l2
Morn1
Morn2
Morn3
Mpnd
Mpp6
Mpv17
Mrc2
Mrfap1
Mrpl10
Mrpl14
Mrpl30
Mrpl32
Mrpl40
Mrpl45
Mrpl48

Mrpl52
Mrpl9
Mrps2
Mrps36
Mrps6
Mrs2
Ms4a10
Msh5
Msl1
Msrb3
Mtf2
Mtif3
Mtmr3
Muc6
Mxi1
Mxra7
Myadm
Myc
Myg1
Myh9
Myl12b
Mylpf
Myo1g
Myo1h
Myo9a
Mzf1
N4bp2
N4bp2l2
Naa16

Naa20
Naa25
Naa50
Nadk
Nagk
Nap1l1
Napa
Nasp
Nat10
Nat2
Nbeal1
Nbeal2
Nbr1
Ncaph2
Nck1
Ncoa3
Ncoa4
Ncor1
Ncor2
Ncrna00085
Ndfip2
Ndrg4
Ndufaf4
Ndufs7
Necap1
Nedd4
Nek10
Nek8
Nek9

Neu1
Neurl2
Nf2
Nfat5
Nfic
Nfil3
Nfix
Nfkbia
Nfx1
Nfxl1
Nhlrc2
Nhp2
Nipbl
Nkrf
Nktr
Nlk
Nol7
Nono
Nop58
Notch3
Npepps
Nphp1
Nploc4
Nppa
Nptn
Nqo2
Nr2f6
Nr3c1
Nr4a2

n-R5s79
Nrf1
Nrg4
Nt5c2
Ntf5
Nub1
Nubp2
Nufip2
Numa1
Nup133
Nup153
Nup205
Nup98
Nyx
Oas1b
Oas1c
Oas2
Ocrl
Ogt
Olfr1414
Oma1
Opn1sw
Orai2
Orc1
Orc2
Osbpl3
Osbpl7
Osbpl8
Otub1

Otud4
Ovol1
Oxnad1
Oxsr1
P2rx4
P4ha1
Pacsin2
Palld
Pan3
Papd4
Papss1
Papss2
Paqr8
Parl
Patz1
Pax2
Pax6
Pbld2
Pbrm1
Pcbd2
Pcbp1
Pcbp2
Pcca
Pccb
Pcgf2
Pcm1
Pcnxl2
Pcsk4
Pde4d

Pdia3
Pdia6
Pdk1
Pdpk1
Pdxdc1
Peg13
Peli1
Pes1
Pex19
Pfkm
Pfn2
Pgam1
Pgap2
Pgd
Phactr4
Phc1
Phc3
Phf12
Phf15
Phf20
Phf21a
Phf6
Phf8
Phgdh
Phip
Phospho1
Phyhd1
Pias4
Picalm

Pif1
Pigl
Pigp
Pigv
Pik3c3
Pik3ca
Pik3cb
Pik3cd
Pik3r1
Pik3r3
Pim1
Pisd
Pisd-ps1
Pisd-ps2
Pitpnc1
Pitpnm2
Pja1
Pkd2l1
Pkig
Pkn3
Pknox1
Pla2g6
Plbd2
Plcg1
Plcl2
Plekha3
Plekha4
Plekha8
Plekhf2

Plekhg2
Plekhg3
Plin3
Plk1s1
Plod3
Plxna2
Plxnd1
Pml
Pmm2
Pnpla8
Poc1a
Poldip2
Pole2
Polg
Polg2
Poll
Polr2h
Polr2i
Polr3c
Polrmt
Pop4
Pou2f1
Pou4f3
Pou6f1
Ppard
Ppcdc
Ppfia3
Ppil1
Ppm1b

Ppm1h
Ppm1k
Ppp1r12a
Ppp1r15a
Ppp1r16a
Ppp1r3f
Ppp1r8
Ppp2cb
Ppp2r5c
Ppp6r2
Prdm1
Prex1
Prickle1
Prkaa1
Prkag1
Prkag2
Prkar1a
Prkcg
Prkrip1
Prpf19
Prpf3
Prpf38a
Prpf38b
Prpf39
Prpf4
Prpf4b
Prpsap1
Prpsap2
Prr12

Prr13
Prr14l
Prrc2a
Prrg2
Psap
Psma1
Psma2
Psma3
Psmb3
Psmb6
Psmc1
Psmd14
Psmd7
Pspc1
Psph
Ptbp3
Ptch1
Ptp4a1
Ptp4a2
Ptplad2
Ptpmt1
Ptpn11
Ptpn6
Ptprj
Ptrh2
Pttg1
Pum1
Pycard
Pycr2

Pygl
Qk
Qrich1
Qsox2
R3hdm2
Rab1
Rab21
Rab28
Rab3gap2
Rab42
Rab5b
Rab6a
Rab7
Rad51ap1
Rad51c
Rad9b
Ralbp1
Ralgapa1
Ralgps1
Rap1b
Rap2a
Rapgef6
Rarg
Rasal2
Rasd1
Rb1
Rbbp5
Rbbp6
Rbck1

Rbm12b2
Rbm27
Rbms1
Rcc1
Rcc2
Rccd1
Rcor1
Rdh10
Rdm1
Rell1
Reps2
Rere
Rexo2
Rffl
Rft1
Rftn2
Rfwd3
Rfx2
Rfx3
Rhbdd2
Rhbg
Rhob
Rhobtb2
Rhot1
Rilpl2
Riok1
Rlim
Rmi1
Rmnd1

Rnase4
Rnf10
Rnf121
Rnf13
Rnf146
Rnf157
Rnf167
Rnf2
Rnf34
Rnf5
Rnft1
Rp9
Rpa1
Rpa2
Rpl10
Rpl10-ps2
Rpl12
Rpl24
Rpl27
Rpl30-ps5
Rpl35a
Rpl35a-ps2
Rpl38
Rpl41
Rpl5
Rpl6
Rpl7
Rpl9
Rpp21

Rprd2
Rps10
Rps15a
Rps26
Rps6ka1
Rps6kb1
Rps8
Rptor
Rreb1
Rrm1
Rrm2b
Rrp8
Rsbn1l
Rsrc2
Rtfdc1
Rtn4rl2
Rufy3
Rundc3a
Runx1
Rybp
S100pbp
Sacm1l
Sae1
Samd1
Samd8
Samd9l
Samhd1
Sap30
Sapcd2

Sarm1
Sbds
Sbf1
Sbno2
Scamp3
Scara5
Scarb1
Scgb1a1
Schip1
Scmh1
Scn1a
Scn3a
Scpep1
Sec14l1
Sec22c
Sec23a
Sec24b
Sec24c
Sec31a
Sec31b
Sec61a1
Seh1l
Selt
Sema3c
Sephs1
Sept5
Sept8
Serf1
Serpinb9

Sertad1
Sertad2
Sesn2
Setd2
Setd3
Setd4
Setd5
Setd7
Setd8
Sfmbt1
Sfpq
Sfxn2
Sgk1
Sgk2
Sgk3
Sgms2
Sh2b3
Sh3bgrl
Sh3bp5l
Sh3glb2
Sh3kbp1
Shc4
Shisa5
Shmt1
Shroom3
Siae
Sigmar1
Sin3a
Sirt1

Sit1
Six6
Skil
Slain2
Slc16a1
Slc18a1
Slc23a2
Slc25a11
Slc25a14
Slc25a3
Slc25a35
Slc25a36
Slc25a38
Slc25a39
Slc25a43
Slc25a51
Slc26a10
Slc30a1
Slc30a7
Slc31a2
Slc32a1
Slc35b1
Slc35b4
Slc38a10
Slc38a2
Slc39a2
Slc3a2
Slc43a2
Slc5a3

Slc5a6
Slc7a7
Slc9a1
Slc9a8
Slu7
Slx1b
Slx4ip
Smad6
Smad7
Smap1
Smarca2
Smarcc2
Smarcd2
Smc4
Smg7
Smim13
Smndc1
Smpd1
Smyd4
Snai1
Snf8
Snhg1
Snhg12
Snhg5
Snora16a
Snora44
Snora61
Snora70
Snord19

Snord21
Snord38a
Snord52
Snord55
Snord7
Snord88a
Snord88c
Snord96a
Snord99
Snrnp35
Snrnp70
Sntb2
Snupn
Snx10
Snx27
Snx29
Snx30
Soat1
Socs1
Socs2
Socs3
Socs7
Sod1
Sorbs1
Sos2
Sp1
Sp3
Spa17
Spag8

Specc1
Spg11
Spin1
Spp1
Sppl2a
Spred1
Spred2
Spry4
Spryd3
Spryd4
Spsb3
Sptan1
Sptlc2
Sqrdl
Srek1
Srgap3
Srrm1
Srrm2
Srsf1
Srsf3
Ssb
Ssbp3
Ssbp4
Ssh2
St13
St6galnac2
Stac2
Stag2
Stam

Stam2
Stard6
Stard9
Stat2
Stim2
Stip1
Stk25
Stk30
Stk38
Stk38l
Stoml1
Strada
Strn3
Stx11
Stx16
Styk1
Suco
Sumo1
Sun1
Suz12
Swsap1
Syne1
Syngr1
Syngr3
Syngr4
Synj1
Synj2
Tacc1
Tacc2

Taco1
Taf1
Taf1c
Taf1d
Taf3
Taf4a
Taf6
Tagln2
Tango2
Tango6
Taok2
Taok3
Tarbp2
Tatdn2
Tbc1d1
Tbc1d10a
Tbc1d10b
Tbcb
Tbcc
Tbl1xr1
Tbx15
Tcam1
Tceanc2
Tcf12
Tcf4
Tcf7l2
Tcof1
TCR-alpha chain
Tctn1

Tdrd3
Tead2
Tecr
Terf2
Terf2ip
Tet2
Tex14
Tex30
Tfap4
Tfdp2
Tfg
Tfrc
Tgif1
Thrap3
Tia1
Tial1
Ticam1
Timm13
Timm8a2
Timm9
Timmdc1
Tipin
Tjap1
Tjp3
Tle2
Tle3
Tle6
Tlk2
Tln1

Tm2d2
Tm9sf4
Tmbim1
Tmcc2
Tmem100
Tmem106a
Tmem120b
Tmem143
Tmem156
Tmem164
Tmem18
Tmem180
Tmem186
Tmem192
Tmem194
Tmem199
Tmem231
Tmem242
Tmem259
Tmem29
Tmem33
Tmem5
Tmem59
Tmem67
Tmem82
Tmem88
Tmpo
Tnfaip8
Tnfrsf9

Tnk2
Tnp2
Tnpo2
Tnpo3
Tnrc18
Tnrc6a
Tob1
Tob2
Tom1l1
Top1
Top2a
Tor1aip1
Tor1aip2
Tpm1
Tprgl
Tpt1
Tpx2
Tra2b
Traf6
Trafd1
Traj58
Traj59
Tram1
Trap1
Trdv5
Trerf1
Triap1
Trib1
Trib2

Trim35
Trim37
Trim59
Trim7
Trim8
Triobp
Trip12
Trmt12
Trpc2
Trpv2
Trpv4
Trub2
Tsc22d3
Tsen54
Tspan10
Tspan14
Tspan17
Tspan31
Ttc17
Ttc19
Ttc28
Ttc3
Ttc7
Ttc9c
Tuba1a
Tuba1c
Tubb5
Tubd1
Tulp1

Tulp3
Txlna
Txn2
Txndc12
Txndc9
Txnl4b
Txnrd1
Txnrd2
Tyw1
U05342
U3
U7
Uba1
Uba5
Uba52
Ubald1
Ubap2l
Ubb
Ubc
Ube2b
Ube2e3
Ube2f
Ube2h
Ube2v1
Ublcp1
Ubn2
Ubr2
Ubtd2
Ubtf

Ubxn1
Ubxn4
Ubxn7
Uchl4
Ulk2
Umodl1
Unc119
Uqcrq
Urgcp
Urm1
Usb1
Usf2
Usp1
Usp10
Usp15
Usp2
Usp20
Usp28
Usp3
Usp32
Usp34
Usp45
Usp48
Usp49
Utp14a
Vac14
Vcp
Vdac1
Vezf1

Vezt
Vgll4
Vhl
Vmp1
Vprbp
Vps13d
Vps29
Vps37b
Vps53
Vps54
Vtn
Wbscr16
Wdfy2
Wdpcp
Wdr1
Wdr34
Wdr37
Wdr47
Wdr5
Wdr6
Wdr63
Wdr75
Wee1
Whsc1
Whsc1l1
Wibg
Wipf1
Wrnip1
Wtap

Wwp1
Wwp2
Xbp1
Xiap
Xpnpep3
Xpot
Yars
Ybey
Ydjc
Yipf2
Yipf4
Ypel2
Ywhag
Yy2
Zan
Zbtb1
Zbtb24
Zbtb25
Zbtb38
Zbtb45
Zbtb7a
Zc3h10
Zc3h6
Zc3hav1
Zc3hc1
Zcchc8
Zdhhc17
Zdhhc5
Zer1

Zfand3
Zfat
Zfp1
Zfp101
Zfp106
Zfp182
Zfp184
Zfp207
Zfp217
Zfp251
Zfp27
Zfp280b
Zfp319
Zfp324
Zfp36l1
Zfp383
Zfp384
Zfp39
Zfp395
Zfp40
Zfp428
Zfp438
Zfp507
Zfp512
Zfp52
Zfp553
Zfp592
Zfp606
Zfp607

Zfp608
Zfp64
Zfp646
Zfp664
Zfp668
Zfp672
Zfp703
Zfp719
Zfp809
Zfp866
Zfp91
Zfp948
Zfpl1
Zfx
Zkscan17
Zkscan3
Zmat1
Zmiz2
Zmym5
Zmynd11
Zmynd8
Znhit1
Znhit3
Zscan25
Zswim7
Zufsp
Zw10